

**Factors Affecting Occupant Risk of Knee-Thigh-Hip
Injury in Frontal Vehicle Collisions**

by: Douglas Heath

A Thesis
Submitted to the Faculty
of the

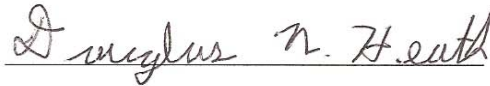
WORCESTER POLYTECHNIC INSTITUTE

In partial fulfillment of the requirements for the

Degree of Master of Science

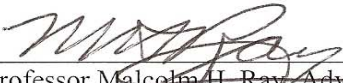
in

Civil Engineering



April 22, 2010

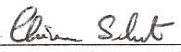
Approved:



Professor Malcolm H. Ray, Advisor
Civil and Environmental Engineering Department



Professor Leonard Albano, Committee Member
Civil and Environmental Engineering Department



Professor Chiara Silvestri, Committee Member
Civil and Environmental Engineering Department



Professor Tahar El-Korchi, Department Head
Civil and Environmental Engineering Department

Abstract

Every year, millions of people are killed or injured in motor vehicle accidents in the United States. Although recent improvements to occupant restraint systems, such as seatbelts and airbags, have significantly decreased life threatening injuries, which usually occur to the chest or head, they have done little to decrease the occurrence of lower extremity injuries. Although lower extremity injuries are not usually life threatening, they can result in chronic disability and high psychosocial cost. Of all lower extremity injuries, injuries to the knee-thigh-hip (KTH) region have been shown to be among the most debilitating. This project used a finite element (FE) model of the KTH region to study injury. A parametric investigation was conducted where the FE KTH was simulated as a vehicle occupant positioned to a range of pre-crash driving postures. The results indicate that foot contact force and knee kinematics during impact affects the axial force absorbed by the KTH region and the likelihood of injury. The results of the study could be used to reevaluate the lower extremity injury thresholds currently used to regulate vehicle safety standards. Also, the results could be used to provide guidelines to vehicle manufacturers for developing safer occupant compartments.

Acknowledgements

Thank you Professor Ray for giving me this opportunity to work on a professional research project. I am certain that I could not have developed as good of a thesis, or learned as much about the research process, if you had not given me this opportunity.

Thank you Chiara for all the help and guidance you gave me during this project. From helping me with LS-DYNA to sharing your thoughts about a given problem, I could not have accomplished as much as I did without your help.

Thank you Professor Albano for being a mentor to me during my time at WPI, both as an undergraduate and graduate student. The time I have spent learning from you inside the classroom and during projects has allowed me to develop problem solving strategies that I can apply in any number of situations.

Thank you to Sia Najafi for all of your help in getting the computers to work for me. In particular, thank you for your hard work in setting up the cluster to run LS-DYNA.

Finally, thank you to my family. The way you supported me and helped me while I was growing up has been a major factor in allowing me to achieve what I have.

Table of Contents

Introduction.....	1
Background.....	3
Anatomy of the KTH	3
KTH Bones	4
KTH Soft Tissues.....	11
KTH Injuries and Injury Criteria	16
Mathematical Modeling in Injury Prediction.....	20
LLNL Model.....	21
KTH Model.....	22
Remarks	25
Methods	27
Effect of Pre-Crash Hip Posture on Injury Susceptibility.....	27
Comparison of Occupant Response in Sled Test and Vehicle Collision	28
Summary of Research Activities.....	29
Results.....	30
Validation of Vehicle Occupant Simulations.....	30
Hip Posture Parametric Study	35
Model Setup	35
Simulation Results	37
Comparison of Sled Test and Vehicle Simulations.....	64
Remarks	65
Conclusions and Discussion	66
References.....	69
Appendix A: Raw Data from Parametric Simulations.....	73
Neutral Results Summary	74
Abduct10° Results Summary	77
Abduct5° Results Summary	80
Adduct5° Results Summary	83
Adduct10° Results Summary	86
Flex7.5° Results Summary.....	89
Flex15° Results Summary.....	92
Flex22.5° Results Summary.....	95

Flex30° Results Summary.....	98
Combined Flex30° Abduct10° Results Summary.....	101
Combined Flex30° Adduct10° Results Summary.....	104
Combined Flex30° Abduct5° Results Summary.....	107
Combined Flex30° Adduct5° Results Summary.....	110
Combined Flex15° Abduct10° Results Summary.....	113
Combined Flex15° Adduct10° Results Summary.....	116
Combined Flex15° Abduct5° Results Summary.....	119
Combined Flex15° Adduct5° Results Summary.....	122
Combined Flex7.5° Abduct10° Results Summary.....	125
Combined Flex7.5° Adduct10° Results Summary.....	128
Combined Flex7.5° Abduct5° Results Summary.....	131
Combined Flex7.5° Adduct5° Results Summary.....	134
Combined Flex22.5° Abduct10° Results Summary.....	137
Combined Flex22.5° Adduct10° Results Summary.....	140
Combined Flex22.5° Abduct5° Results Summary.....	143
Combined Flex22.5° Adduct5° Results Summary.....	146

Table of Figures

Figure 1: Full View KTH Region	3
Figure 2: Osteons of Cortical Bone.....	4
Figure 3: Anatomy of Trabecular Bone	5
Figure 4: Knee Joint Anatomy	6
Figure 5: Femoral Condyles.....	7
Figure 6: Femoral Shaft and Linear Aspera.....	8
Figure 7: Arrangement of Trabecules in the Femoral Shaft	9
Figure 8: Geometry of the Proximal Femur.....	10
Figure 9: Arrangement of Trabecules in the Proximal Femur	10
Figure 10: Greater Pelvis (left) and Lesser Pelvis (right)	11
Figure 11: Ligament Hierarchy.....	12
Figure 12: Non-Linear Stress Strain Curve of Ligaments	12
Figure 13: Iliofemoral Ligament (left) and Ischiofemoral Ligament (right)	13
Figure 14: Ligaments of the Knee.....	14
Figure 15: Anterior (left), Medial (center), and Posterior and Guteal (left) Muscles	16
Figure 16: AP Motion of the Tibia and Femur During Compressive Loading	19
Figure 17: LLNL Model	22
Figure 18: KTH Model	22
Figure 19: Femoral Shaft Validation Force Time History	23
Figure 20: Silvestri's Ligament Validation Simulation.....	24
Figure 21: Initial Sled Test Position in Physical Test (left) and FE Simulation (right).....	24
Figure 22: Femur Axial Force Time Histories (top), Location of Initial Fracture in FE KTH based on von Mises Stresses (bottom left), Fracture Location in Physical test (bottom right) in Full Scale Validation..	25
Figure 23: FE KTH Inside Reduced FE Taurus.....	28
Figure 24: 2001 Ford Taurus Model, Exterior (left) and Occupant Compartment (right).....	30
Figure 25: FE Hybrid.....	31
Figure 26: Initial FE Hybrid Position (left) and FE Hybrid Position at Time of Maximum Femur Axial Force	32
Figure 27: Reduced FE Taurus, Front View (left) and Back View (right)	32
Figure 28: FE Hybrid in Reduced FE Taurus Model, Initial Position (left) and Position at Time of Maximum Femur Force (right)	33
Figure 29: FE KTH in the Reduced FE Taurus, Initial Position (left) and Position at Maximum Axial Femur Force (right).....	34
Figure 30: Examples of Pre-Crash Hip Posture, 0° Adduction (top left), 0° Flexion (top right), 10° Abduction (bottom left), 30° Flexion (bottom right)	36
Figure 31: 10° Adducted Hip Posture	37
Figure 32: Injury to Various KTH Components	38
Figure 33: Basic Description of Occupant Kinematics During Impact: Both Legs Directly Impacting the Knee Bolster (left) and Left Leg Directly Impacting the Knee Bolster and Right Leg Sliding Along It (right)	39
Figure 34: Large Tibia Displacement Relative to the Femur.....	40
Figure 35: Maximum Femur Axial Force Distribution Left Leg (top); Right Leg (bottom)	42
Figure 36: Effect of Knee Impact Location on Maximum Femur Axial Force	43

Figure 37: Distribution of Femur Axial Force Required to Cause Acetaublum Injury, in the Left Leg (top), and Right Leg (bottom).....	45
Figure 38: Distribution of Femur Axial Force at the Time of Initial Femoral Head Fracture, Left Leg (top) and Right Leg (bottom).....	47
Figure 39: Distribution of Femur Axial Force at the Time of Initial Femoral Neck Fracture, Left Leg (top) and Right Leg (bottom).....	49
Figure 40: Distribution of Femur Axial Force at the Time of Initial Proximal Femoral Shaft Fracture, Left Leg (top) and Right Leg (bottom).....	51
Figure 41: Femur Axial Force Distribution at the Time of Initial Mid Femoral Shaft Fracture, Left Leg (top) and Right Leg (bottom).....	53
Figure 42: Distribution of Femur Axial Forces at the Time of Initial Fracture to the Femoral Condyles, Left Leg (top) and Right Leg (bottom).....	55
Figure 43: Distribution of Injuries by KTH Region.....	56
Figure 44: Comparison of Maximum Femur Axial Force to Axial Force at time of Initial KTH Component Fracture, Left Leg, 0° Flexion.....	57
Figure 45: Comparison of Maximum Femur Axial Force to Axial Force at time of Initial KTH Component Fracture, Left Leg, 7.5° Flexion.....	57
Figure 46: Comparison of Maximum Femur Axial Force to Axial Force at time of Initial KTH Component Fracture, Left Leg, 15° Flexion.....	58
Figure 47: Comparison of Maximum Femur Axial Force to Axial Force at time of Initial KTH Component Fracture, Left Leg, 22.5° Flexion.....	58
Figure 48: Comparison of Maximum Femur Axial Force to Axial Force at time of Initial KTH Component Fracture, Left Leg, 30° Flexion.....	59
Figure 49: Comparison of Maximum Femur Axial Force to Axial Force at time of Initial KTH Component Fracture, Right Leg, 0° Flexion.....	59
Figure 50: Comparison of Maximum Femur Axial Force to Axial Force at time of Initial KTH Component Fracture, Right Leg, 7.5° Flexion.....	60
Figure 51: Comparison of Maximum Femur Axial Force to Axial Force at time of Initial KTH Component Fracture, Right Leg, 15° Flexion.....	60
Figure 52: Comparison of Maximum Femur Axial Force to Axial Force at time of Initial KTH Component Fracture, Right Leg, 22.5° Flexion.....	61
Figure 53: Comparison of Maximum Femur Axial Force to Axial Force at time of Initial KTH Component Fracture, Right Leg, 30° Flexion.....	61
Figure 54: Resultant Foot Contact Force for Neutral Posture Impact (Direct).....	63
Figure 55: Resultant Foot Contact Force for 10° Abduction Posture Impact (Indirect).....	63
Figure 56: Comparison of Floor Placement in Vehicle Simulation (left) and Sled Test Simulation (right).....	64

Table of Tables

Table 1: AIS Summary	17
Table 2: Hip Posture Test Matrix.....	27
Table 3: Basic Occupant Impact Scenario	40
Table 4: Maximum Femur Axial Force (kN).....	41
Table 5: Femur Axial Force at the Time of Initial Fracture to the Acetabulum (kN).....	44
Table 6: Femur Axial Force at Time of Initial Femoral Head Fracture (kN)	46
Table 7: Femur Axial Force at the Time of Initial Femoral Neck Fracture (kN)	48
Table 8: Femur Axial Forces at the Time of Initial Fracture of the Proximal Femoral Shaft (kN)	50
Table 9: Femur Axial Force at the Time of Initial Fracture to the Mid Femoral Shaft (kN).....	52
Table 10: Femur Axial Force at the Time of Initial Femoral Condyle Fracture (kN)	54
Table 11: Comparison of Maximum Femur Axial Forces in Direct and Indirect Impacts	62
Table 12: Percent Occurrence of Right Leg Fracture in Direct and Indirect Impacts.....	62

Introduction

In the year 2000, 5.3 million persons were injured and nearly 42000 fatalities occurred in over 16 million motor vehicle crashes in the United States alone. These injuries resulted in \$32.6 billion in medical costs, making injuries due to motor vehicle crashes the second largest contributor to total medical costs in the U.S. (Blincoe, 2002). It is therefore important for engineers to develop ways for decreasing motorists' risk of injury or death in highway crashes.

The widespread use of safety restraints such as seatbelts and airbags has significantly decreased the incidence of life threatening injury and death in motor vehicle collisions. Despite these improvements in highway safety, many people involved in frontal motor vehicle collisions still suffer from lower extremity injuries. Although these injuries are not usually life threatening, they can result in serious injury, and make up a significant portion of the total medical costs due to motor vehicle accidents. Of all types of lower extremity injuries, injuries to the knee-thigh-hip (KTH) region account for a significant portion (50%) (Kuppa, 2002). As a result, engineers are now trying to find ways of decreasing the risk and the severity of injuries to the lower extremities, particularly the KTH.

Computer simulation has proven to be an effective way of studying injuries. Ray and Silvestri (2009) developed a finite element (FE) model of the lower extremities that can be used to study injury to the KTH region (referred to as the FE KTH in this paper). The model was validated against experimental results from a cadaveric specimen in a sled test. It is highly detailed and includes an accurate geometry of the skeletal structure, an accurate representation of many muscles and ligaments, and appropriate material models for all parts of the model.

Although much has been learned about injury to the lower extremities through numerical models and physical experiments, much still remains to be learned about occupant response to a head on collision. One reason for this is because a popular test used for studying lower extremity injury, the sled test, fails to accurately capture all of the factors that characterize an actual vehicle collision. For example,

in a typical sled test, the knee is impacted by a blunt, deformable interface, usually a piece of foam. In an actual collision, the knee is likely to impact the knee bolster, which is usually made of a stiffer material such as plastic or metal. The knee bolster can respond differently from the foam during impact because of differences in stiffness and geometry. Furthermore, limited amounts of cadavers available for experimental testing prohibit researchers from studying a wide range of impact scenarios. The lack of availability and high variability in mechanical properties between cadavers makes it difficult to study injury over a range of pre-crash hip postures, a parameter that has been shown to affect injury tolerance (Rupp, 2003). This project studied occupant response to an actual vehicle collision using computer simulation. A range of pre-crash hip postures was considered to determine the effects on injury tolerance and mechanism.

This project used the LS-DYNA finite element code to study occupant response to the effects of frontal collisions. The FE KTH was simulated as an occupant in a FE vehicle model. The response of the FE KTH in the vehicle simulation was compared to results observed in full scale physical crash tests. Next, the FE KTH was simulated in the FE vehicle over a range of pre-crash hip postures. Finally, differences between the FE KTH's response to impact in a vehicle was compared to its response to a sled test impact observed by Silvestri (2009). The results of this study could be used to help researchers understand the differences between occupant response to a sled test and an actual vehicle collision. An understanding of these differences could provide a deeper understanding of the implication of the results of sled tests. This study may also be used to help regulators re-evaluate lower extremity injury thresholds used to regulate vehicle safety, or to provide guidelines to vehicle manufacturers for designing safer occupant compartments.

Background

This chapter presents the background research conducted to complete this project. Topics covered include an overview of the anatomy of the KTH region, common KTH injury mechanisms in frontal vehicle collisions, and the use of mathematical modeling for studying injury. The chapter concludes with the presentation of research questions that the work is intended to answer.

Anatomy of the KTH

The KTH complex consists of the bones and soft tissue (muscles and ligaments) in the knee-thigh-hip region. Figure 1 gives a full view of the KTH region.

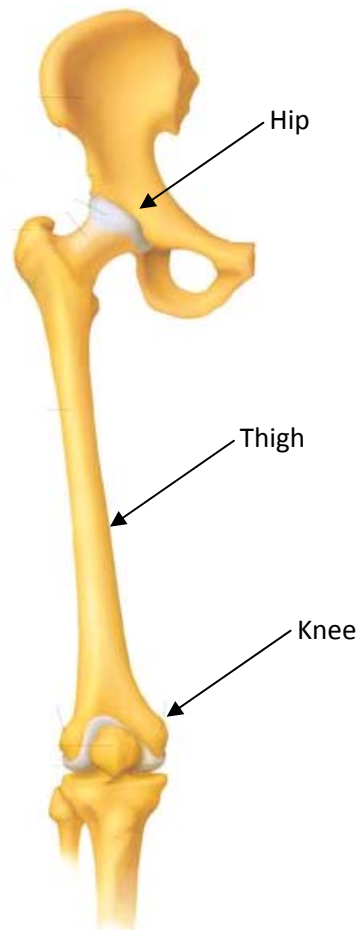


Figure 1: Full View KTH Region
http://skeletonsandmore.com/cart/index.php?main_page=product_info&products_id=331

KTH Bones

To understand the anatomy of the KTH bones, it is first important to understand the basic structure of bone in the human body. Bone is the hardest material in the human body. Although it is typically thought of as a brittle material, it has been shown to exhibit some elastic properties, and toughness when loaded beyond its elastic limit (Grey, 1918).

Bone primarily consists of two materials: cortical bone and trabecular bone. Cortical bone is denser than trabecular bone, and has a higher ultimate strength but lower toughness. It is organized in cylindrically shaped elements called osteons. Cortical bone is an anisotropic material, and is often considered a transversely isotropic material. As a result of its anisotropy, the direction that the osteons arrange themselves dictates the stiffness of the cortical bone in response to load. Because of its porous nature, cortical bone is stronger in compression than in tension, similar to concrete (Mechanical Properties of Bone, 2010). Figure 2 shows cortical bone organized into groups of osteons.

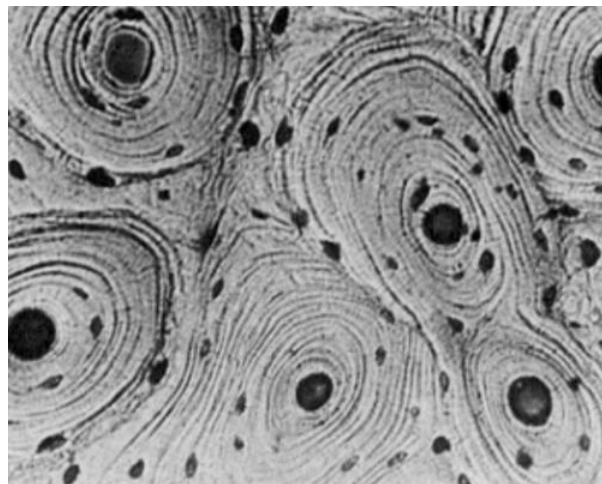


Figure 2: Osteons of Cortical Bone

http://www.feppd.org/ICB-Dent/campus/biomechanics_in_dentistry/ldv_data/mech/basic_bone.htm

Trabecular bone, sometimes referred to as cancellous bone, is more complicated than cortical bone from a biomechanical point of view. It is even more porous than cortical bone. Although it has a lower ultimate strength, it is often described as “spongy” and, as a result, is capable of absorbing large amounts of energy. It is organized into small structures called trabecules. The trabecules arrange

themselves in a manner to maximize load carrying efficiency, a principle known as Wolf's Law (Mechanical Properties of Bone, 2010). Koch describes this principle as it applies to the femur in his article "The Laws of Bone Architecture." (1917)

"...in every part of the femur there is a remarkable adaptation of the inner structure of the bone to the mechanical requirements due to the load on the femur-head. The various parts of the femur taken together form a single mechanical structure wonderfully well-adapted for the efficient, economical transmission of the loads from the acetabulum to the tibia; a structure in which every element contributes its modicum of strength in the manner required by theoretical mechanics for maximum efficiency."

This principle is highlighted in the following paragraphs to show the fundamental biomechanics related to the femur and the rest of the KTH region. Figure 3 shows the arrangement of trabecules in trabecular bone.

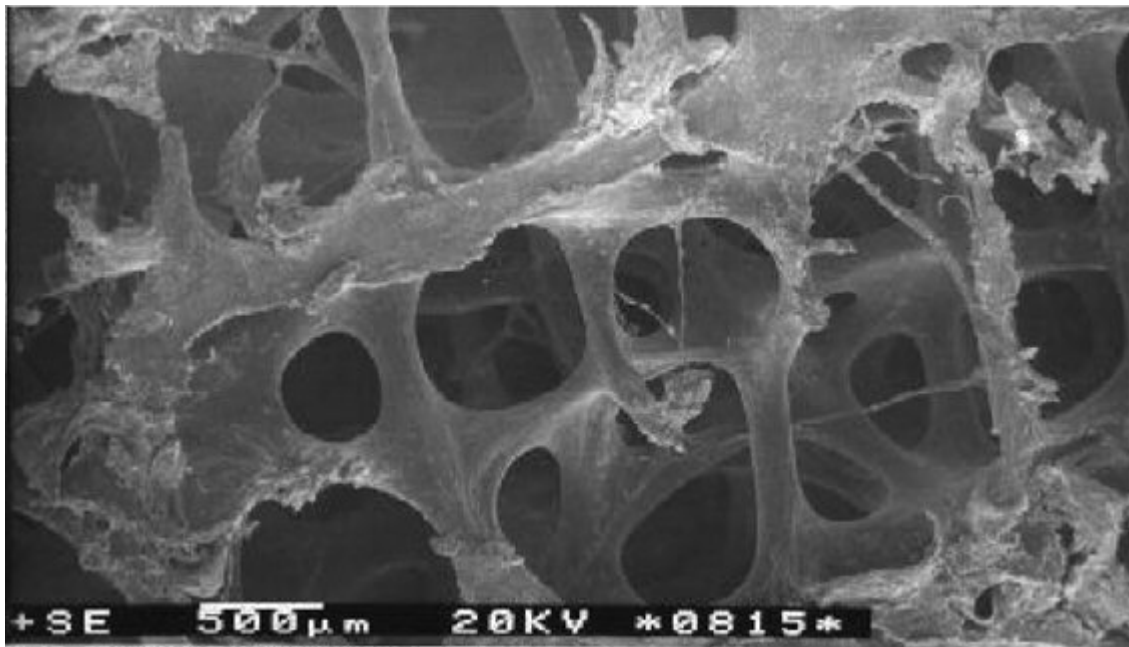


Figure 3: Anatomy of Trabecular Bone
http://www.feppd.org/ICB-Dent/campus/biomechanics_in_dentistry/ldv_data/mech/basic_bone.htm

The Knee

The first major part of the KTH complex is the knee, which consists of the patella bone and the femoral condyles, as shown below in Figure 4.

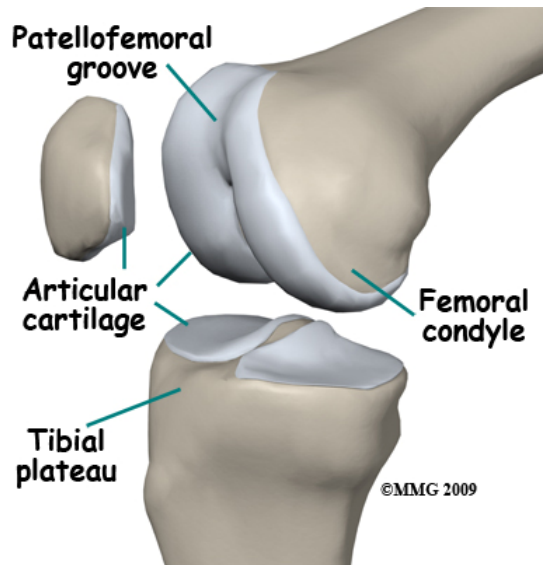


Figure 4: Knee Joint Anatomy
http://www.eorthopod.com/sites/default/files/images/knee_anatomy02a.jpg

The patella is more commonly known as the knee cap and serves to protect the front of the knee joint and increase the leverage of the quadriceps tendon. The patella is made up mostly of dense trabecular bone, with a thin layer of cortical bone on its outside. The quadriceps tendon is located on the anterior face of the patella, while the posterior surface consists of cartilage where the patella meets the femoral condyles (Grey, 1918).

The femoral condyles are part of the femur, and are located distal from the hip. They serve to transfer loads from the proximal femur to the tibia, and vice-versa. The condyles consist of a medial and lateral condyle, which are separated by the patellofemoral groove. The patellofemoral groove is the location where the patella meets the knee. The condyles consist of an outer layer or cortical bone, and an inner layer of trabecular bone. The trabecules in the condyles primarily arrange themselves in the longitudinal direction of the femur however, they begin to curve, following the general shape of the condyles, at the location where the condyles start to become wider than the mid-section of the femoral shaft. The trabecules terminate at the medial and lateral faces of the condyles. This leaves the patellofemoral groove to consist only of dense cortical bone, which is thicker than in the femoral shaft. It is believed that the increased thickness of the cortical bone is the result of additional loads applied to this

region from the anterior and posterior cruciate ligaments. Figure 5 shows the condyles, and the arrangement of trabecules in them (Grey, 1918).

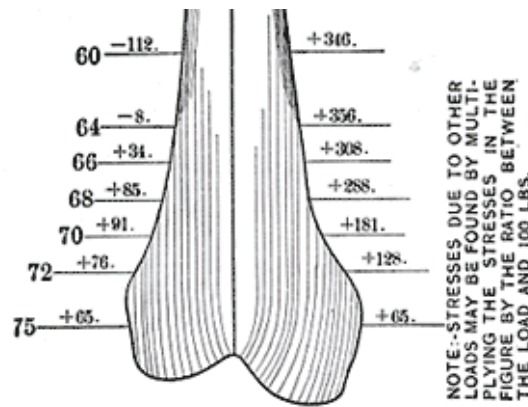
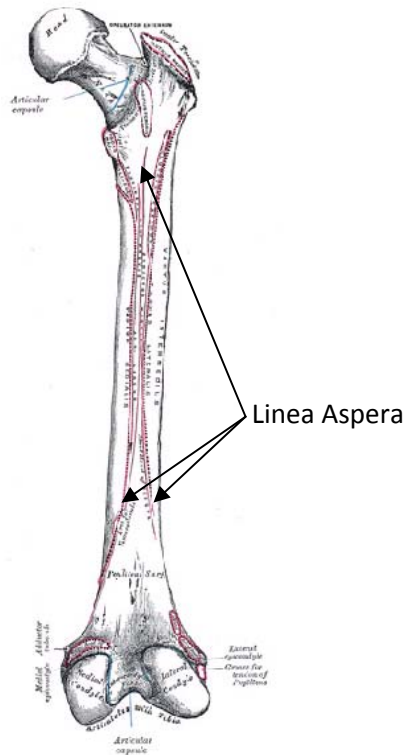


Figure 5: Femoral Condyles
Grey, 1918

The Thigh

The thigh is in the midsection of the KTH region and consists of the femoral shaft. The femur is the longest and strongest bone in the body. The shaft is slightly concave downwards and inwards. It is strengthened by a ridge that runs longitudinally down its midline, known as the linea aspera. The linea aspera runs from the lesser trochanter of the proximal femur to the condyles of the distal femur. Figure 6 shows the femoral shaft and the linea aspera (Grey, 1918).



**Figure 6: Femoral Shaft and Linear Aspera
Grey, 1918**

The femoral shaft experiences minimal shear effects. Based on Wolf's Law and basic shearing stress theory, it is expected that the femoral shaft has little material at its center. The hollow femoral shaft shows that there is little trabecular bone in this region, which is consistent with Wolf's Law. Bending moment is at a maximum in the proximal shaft, near the femoral neck, at sections 16-18 shown in Figure 7. As predicted by Wolf's Law and basic bending stress theory, the shaft is strongest at its extreme fibers, farthest away from the center. The strength comes from a thick layer of cortical bone and some trabecular bone near the outside of the femoral shaft. Figure 7 shows the distribution of trabecules along the femoral shaft (Grey, 1918).

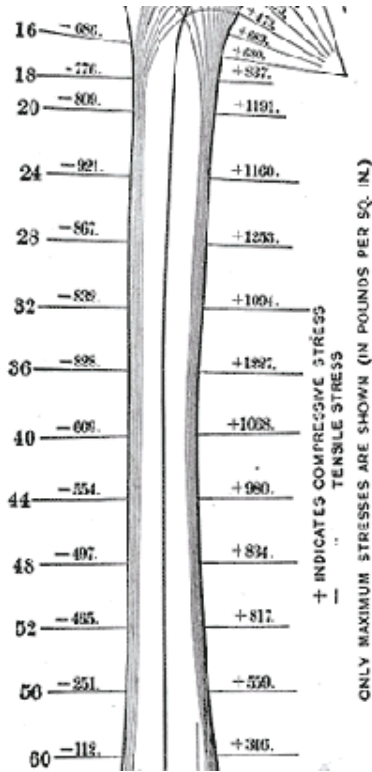
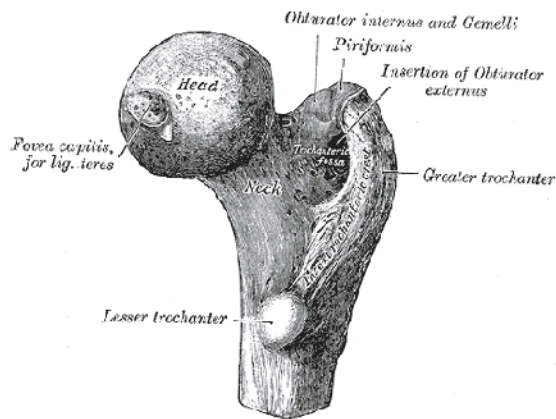


Figure 7: Arrangement of Trabecules in the Femoral Shaft
Grey, 1918

The Hip

The hip consists of the proximal femur and the pelvis. The proximal femur includes the femoral neck, head, and greater and lesser trochanter. The femoral head is somewhat spherical in shape and is covered with cartilage. It is directed upward, medialward, and posteriorward, and frames into the acetabulum of the pelvis. Below the head is the femoral neck, which connects the femoral head to the trochanter and the rest of the lower extremity. It creates a wide angle (approximately 125°) with the body, which faces medialward. The femoral neck meets both the greater and less trochanter, both of which provide leverage to the muscles that rotate the KTH region. The greater trochanter is an irregularly shaped, lateral projection of the femur. The lesser trochanter is conical in shape, and is where the linea aspera meets the proximal femur. Figure 8 shows the geometry of the proximal femur (Grey, 1918).



**Figure 8: Geometry of the Proximal Femur
Grey, 1918**

The trabecules of the proximal femur can be organized in two groups: compressive trabecules on the medial side and tensile trabecules on the lateral side. These groups intersect each other at right angles. The trabecular bone on the medial side is thicker than the bone on the lateral side, because compressive stresses are higher than the tensile stresses in the proximal femur. Closer to the femoral shaft, where shearing forces and bending moments are smaller, there is less trabecular bone. Figure 9 shows the orientation of trabecules in the proximal femur (Grey, 1918).

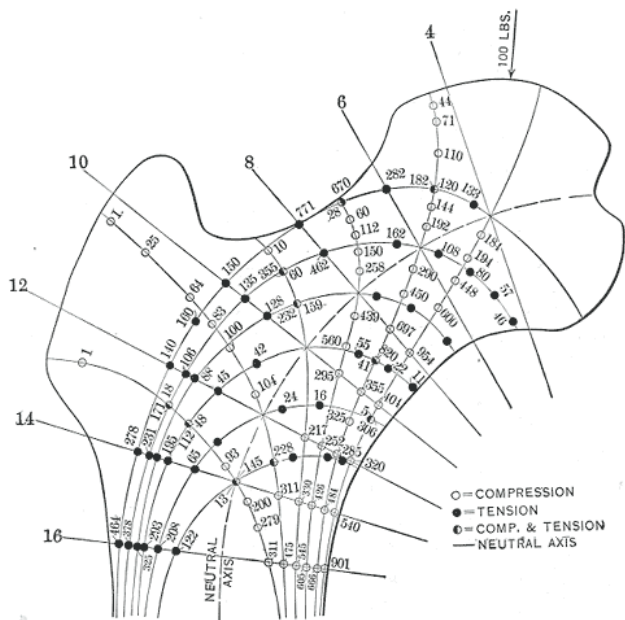


**Figure 9: Arrangement of Trabecules in the Proximal Femur
Grey, 1918**

The pelvis is an irregularly shaped bony ring that is centered about the spine and is supported by the lower extremities. It consists of the two hip bones on either side, the sacrum on the front and the coccyx in the back. The pelvis can be divided into two groups: the greater and lesser pelvis. The greater pelvis is the top part of the pelvis and contains the iliac wings. The greater pelvis is somewhat incomplete, creating space between the iliac wings. This space is filled by the abdomen. The lesser pelvis is the lower part of the pelvis. The lesser pelvis is more complete than the greater pelvis, and therefore has less space at its center (Grey, 1918). Figure 10 shows the greater and lesser pelvis.

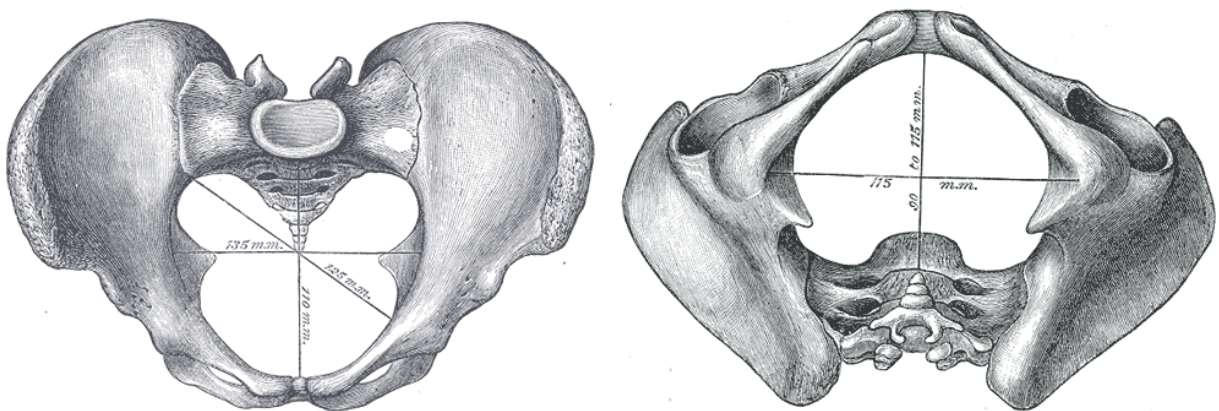


Figure 10: Greater Pelvis (left) and Lesser Pelvis (right)
Grey, 1918

Because the load paths through the pelvis are very complex, little is known about the arrangement of trabecules in this region. Trabecule arrangement in the pelvis is the topic of many current research studies, such as in Martinon-Torres (2003).

KTH Soft Tissues

The soft tissue of the KTH region (ligaments and muscles) is an important factor in the assessment of risk to injury during frontal vehicle crashes. The ligaments are susceptible to injury, such as tearing of the anterior or posterior cruciate ligaments. The muscles can stress the bones during contraction, and alter the injury mechanism based on the level of contraction (Silvestri, 2008). This section summarizes the basic anatomy of these features.

KTH Ligaments

Ligaments and tendons behave in a very similar way. The principle difference between the two is that ligaments connect two bones, while tendons connect a bone to a muscle. The structure of ligaments in the KTH region, and in all regions of the body, is hierarchical. The structure can be seen in Figure 11.

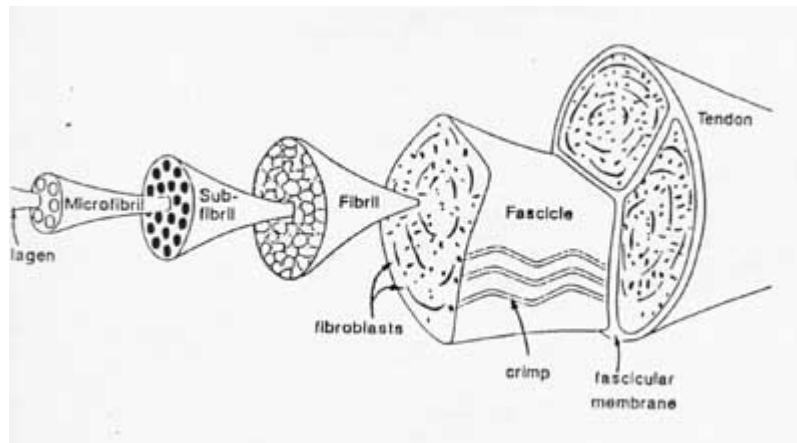


Figure 11: Ligament Hierarchy
<http://www.engin.umich.edu/class/bme456/ligten/ligten.htm>

The top of the hierarchy is the ligament or tendon itself. Ligaments are composed of several fascicles, which are composed of fibrils and fibroblasts. These are the biological cells that make up the ligament or tendon, and are the main contributors to the non-linear stress-strain curve associated with them. This is illustrated in Figure 12.

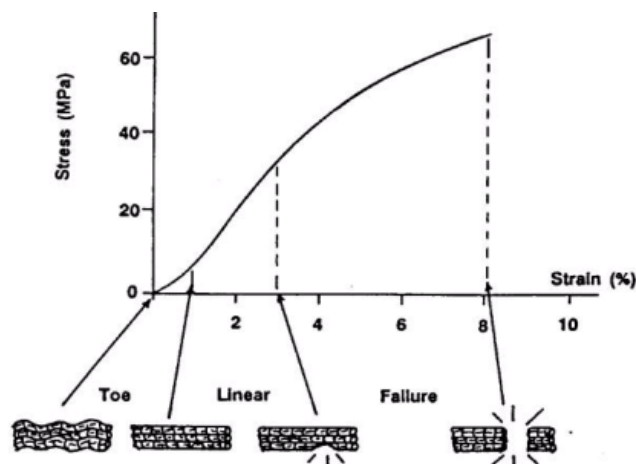
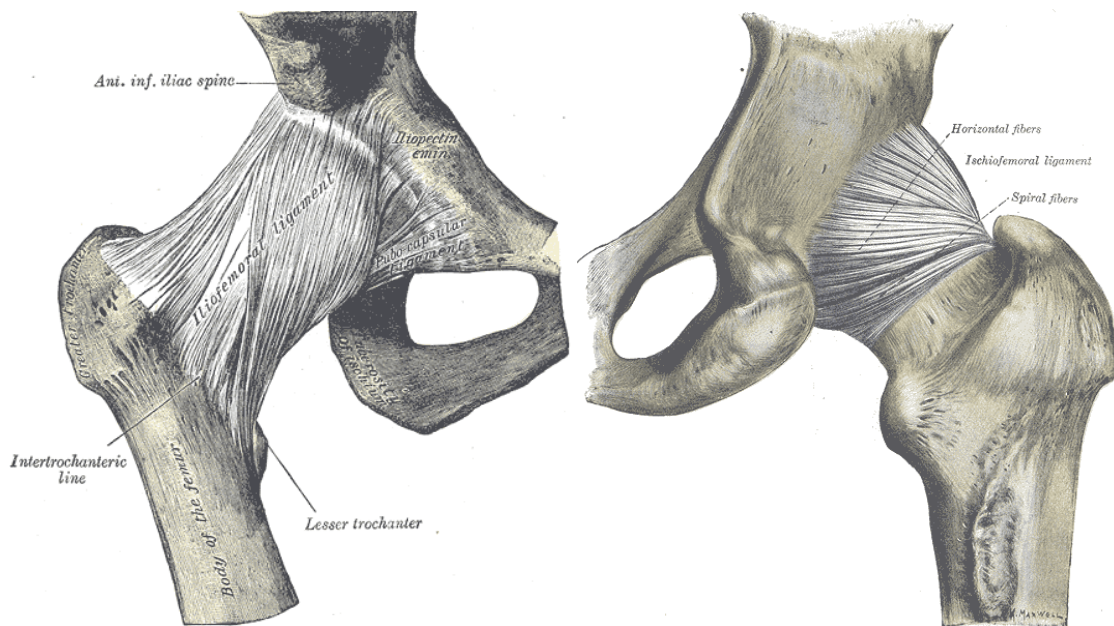


Figure 12: Non-Linear Stress Strain Curve of Ligaments
Biomedcentral.com

The stress strain curve is divided into three regions: the toe, the linear region, and the failure region. In the toe region, the ligaments and tendons are experiencing very small strains, as shown on the bottom of Figure 12. As a result, the fibroblasts are “wrinkled” and have very low stiffness. As the ligament or tendon is strained, and fibroblasts “flatten out,” their stiffness is increased. This phenomenon is reflected in the “linear” portion of Figure 12. Once the ligament or tendon has been loaded to its limit, it begins to fail and enters the “failure” region of the plot in Figure 12. The ligament or tendon completely fails once it has reached its ultimate strain, approximately eight percent for the one shown in Figure 12 (Ligament and Tendon Structure and Function, 2010).

There are three main ligaments and tendons in the KTH region: the ligaments at the hip, the knee, and the quadriceps tendon and patella ligament. The ligaments of the hip primarily consist of the iliofemoral and ischiofemoral ligaments. These ligaments connect the acetabulum of the pelvis to the femoral neck of the proximal femur. They are very strong and play a major role in allowing humans to walk upright without experiencing serious muscle fatigue (Grey, 1918). Figure 13 shows the ligaments of the hip.



**Figure 13: Iliofemoral Ligament (left) and Ischiofemoral Ligament (right)
Grey, 1918**

The ligaments of the knee consist of the anterior and posterior cruciate ligaments (ACL and PCL), and the medial and lateral collateral ligaments (MCL and LCL). The ACL and PCL are located in the middle of the knee, and are termed “cruciate” because they cross each other in an (X) shape. The ACL is connected to the top of the tibia and passes upward, lateralward, and backward, to the back of the lateral condyle of the femur. The PCL is stronger and shorter than the ACL. It is connected to the top of the tibia and passes upward, medialward, and forward to the front of the medial condyle. The MCL is a broad, flat band of ligaments located closer to the back of the knee joint than the front. It is connected to the medial side of the tibia, and passes backwards and upwards to the medial condyle. The LCL is a strong, round band of ligaments, which connects the lateral condyle of the tibia to the lateral side of the head of the fibula (Grey, 1918). Figure 14 shows the ligaments of the knee.

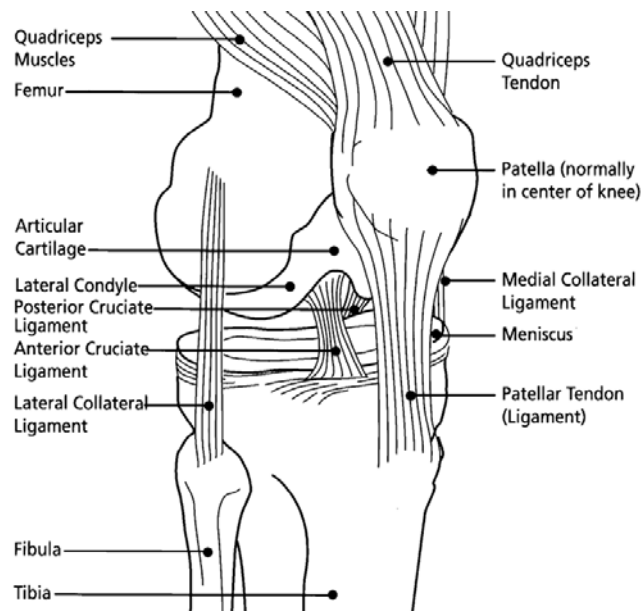


Figure 14: Ligaments of the Knee
http://en.wikipedia.org/wiki/File:Knee_diagram.svg

The final major tendons of the KTH region are the quadriceps tendon and the patella ligament (commonly known as the patellar tendon), and are shown in Figure 14. The quadriceps tendon connects the rectus femoris muscle to the patella, and the patella ligament connects the patella to the tibial tuberosity. The patella ligament is continuous with the quadriceps tendon over the patella, and extends

across the width of the patella. The patella ligament and quadriceps tendon are strong and fairly flat (Grey, 1918).

KTH Muscles

Muscles are fibrous entities that allow movement of different parts of the body. They connect bones, cartilage, ligaments, and skin either directly or through tendons (Grey, 1918). There are two popular mechanical models for muscles: Hill's model and Huxley's model. Hill's model reduces muscles to one-dimensional entities consisting of a spring-mass-damper system. Huxley's model follows a more fundamental approach, looking at muscles from a microscopic, biomechanical level. Both models have gone through considerable revision since they were first proposed (Silvestri, 2008). Because of its simplicity, the FE KTH utilizes Hill's model.

The muscles of the KTH can be divided into four categories: the anterior, posterior (sometimes called hamstring muscles) and medial thigh, and the gluteus. Figure 15 illustrates these groups.

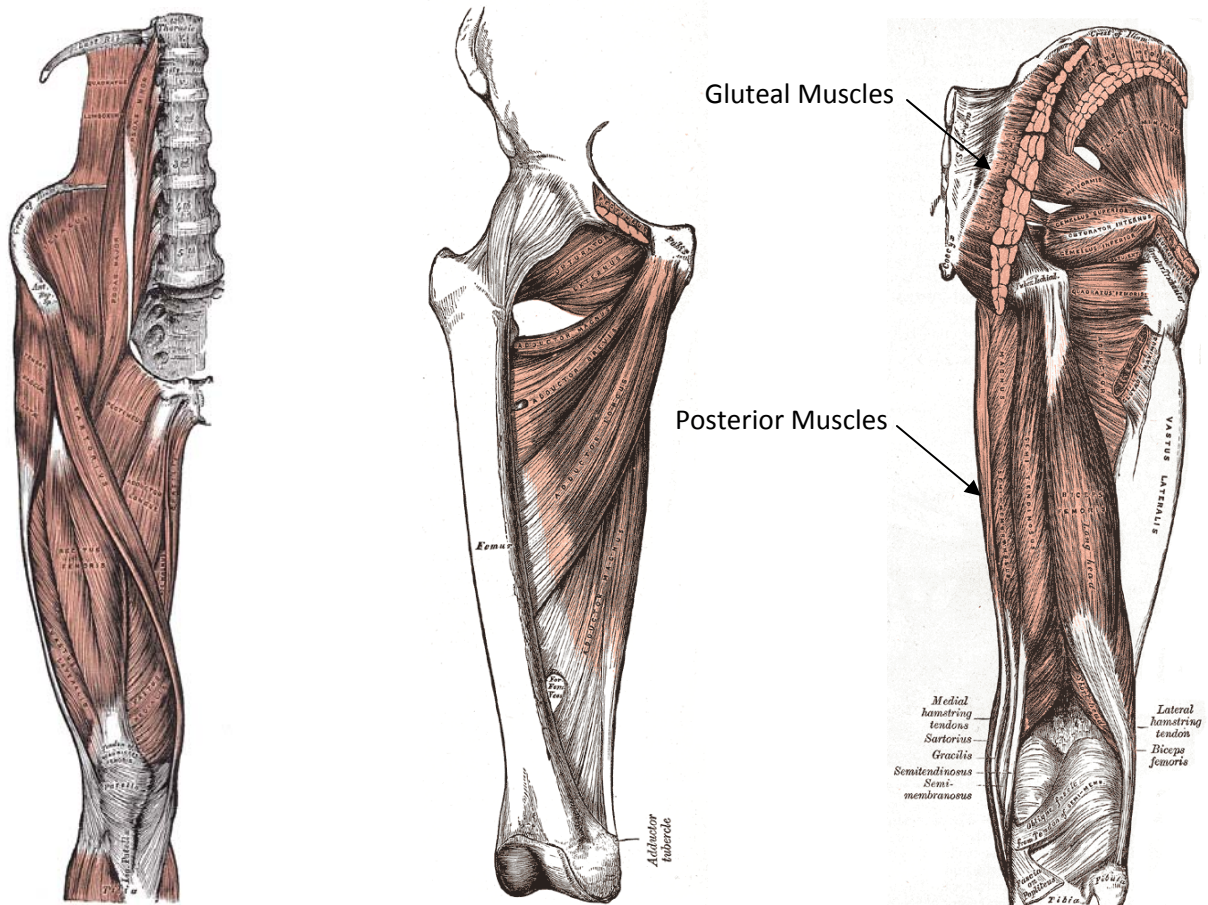


Figure 15: Anterior (left), Medial (center), and Posterior and Gluteal (left) Muscles
 Grey, 1918

Major muscles of each group include the quadriceps femoris and Sartorius of the anterior muscles, the adductor longus, adductor brevis, and adductor magnus of the medial muscles, the gluteus maximus, gluteus medius, and gluteus minimus of the gluteal muscles, and the biceps femoris and semitendinosus or the posterior muscles (Grey, 1918).

KTH Injuries and Injury Criteria

Kuppa (2003) examined the prevalence of KTH injuries in frontal crashes by analyzing crash and injury report data from vehicle crashes in the United States in the years 1993-2001. The results of the study relate a given level of risk of injury to a given injury severity using the Abbreviated Injury Scale

(AIS), a concept known as an injury criterion. The AIS system was first proposed in 1969, and is used to rate the severity of injury (Trauma.org, 2010). Table 1 summarizes the scoring system.

Table 1: AIS Summary
Trauma.org, 2010

AIS Score	Injury
1	Minor
2	Moderate
3	Serious
4	Severe
5	Critical
6	Unsurvivable

The results of Kuppa's study show that lower extremity injuries are the most frequently AIS 2+ injured region of the body in frontal crashes. Of all lower extremity injuries, 50% occur in the KTH region. Furthermore, risk of AIS 2+ injury for occupants restrained with seatbelts and airbags is comparatively higher than risk of injury to the upper body. Finally, the results show that of all KTH injuries considered in the study, injuries to the hip results in the highest impairment levels. The study concludes that increased use of seatbelts and wider availability of airbags has changed the injury profile for frontal crashes from predominately injuries to the head, neck, or thorax to increased lower extremity injuries. Kuppa recommends new efforts be made to mitigate risk of injury to the KTH (Kuppa, 2003).

To aid lower extremity injury studies, Kuppa (2001) published another article that proposes injury risk curves for parts of the lower extremity, which relate a measureable parameter in a physical test to a given risk of AIS injury. The parameters considered by Kuppa were based on the most influential factors affecting injury to a given region reported by other researchers. These parameters suggest that femur axial force magnitude has the largest influence on bone fracture in the KTH region, while relative tibia/femur displacement influences KTH ligament injury the most. The curves were developed by conducting regression analyses of cadaveric tests, considering the largest influences of injury given above and the resulting level of AIS injury experienced by the cadaver. Because of insufficient data, Kuppa was

not able to develop curves for ligament injuries. The curves for risk of AIS 2+ and AIS 3+ injury are given in Equation 1.

Equation 1: KTH Injury Risk Curves

$$p(AIS\ 2\ +) = \frac{1}{1 + e^{5.7949 - 0.5196F}} \quad p(AIS\ 3\ +) = \frac{1}{1 + e^{4.9795 - 0.326F}}$$

Where (F) denotes femur axial force (Kuppa, 2001).

Rupp (2003) conducted additional research on injury to the KTH complex. In a previous study, Rupp analyzed crash data and found that hip injuries tended to occur on the side (left or right hip) that corresponded to the lateral direction the occupant moved during the crash (2002). Based on this finding, Rupp et. al. hypothesized that this trend was due to occupant hip flexion or adduction. The researchers proposed that when the KTH region is in flexion or adduction, the contact area between the femoral head and acetabular cup is decreased, which decreased injury tolerance.

To study the effect of flexion and adduction on KTH injuries, Rupp et. al. conducted tests on 35 different KTH specimens. Twenty five of these tests were carried out on specimens in a neutral posture, four tests were carried out on specimens in 30° flexion, and six tests were carried out on specimens in 10° adduction. In the tests, the pelvis was fixed to a mounting device, the KTH region was placed in the desired position (neutral, flexion or adduction) and the knee was impacted with a blunt deformable interface. The researchers found that all fractures occurred to the hip or to the pelvis, not to the knee or to parts of the femur far from the hip. They also found that specimens in flexion experienced fracture at a load of 4.1 kN, a 34% decrease from the 6.1 kN load required to cause fracture in the specimens in the neutral position. They found that specimens in adduction experienced fracture at a femur load 5 kN, an 18% decrease. The researchers did not study the effects of hip abduction, but they suggest that it would increase the fracture load by increasing the surface area between the femoral cap and acetabular cup (Rupp, 2003).

In the paper *Effects of Anterior-Posterior Constraint on Injury Patterns in the Human Knee During Tibial-Femoral Joint Loading from Axial Forces Through the Tibia* by Jayaraman et. al, (2001)

the amount of anterior-posterior (AP) constraint provided to a knee was shown to affect the injury mechanism and associated load required to cause injury. Jayaraman et. al. theorized that because of the sloped interface between the tibia and femur (shown in Figure 16) the tibia translates anteriorly relative to the femur during compressive loading.

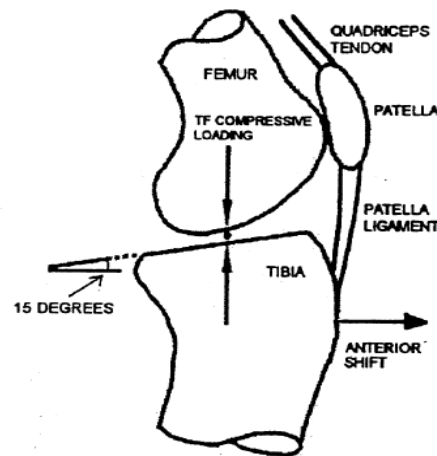


Figure 16: AP Motion of the Tibia and Femur During Compressive Loading
Jayaraman, Vijay M., Eric T. Sevensma, Masaya Kitagawa, and Roger C. Haut. "Effects of Anterior-Posterior Constraint on Injury Patterns in the Human Knee During Tibial-Femoral Joint Loading from Axial Forces through the Tibia." *Stapp Car Crash Journal* 45 (2001): 449-68.

To study this phenomenon, Jayaraman et. al. developed a testing device in which the tibiofemoral joint and sections of the tibia and femur were placed, and then impacted the tibia with a compressive load. The load through the tibia and femur was able to be measured, as were relevant displacements. The researchers carried out tests on six pairs of joints. For each pair of joints, the joint from one leg was tested with AP motion of the tibia relative to the femur constrained, and one joint was tested with AP motion unconstrained. The joint was loaded repeatedly to failure, with each successive load being greater than the previous one.

The researchers found that in the unconstrained tests, failure occurred at a femur load 5.8 kN and the primary failure mode was rupture of the anterior cruciate ligament (ACL). A displacement between the tibia and femur of 18 mm was recorded. In the constrained tests, failure occurred at a femur load of 9.2 kN and the primary failure mode was fracture of the femoral condyles. This shows that the amount of

load that can be carried by the knee joint without causing injury can be increased by providing adequate AP constraint. Jayaraman et. al. suggest that in an actual crash event, this constraint could be provided by the knee bolster.

The paper *The Effect of Axial Load in the Tibia on the Response of the 90° Flexed Knee to Blunt Impacts with a Deformable Interface* by Meyer et. al. (2004) presents the results of a study similar to the one conducted by Jayaraman. In this study, the researchers theorized that impacting the knee with a blunt interface causes posterior translation of the tibia relative to the femur. They hypothesized that introducing an axial force through the tibia during the knee impact would counter the posterior translation by causing anterior translation, as described in the Jayaraman study.

In this study by Meyer et. al., tests were conducted on 10 knee joints. In the tests, specimens consisting of the tibia and femur were placed in the testing device. The knee joint was impacted with a blunt interface. For each pair of knee joints, one joint was impacted uniaxially (with only the blunt interface to the knee) and one joint was impacted biaxially, with an impact occurring with both the blunt interface at the knee and an axial load through the tibia. Meyer et. al. found that in joints with the axial load through the tibia, AP translation between the tibia and femur was reduced, and the load required to cause injury was increased.

In both the Jayaraman and the Meyer studies, the tibia was loaded with an axial force, and the relative AP displacements of the tibia and femur were studied. In the Jayaraman study, the femur was constrained by physically fixing the femur, thereby preventing movement. One can think of the Meyer study as doing the same thing; however, in the Meyer study, the AP constraint was provided by the impact by the blunt interface to the knee.

Mathematical Modeling in Injury Prediction

Traditionally, biomechanical studies related to motor vehicle accidents have consisted of physical tests on cadaveric test subjects. A limited supply of cadaveric specimens prohibits researchers from studying a wide range of impact scenarios. This is because of the destructive nature of the tests. This

means that once a cadaver is used in an experiment to study fracture, it cannot be used in another experiment. In addition, cadavers exhibit a wide range of responses to the same impact scenario. Therefore, even if an unlimited supply of cadavers were available, it would be difficult to determine if differences in injury mechanism were due to changes in the impact scenario or a result of cadaveric variability (Rupp, 2003 and Meyer, 2001).

Improvements to computer simulation technology have allowed researchers to develop detailed analytical models that can be used to study injury. Advantages of using analytical models are that many impact scenarios can be explored at very low cost, and that they have no variability over the same impact scenario. Several models of the lower extremity have been developed to date. Two models are presented in this section: a model developed by Lawrence Livermore National Laboratories (LLNL) and a model proposed by Silvestri. The LLNL model was the basis for the Silvestri model, and is referred to as the LLNL model. The Silvestri model was used in this project, and is referred to as the KTH model.

LLNL Model

The LLNL model was developed in 1997, and depicts the geometry of a 50th percentile male. It provides a fairly biofidelic representation of the skeletal structure of the lower extremity, including the foot, tibia, fibula, femur, and pelvis. A few ligaments are provided to the knee joint to improve stability. Silvestri (2008) summarized the basic characteristics of the LLNL model as the following:

- The model contains 14,126 elements and 18,800 nodes. It experiences hourglassing problems for some impact scenarios.
- The bones are modeled with a solid cross-section (no differentiation is made between cortical and trabecular bone). The material properties are isotropic with a bilinear stress-strain curve.
- The inertial effects of the flesh were represented by discrete mass elements attached to the bones at select locations.

The LLNL model was developed for use with LLNL DYNA 3D, the predecessor of LS-DYNA (Perfect, 1997). Figure 17 shows the LLNL model.



Figure 17: LLNL Model
Perfect, 1997

KTH Model

Silvestri made several changes to the LLNL model. These included re-meshing the skeletal structure to allow for a more accurate geometric representation (in terms of bone shape and differentiating between cortical and trabecular bone), providing accurate anisotropic bone material properties based on published literature, providing representation of all major muscles and ligaments with discrete spring elements and appropriate material properties, and providing representation of flesh at the thighs, buttocks, and torso with solid elements (2008 and 2010). Figure 18 shows Silvestri's KTH model.

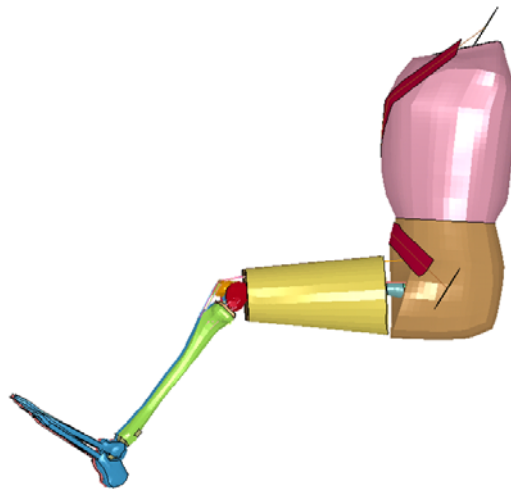


Figure 18: KTH Model
Silvestri, 2010

The KTH model was validated against physical tests at the component and full scale level. Component validations included the femoral condyles, femoral shaft, pelvis bones, and the ligaments. The bone validation simulations were compared to tests conducted by Rupp at the University of Michigan

Transportation Research Institute (UMTRI) (2002). The simulations involved fixing part of the bone in the same manner as was done in the physical tests, then impacting the knee with a deformable interface. The reaction forces at the fixed point and the resulting injury mechanisms were compared to the physical test. In all simulations, the model performed acceptably well compared to the physical test. Figure 19 shows the force time history for the femoral shaft.

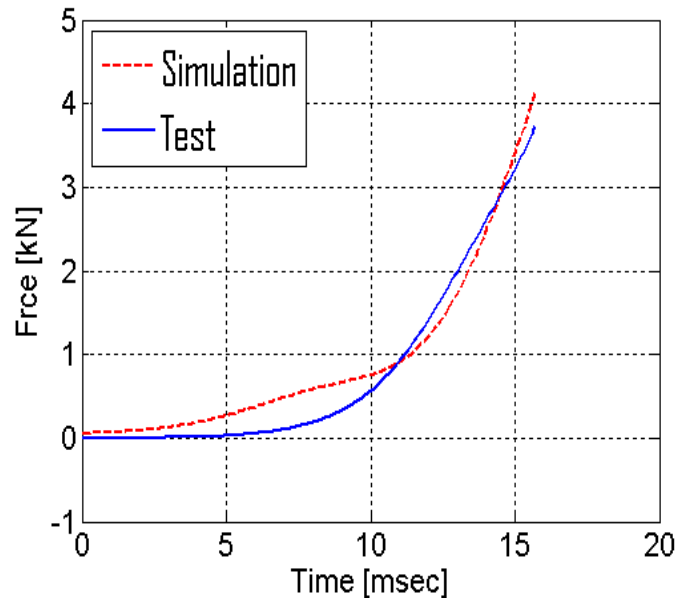


Figure 19: Femoral Shaft Validation Force Time History
Silvestri, 2008

The ligaments were validated against physical tests conducted by Viano (1978). In Viano's tests, the tibial and femoral shafts were cut at their midpoint. The femoral shaft was fixed, and a dynamic posterior displacement was applied to the tibial shaft. The results showed that partial failure occurred at a displacement of 14.4 mm and complete failure occurred at 22.6 mm. Silvestri replicated Viano's test in a FE simulation with the same test set-up. The FE results showed partial failure at a displacement of 14.24 mm and complete failure at 22.94 mm (Silvestri, 2008). Failure was defined by the discrete spring elements representing the ligaments detaching from the bones at their insertion site. This represents an avulsion failure. Figure 20 shows the FE simulation.

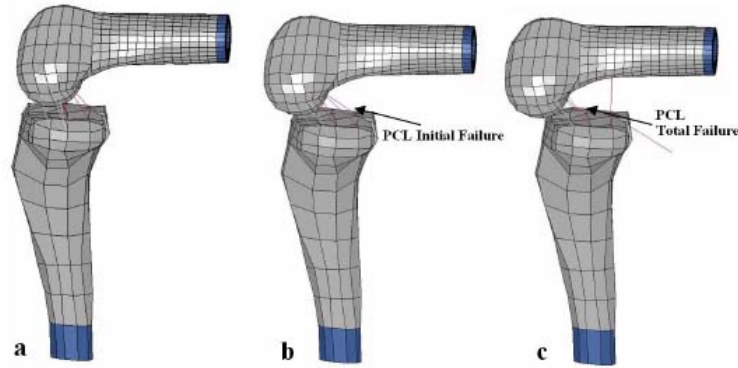


Figure 20: Silvestri's Ligament Validation Simulation
 Silvestri, 2009

The KTH model was validated at the full scale level against a full scale sled test conducted by Rupp at UMTRI (2002). The KTH validation simulation contained all components of the model, including bones, muscles, ligaments, and flesh. In both the physical test and the simulation, the cadaver and FE model respectively were positioned to a typical driving position and restrained with a three-point seatbelt. They were then accelerated into a piece of foam meant to represent the knee bolster in a vehicle. The KTH model was validated by comparing the femur axial force time history predicted by the FE model to the force measured in the physical test. Also, the resulting injury mechanisms were compared. Fracture in the FE KTH was based on element von Mises stresses. Figure 21 shows the initial position of the physical test and FE simulation, and Figure 22 shows that there was good agreement between the FE model and the physical test (Silvestri, 2010).



Figure 21: Initial Sled Test Position in Physical Test (left) and FE Simulation (right)
 Rupp 2002 and Silvestri 2010

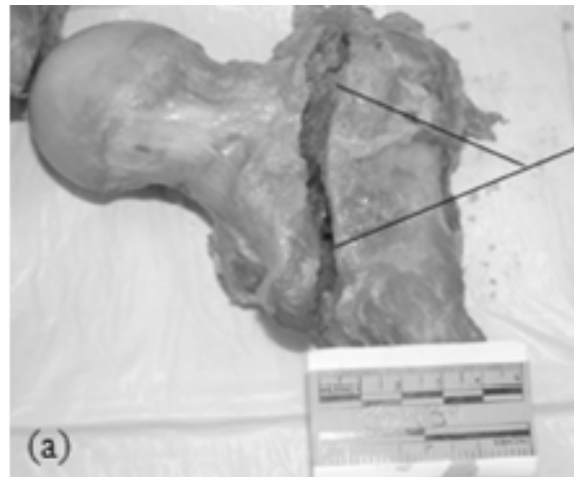
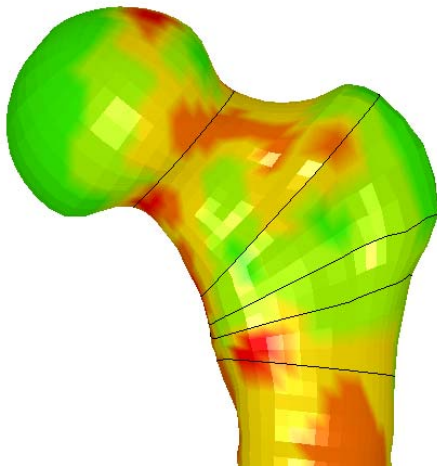
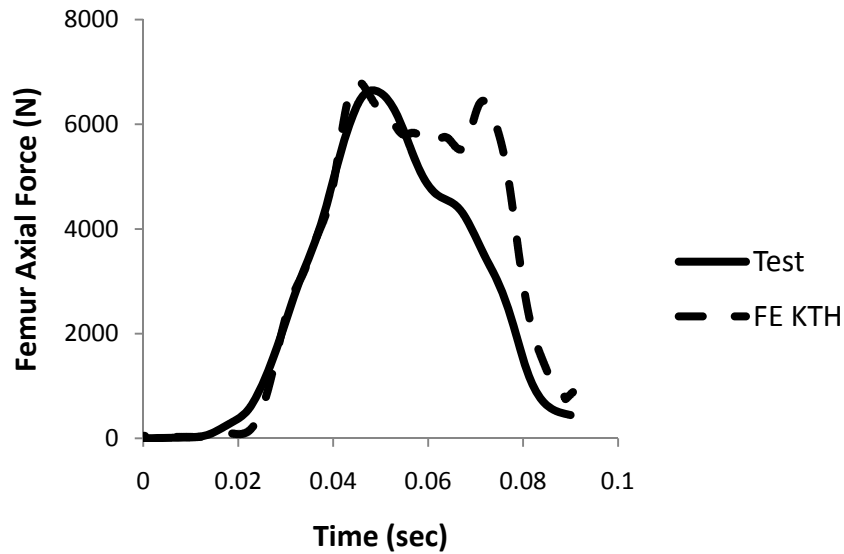


Figure 22: Femur Axial Force Time Histories (top), Location of Initial Fracture in FE KTH based on von Mises Stresses (bottom left), Fracture Location in Physical test (bottom right) in Full Scale Validation Silvestri, 2010 and Rupp, 2002

Remarks

This chapter has presented the background research conducted to complete this project. First, a description of the KTH region was presented, with an emphasis on biomechanics. Next, an overview of KTH injuries in frontal crashes was presented, as was the concept of injury criteria and AIS injury. Finally, the use of mathematical models in studying injury was presented, and the model used in this report was introduced.

It is clear that Silvestri has conducted a detailed study of the injury mechanisms of the KTH region with the FE KTH model. However, the work exclusively dealt with tests carried out in a

laboratory setting. Because of differences between vehicle occupant compartments and laboratory test setups, this project hypothesizes that there may be differences in occupant kinematics in an actual vehicle collision and in an experimental test. Also, the results of the Rupp study suggest that initial hip posture affects injury susceptibility. In light of this, the project proposes the following two research questions to help researchers gain insight into occupant response to an actual vehicle collision.

1. How does an occupant's pre-crash hip posture affect injury susceptibility and the resulting injury mechanism? Are there other parameters that affect injury?
2. How does the FE KTH response in the full scale sled test differ from its response to an impact in a FE vehicle model?

These questions were answered by simulating the FE KTH as an occupant in an FE vehicle model. The following chapters present the methodology followed to answer the questions, and the findings of the study.

Methods

This chapter presents the basic approach followed to answer the research questions proposed at the end of the background chapter. The major research activities are presented, and the major steps in completing each activity are described.

Effect of Pre-Crash Hip Posture on Injury Susceptibility

To assess the effect of pre-crash hip posture on injury susceptibility, 25 simulations were run with the FE KTH being an occupant in a reduced FE Ford Taurus. In each of the 25 simulations, the FE KTH was positioned with a different hip posture at the start of the simulation. Table 2 shows the test matrix considered for this part of the project. It shows the range of hip postures considered, and the order in which the simulations were run.

Table 2: Hip Posture Test Matrix

		Flexion °				
		0	7.5	15	22.5	30
Adduction °	-10	3	14	9	15	6
	-5	5	22	20	23	18
	0	1	11	4	12	2
	5	17	24	21	25	19
	10	7	13	10	16	8

***Note: (-) Adduction implies Abduction**

As show in Table 2, a range of (-10°) to (10°) adduction was considered and a range of (0°) to (30°) flexion was considered. The numbers in each cell denote the order in which the simulation was run, e.g. 0° adduction and flexion was run first, 0° adduction and 30° flexion run second etc. The order was selected to ensure that simulations most likely to affect the overall trend of the results were run first. This helped avoid potential problems in the final project results caused by errors in the results of individual simulations.

The injury tolerance (femur axial force required to initiate fracture) and corresponding mechanism were noted for each simulation shown in Table 2. These results were plotted as a function of hip posture angle to determine the minimum injury tolerance over a range of typical driving postures.

Comparison of Occupant Response in Sled Test and Vehicle Collision

To assess differences in occupant response in the sled test compared to an actual vehicle collision, the sled test simulation used by Silvestri (2010) was studied. Occupant kinematics, knee and foot contact forces, and relevant forces through the femur were noted in Silvestri's simulations.

Also, the FE KTH was simulated as an occupant in a FE Ford Taurus developed by the National Crash Analysis Center (NCAC) (Finite Element Model Archive, 2009). Because the FE Ford Taurus model had many nodes and elements, simulations involving the FE Taurus and FE KTH were very computationally demanding. To decrease computation times, the full FE Taurus model was "reduced" to only include parts of the vehicle required to simulate the frontal impact. These included the seat, steering wheel, floor, and instrument panel. Figure 23 shows the FE KTH inside the reduced FE Taurus.

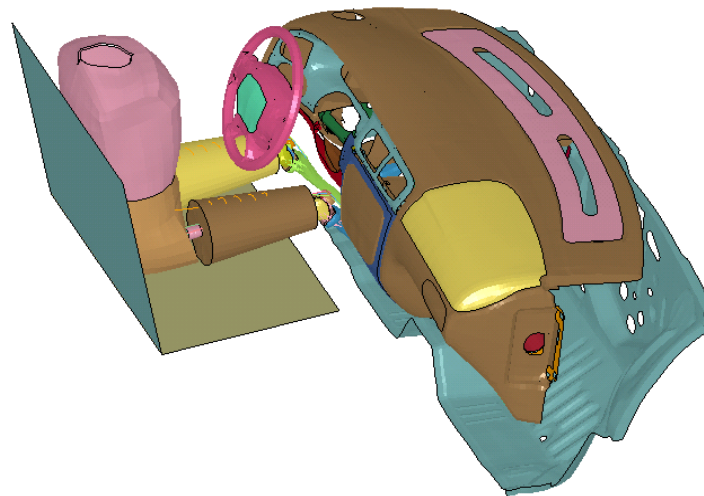


Figure 23: FE KTH Inside Reduced FE Taurus

Similar parameters were recorded in the reduced vehicle simulations as were recorded in the sled test simulations. The parameters from each simulation were then compared, and the possible implications of differences in the simulations were considered.

Summary of Research Activities

The following list summarizes the activities undertaken to complete this project.

1. Develop and validate reduced Ford Taurus vehicle model from NCAC model,
2. Simulate FE KTH over a range of pre-crash hip postures,
 - a. Note differences in injury tolerance and mechanism
3. Study FE KTH sled test simulations conducted by Silvestri; note important characteristics and
4. Compare the results of (2) and (3).

These activities were intended to help answer the research questions proposed at the end of the Background chapter. The results of the activities are presented in the following chapter.

Results

This chapter presents the results of the study. First, the results of the vehicle/occupant simulations are compared to physical tests. Next, the results of the parametric study of the effect of pre-crash hip posture on injury tolerance are presented. Finally, a comparison is made between the FE KTH response to impact in the sled test and the vehicle simulations.

Validation of Vehicle Occupant Simulations

The first step in completing this project was ensuring that the occupant and vehicle interacted properly during the frontal impact. Gabauer and Thomson (2005) presented the results of several full scale physical crash tests in which a Hybrid III anthropomorphic test dummy (ATD) was placed in a vehicle, restrained with only an airbag, and the vehicle was subject to a frontal impact at 30 mph. The research showed that the ATD's femur axial force ranged from 4.5 kN to 7.5 kN. Bedewi and Digges (1999) showed that maximum femur axial forces in 12 different 35 mph frontal crashes ranged from two to eight kN. The objective of this part of the study, therefore, was to observe a maximum femur axial force within the range observed in physical tests.

To validate the vehicle-occupant simulations, this project obtained a detailed FE model of a 2001 Ford Taurus developed by the National Crash Analysis Center (NCAC). Validation material for this model can be found on the NCAC website (Finite Element Model Archive, 2009). Figure 24 shows this model.

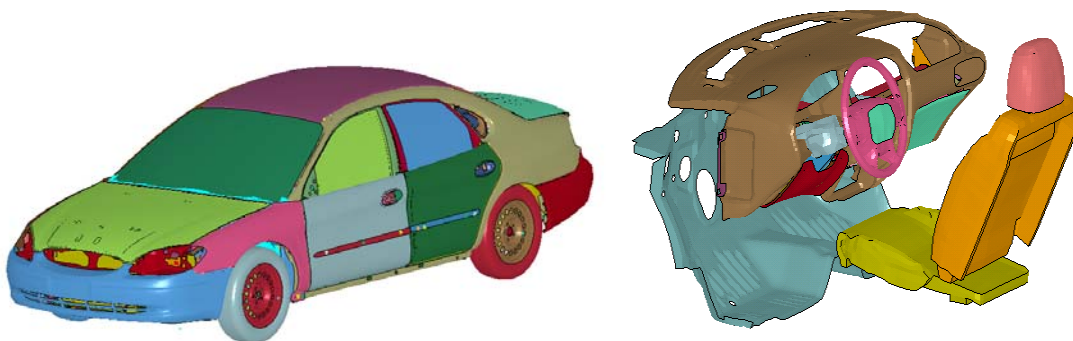


Figure 24: 2001 Ford Taurus Model, Exterior (left) and Occupant Compartment (right)

Next, a FE Hybrid III crash dummy developed by LSTC was obtained. The documentation validating the FE Hybrid can be found in Guha, Bhalsod, and Krebs (2008). Figure 25 shows the FE Hybrid.



Figure 25: FE Hybrid

The FE Hybrid was placed in the driver's seat of the FE Taurus and positioned in a typical driving posture. This was done by consulting a test report for the New Car Assessment Program (NCAP). In the NCAP test referenced in this project, a standard Hybrid III crash test dummy was placed in the driver's seat of a 2000 Ford Taurus, and positioned in a typical driving position. The report specifies the geometry of the driver compartment and Hybrid dummy. The FE Hybrid was positioned in manner to match the NCAP specifications as closely as possible. This involved ensuring that the vertical and horizontal distances of the FE Hybrid knee to the knee bolster were correct, the amount of knee flexion was correct and the pelvic angle was correct, etc (NCAP, 2003). All nodes in the model were given an initial velocity of 30 mph, and a rigid wall was defined one millimeter away from the front of the vehicle to simulate the frontal impact. Figure 26 shows the initial simulation setup, and the response of the FE Hybrid at the time of maximum femur axial force.

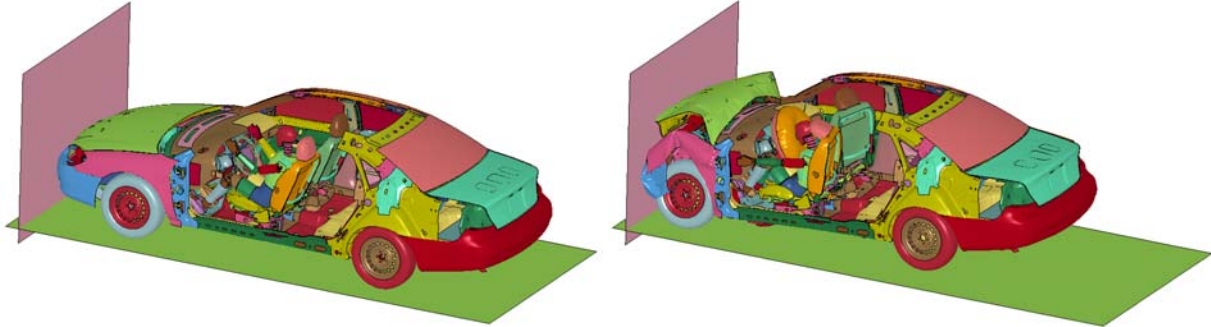


Figure 26: Initial FE Hybrid Position (left) and FE Hybrid Position at Time of Maximum Femur Axial Force

The maximum axial forces in the left and right femurs were 5.63 kN and 4.92 kN respectively, which falls within the bounds described above. The occupant-vehicle simulations with the FE Hybrid were therefore considered validated with respect to reproducing a femur force in the observed test range.

The FE KTH was simulated in the FE Taurus in a similar manner as described above however, these simulations were extremely computationally demanding, requiring approximately 16 days of computation time. To decrease the required computation time, the FE Taurus was reduced to only include the parts needed to simulate occupant response to frontal impact. These parts included the seat, floor, dashboard, and steering wheel. Figure 27 shows the reduced FE Taurus model.

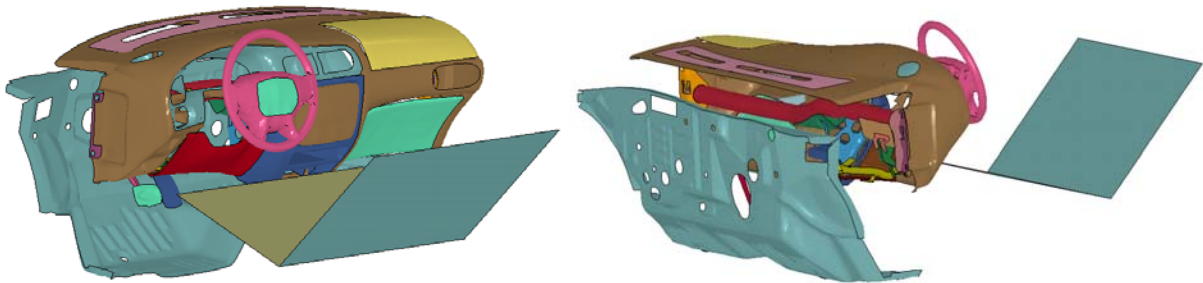


Figure 27: Reduced FE Taurus, Front View (left) and Back View (right)

To simulate the frontal impact event using the reduced FE Taurus, the following procedure was followed.

1. Simulate the full FE Taurus impacting a rigid wall at 30 mph.
2. Record the nodal displacement time histories at the steering column and driver's side B-pillar during the impact event in (1). These parts of the vehicle experienced little to no deformation during the impact.

3. Apply the B-pillar and steering column nodal displacement time histories from (2) as displacement boundary conditions to the seat and steering wheel respectively in the reduced FE Taurus.
4. Merge some of the nodes on the exterior of the dashboard and floor (left and rightmost portions when viewing the left side of Figure 27) to have coupled motion with the steering wheel.
5. Position the FE occupant model on the driver's seat in the reduced model.
6. Apply an initial velocity of 30 mph to all nodes of the reduced Taurus model and the occupant model.

The reduced FE Taurus model was validated by placing the FE Hybrid on the driver's seat and recording the maximum femur axial force. Figure 28 shows the FE Hybrid's initial position and position at the time of maximum femur axial force in the reduced FE Taurus simulations. It should be noted that in the reduced FE Taurus simulations, no airbag restraint was included because no restraint was to be included when the FE KTH was simulated as the occupant. This was because this project aimed to study the worst case impact scenario, which corresponds to a completely unrestrained occupant.

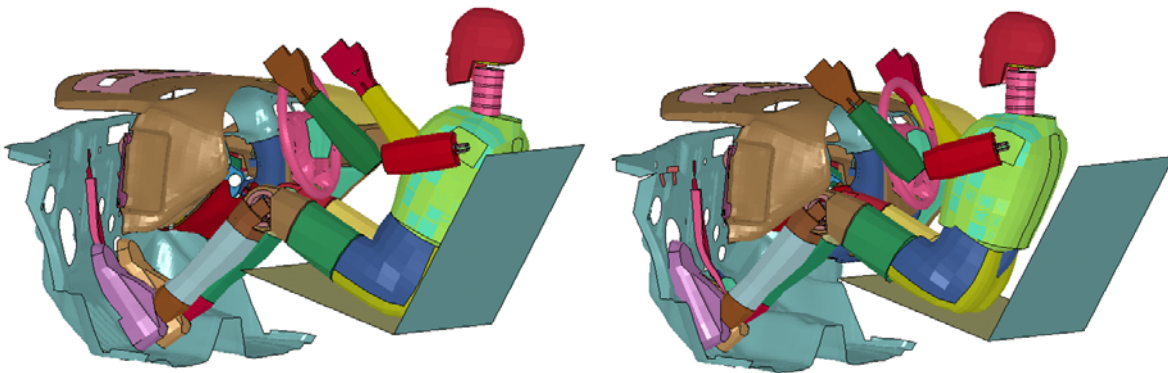


Figure 28: FE Hybrid in Reduced FE Taurus Model, Initial Position (left) and Position at Time of Maximum Femur Force (right)

The FE Hybrid experienced a maximum femur force of 6.72 kN on the left leg and 6.27 kN on the right leg. These values are reasonably close the values obtained in the full FE Taurus model, and are within the range observed in physical tests described above. Therefore, the reduced FE Taurus model was considered validated.

The FE KTH was simulated in the reduced FE Taurus in the same way as the FE Hybrid. Figure 29 shows the FE KTH in the reduced FE Taurus.

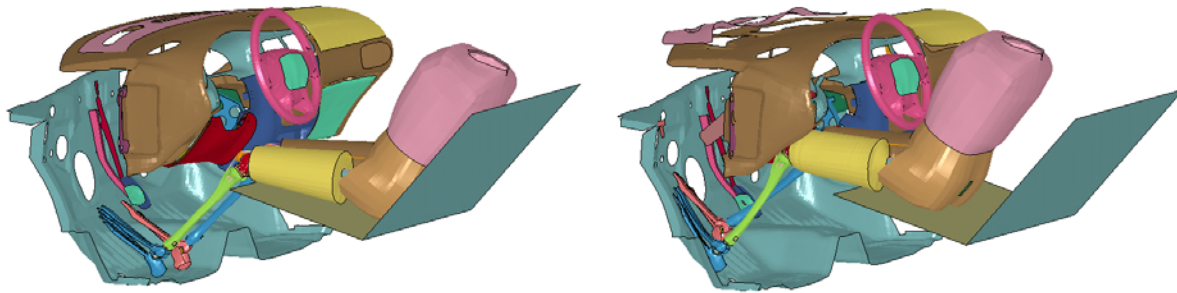


Figure 29: FE KTH in the Reduced FE Taurus, Initial Position (left) and Position at Maximum Axial Femur Force (right)

In all of the simulations involving the FE KTH and reduced FE Taurus, the left maximum femur forces ranged from 3.86 kN to 10.7 kN while the right maximum femur forces ranged from 4.00 kN to 11.6 kN. Although these femur forces are slightly outside the range observed in physical tests, the physical tests measured the response of an ATD, while the FE KTH represents an actual human's response. The differences in response may be attributed to differences in geometry and material properties in an ATD compared to an actual human. Also, the range of hip postures considered in the FE KTH simulations may be outside the range that ATDs are positioned to in physical tests. As shown later in this chapter, femur axial force varies with hip posture.

The FE KTH was treated as rigid during the first 50 milliseconds of the simulation to decrease the required computation time. After this time, it was switched back to deformable, with the same material modeling proposed by Silvestri (2010). This was a valid simulation strategy because the FE KTH did not impact the knee bolster, or contact the floor with substantial force, until after it was switched back to deformable. The implementation of the deformable-rigid switch and the development of the reduced Taurus model allowed for a 95% reduction of computation time, from 16 days to 18 hours.

Hip Posture Parametric Study

This parametric study involved simulating the FE KTH as a vehicle occupant in 25 different pre-crash hip postures. The results of the parametric study are broken into two categories: model setup and simulation results.

Model Setup

The first step in setting up the models for the parametric study was to position the FE KTH to the various hip postures described in the Methodology chapter. The hip postures considered involved different combinations and degrees of adduction and flexion. The definition of adduction and flexion angle used in this study was the same as was used by Rupp (2003), and are as follows:

Adduction Angle: When looking at the lower extremity from a top view, a line connecting the center of the femoral condyles to the center of the hip joint being perpendicular to a line connecting the two hip joints corresponds to a zero degree adduction posture. If this angle is less than 90° , the hip is considered to be adducted, if the angle is greater than 90° , the hip is considered to be abducted.

Flexion Angle: When looking at the lower extremity from a side view, an angle of 120° between a line drawn along the longitudinal axis of the femur and a line connecting the anterior-superior iliac spine and the pubic symphysis corresponds to a zero degree flexion posture. If this angle is less than 120° , the hip is considered flexed.

Figure 30 demonstrates how the FE KTH was positioned to a neutral, 10° abduction, and 30° flexion hip posture.

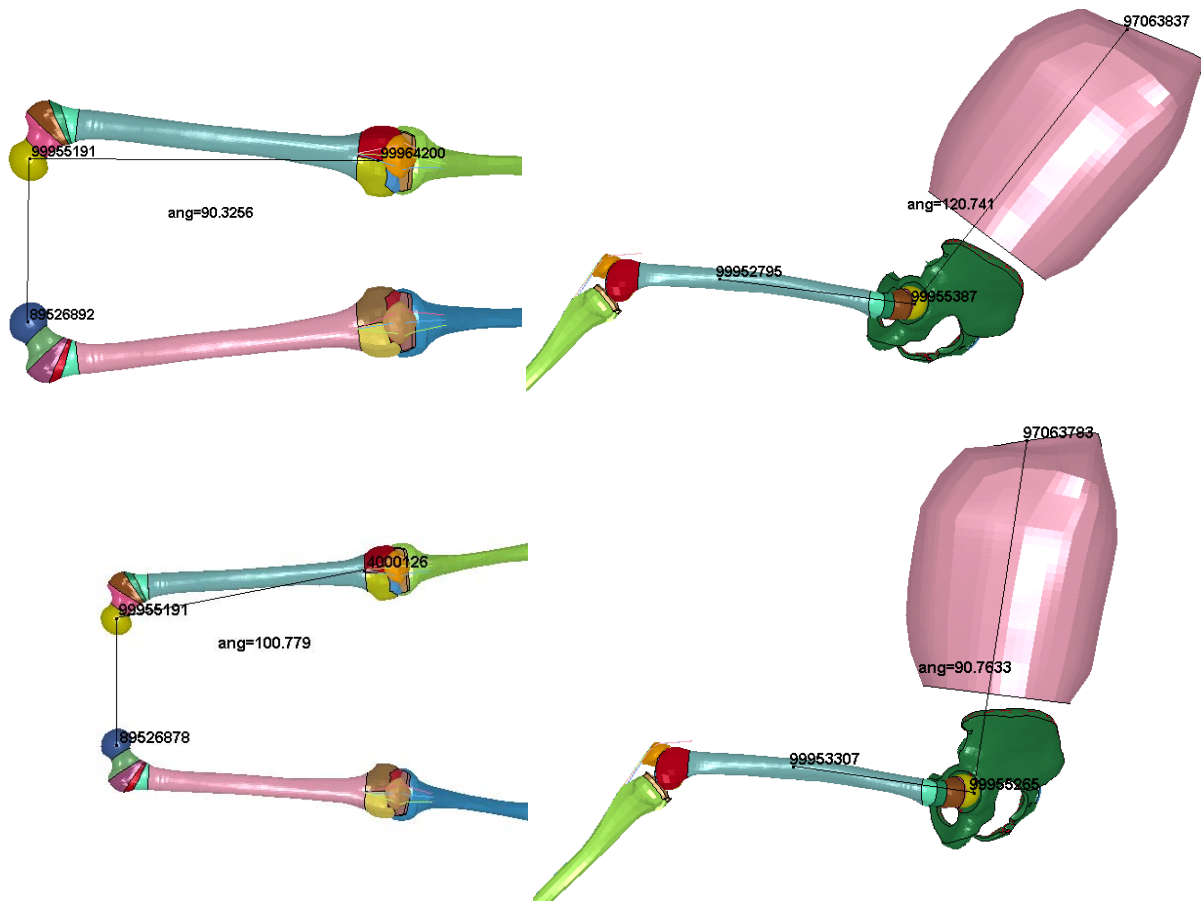


Figure 30: Examples of Pre-Crash Hip Posture, 0° Adduction (top left), 0° Flexion (top right), 10° Abduction (bottom left), 30° Flexion (bottom right)

Of course, there is some amount of approximation required in positioning the FE KTH to the specified hip posture. As a result, the angles shown in Figure 30 are not exactly what is described in the adduction and flexion angles defined above.

As described in the Methodology chapter, this project planned to study both five degrees and 10° adducted hip postures. When the FE KTH was positioned to these postures, it was found that the legs crossed in a non-physical way. As a result, in the adducted simulations, the right leg was adducted five or 10 degrees, and the left leg was abducted the same amount. Figure 31 demonstrates this for a 10° adducted posture.

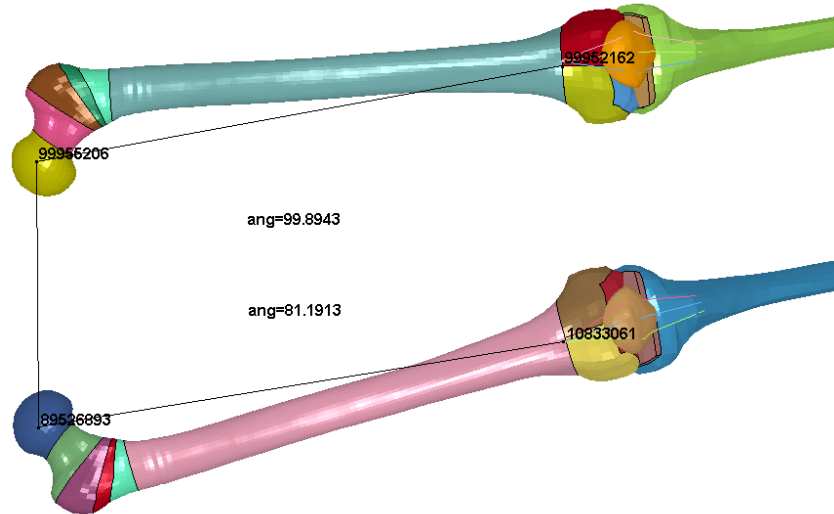


Figure 31: 10° Adducted Hip Posture

Once the FE KTH was positioned correctly, the simulations were run in a similar manner as described earlier in this chapter. The appropriate displacement boundary conditions were applied to the reduced FE Taurus, and the FE KTH was treated as rigid during the first 50 ms of the simulation.

Simulation Results

Several parameters were recorded in the parametric study to describe the FE KTH's response to impact. These included maximum femur axial force and femur axial force at the time of initial fracture of a given part of the KTH. The KTH region was divided into the following sections: acetabulum, femoral head, femoral neck, proximal femoral shaft, mid-shaft (of the femur), and the femoral condyles. Figure 32 shows injuries to the various FE KTH components (injured parts shown in red).

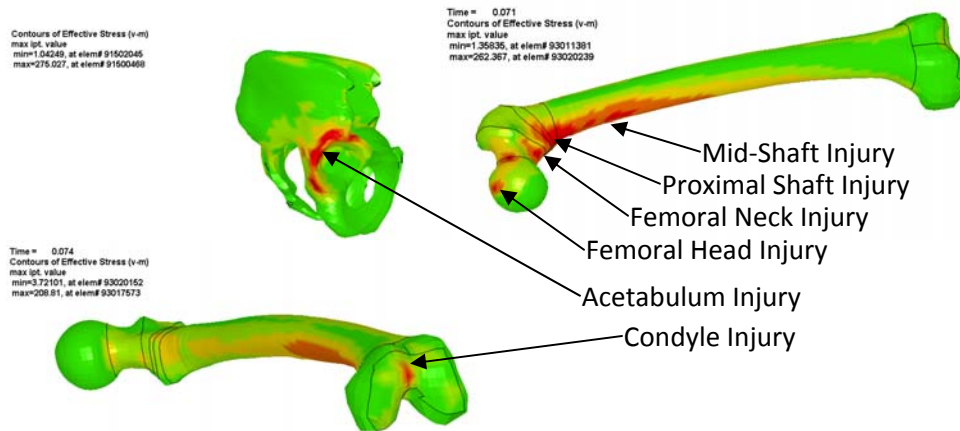


Figure 32: Injury to Various KTH Components

It is important to understand how injury (or fracture) of the various KTH components was evaluated. Fracture was evaluated based on element von Mises stresses. Stresses of 160 MPa in the pelvis or 190 MPa in the femur constituted fracture (Silvestri, 2009). Therefore, in Figure 32, the colors represent different magnitudes of von Mises stress (or effective stress). In the pelvis, the red contours represent the 160 MPa injury threshold, while the yellow represents 80 MPa, while the green represents low levels of stress (~0 MPa). In the femur, the red contours represent the threshold value of 190 MPa, the yellow represents 95 MPa, and the green represents low stress levels (~0 MPa).

In the following sections, femur axial forces are given at the time of initial fracture of the various KTH components, i.e. when elements in a given region first reach the threshold value given above. Although the first initiation of fracture would theoretically change the load path through the KTH complex, rendering the remaining parts of the simulation void (because the fractured bone elements are still capable of carrying load in this model), this project reports the progression of KTH component fractures up to the termination of the simulation. It is believed that this is a valid approach because of the approximate nature of the analytical model. Because of the approximate nature of the model, this project sought to provide conservative results in terms of femur force required to cause fracture by defining fracture at its initiation. The force required to cause total fracture would be higher than the forces reported in this project.

Overall, the results seem to indicate that occupant injury tolerance is primarily dictated by occupant kinematics during the impact event. This section presents the overall occupant kinematics observed in all the simulations, followed by the femur axial force and injury tolerance for each region of the KTH complex. The section concludes by summarizing the injury tolerance data, and commenting on observable trends. The raw data, summarizing contact forces, femur axial forces, and showing von Mises stress distributions can be found for all simulations in Appendix A.

Occupant Kinematics

The occupant kinematics in the parametric investigation can be grouped into two basic categories which relate to the knee's response with the knee bolster after impact. In the first, both knees impacted the knee bolster fairly directly, which resulted in an upward rotation of the femur at the hip joint and a fairly even amount of femur axial force in both legs; this is referred to as a "direct impact". In the second, the left leg responded in the same way as described in the first however, the right leg was pushed downward along the plane of the knee bolster; this is referred to as an "indirect impact". This resulted in the left leg suffering from much higher femur axial force than the right leg. Figure 33 depicts these two scenarios.

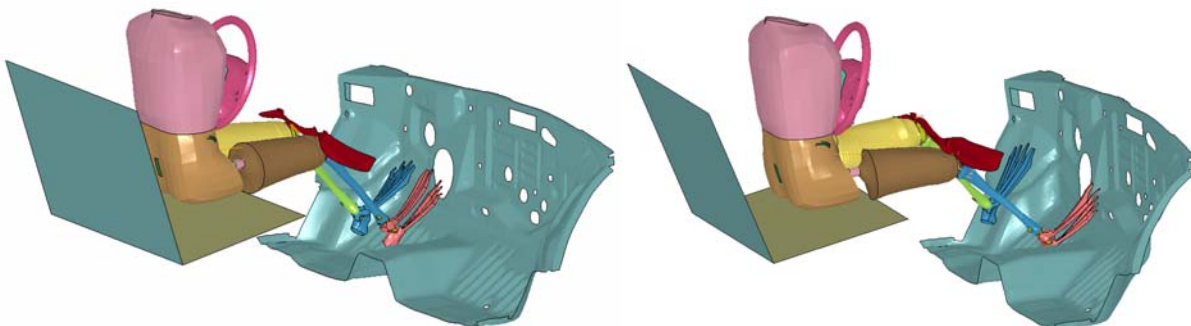


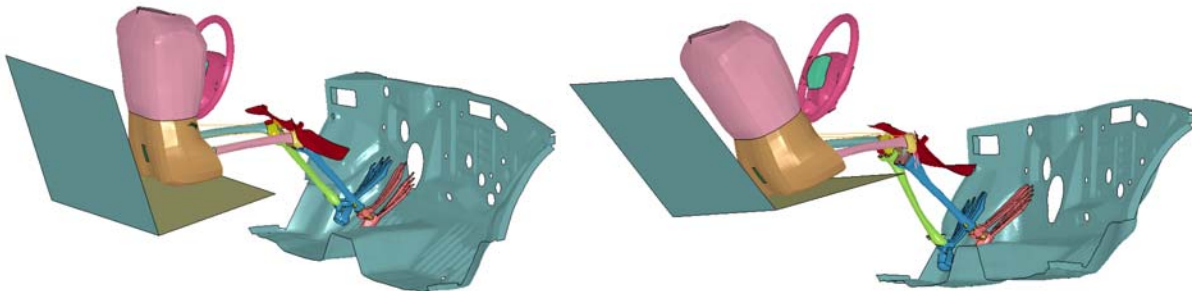
Figure 33: Basic Description of Occupant Kinematics During Impact: Both Legs Directly Impacting the Knee Bolster (left) and Left Leg Directly Impacting the Knee Bolster and Right Leg Sliding Along It (right)

The left side of Figure 33 represents a pre-crash hip posture of zero degrees adduction and 30° flexion, while the right side represents 10° abduction and 30° flexion. Table 3 describes the impact kinematics over all simulations run.

Table 3: Basic Occupant Impact Scenario

Direct Impact	Indirect Impact
Neutral	10° Abduction
5° Adduction	5° Abduction
10° Adduction	30° Flexion - 10° Abduction
7.5° Flexion	30° Flexion - 10° Adduction
15° Flexion	30° Flexion - 5° Abduction
22.5° Flexion	30° Flexion - 5° Adduction
30° Flexion	15° Flexion - 10° Abduction
15° Flexion - 5° Abduction	15° Flexion - 10° Adduction
15° Flexion - 5° Adduction	7.5° Flexion - 10° Abduction
7.5° Flexion - 5° Abduction	7.5° Flexion - 10° Adduction
22.5° Flexion - 10° Adduction	7.5° Flexion - 5° Adduction
22.5° Flexion - 5° Abduction	22.5° Flexion - 10° Abduction
	22.5° Flexion - 5° Adduction

In addition to the knee's response to impact, it is also interesting to note the kinematic response based on foot contact force with the floor. In one set of circumstances, both feet impacted the floor with a fairly equal contact force. In the second, the left foot impacted the floor in similar manner as the first however, the right foot's contact force was comparatively very low. This resulted in large relative displacements of the tibia relative to the femur, as shown in Figure 34. These large relative displacements can result in injuries to the knee ligaments, such as the anterior and posterior cruciate ligaments (ACL and PCL).

**Figure 34: Large Tibia Displacement Relative to the Femur**

The left side of Figure 34 corresponds to a pre-crash hip posture of 30° flexion – 0° adduction while the right side corresponds to 0° flexion – 10° adduction. This phenomenon was demonstrated in a study involving physical tests conducted by Meyer (2004). Although the FE KTH model used in this

parametric investigation was not validated against Meyer’s study since the model below the knee is not validated, the revisions to the model required to validate it are described in Silvestri and Heath (2010).

Maximum Femur Axial Force

Injury susceptibility in the KTH region is evaluated by vehicle safety regulators based on femur axial force. It is, therefore, interesting to note the maximum femur axial force experienced by the FE KTH during each simulation. Table 4 gives the maximum recorded femur axial force in the left and right legs for all the simulations run. It should be noted that in Tables 4-10, cells highlighted in red represent direct impacts, while cells highlighted in green represent indirect impacts.

Table 4: Maximum Femur Axial Force (kN)

Maximum Femur Axial Force: Left Leg						
		Flexion °				
		0	7.5	15	22.5	30
Adduction °	-10	10.3	9.01	9.98	9.3	9.15
	-5	10.7	9.27	8.37	10.1	8.01
	0	6.48	7.76	6.41	4.8	3.86
	5	6.2	9.44	5.27	7.56	8.43
	10	9.28	8.11	7.58	7.59	8.03
	Maximum Femur Axial Force: Right Leg					
		Flexion °				
		0	7.5	15	22.5	30
Adduction °	-10	7.12	6.54	7	6.68	7.14
	-5	8.79	8.67	11.6	8.06	6.32
	0	9.36	7.79	6.94	5.96	5.39
	5	6.88	5.47	5.17	4.71	4.76
	10	8.68	6.11	4.94	9.19	4

The average maximum femur axial force in all the simulations was 8.04 kN on the left leg and 6.93 kN on the right leg. The maximum force was 10.7 kN on the left leg and 11.6 kN on the right leg. The minimum was 3.86 kN on the left leg and 4.00 kN on the right leg. For comparison, it should be noted that the maximum femur axial force allowed in FMVSS 208 regulatory testing is 10 kN. Figure 35 shows the distribution of maximum recorded femur axial force in the left and right legs for all the simulations run.

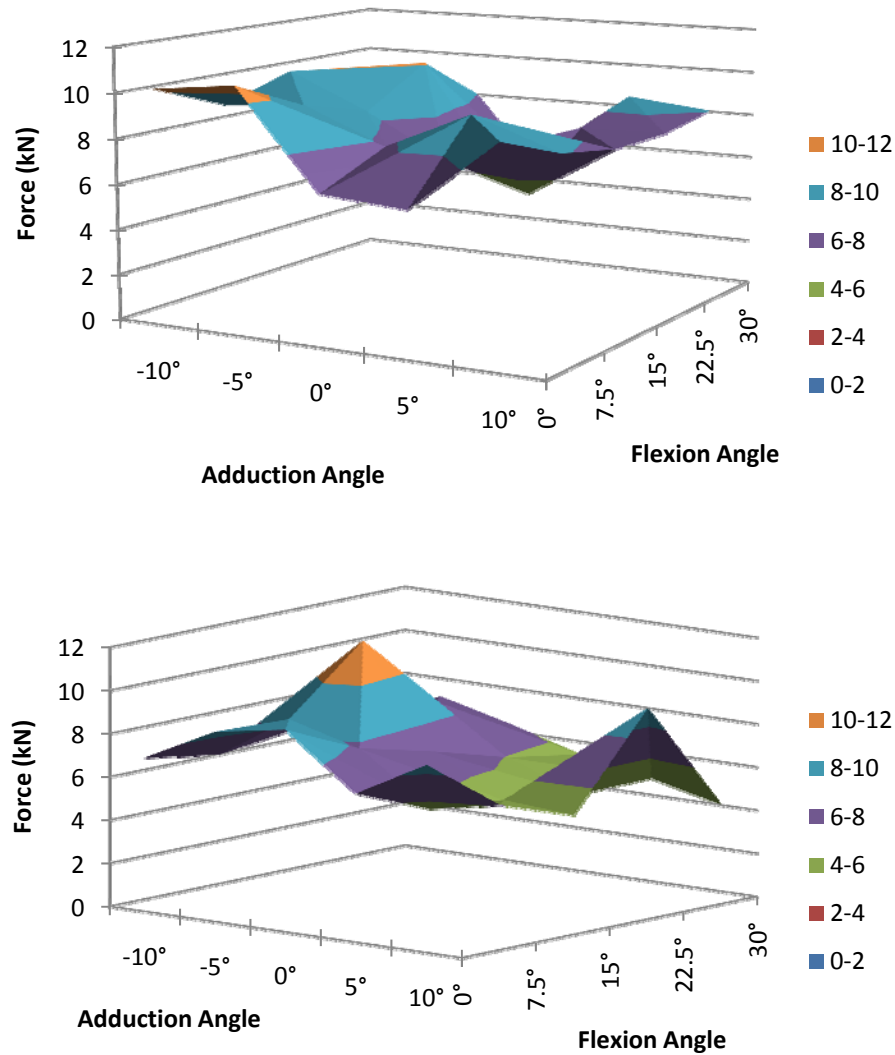
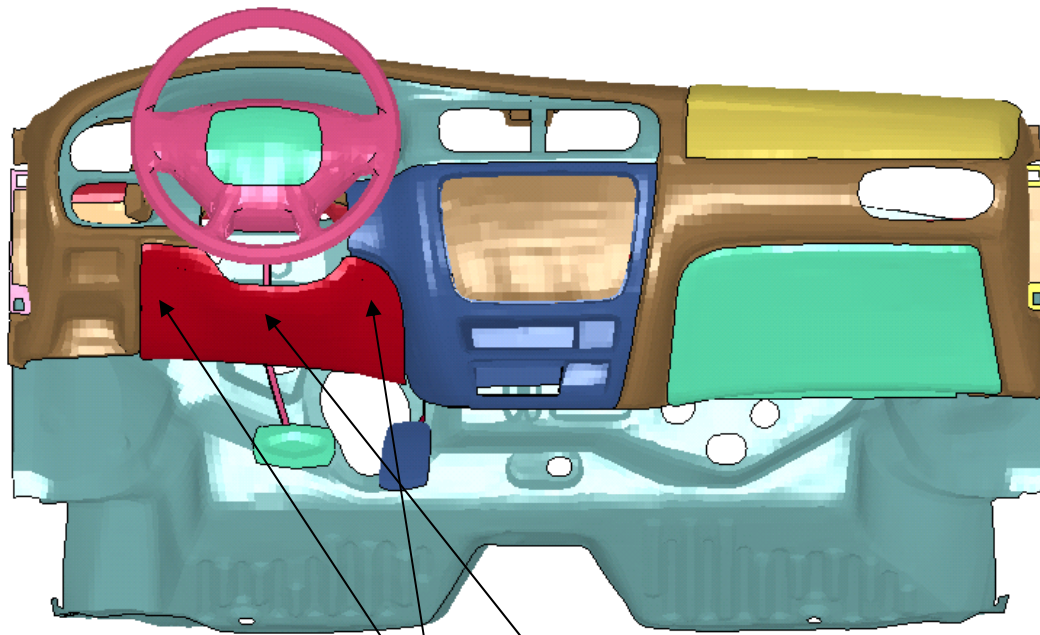


Figure 35: Maximum Femur Axial Force Distribution Left Leg (top); Right Leg (bottom)

Figure 35 shows a valley for all flexion angles along the zero degree adduction posture, particularly in the left leg. This indicates that adduction angle plays a larger role in determining maximum femur axial force than flexion angle. This may be a result of occupant kinematics. Adduction angle plays a major role in the part of the knee bolster impacted by the knee, particularly for the right leg. If the knee impacts the center of the knee bolster, the bolster is able to achieve maximum deformation and therefore absorbs a maximum amount of energy. If the knee impacts the edge of the bolster, closer to the dash, the bolster's

support is increased and smaller deformation is expected, requiring the KTH to absorb more of the impact force. Figure 36 demonstrates this phenomenon.



If the knee impacts here, the bolster cannot deform as much, requiring the KTH to absorb much of the impact force

If the knee impacts here, the bolster can achieve maximum deformation, and absorb the most energy.

Figure 36: Effect of Knee Impact Location on Maximum Femur Axial Force

Also, a comparison of foot-floor and knee-bolster contact forces shows a trend related to maximum femur axial force. This idea is developed further at the end of this chapter.

Acetabulum Injury Tolerance

Table 5 gives the femur axial force at the time of initial acetabulum fracture for the left and right leg.

Table 5: Femur Axial Force at the Time of Initial Fracture to the Acetabulum (kN)

Left Leg						
Flexion °						
		0	7.5	15	22.5	30
Adduction °	-10	5.99	4.81	4.8	4.54	3.73
	-5	4.59	5.85	5.18	2.61	3.88
	0	4.55	5.97	5.84	4.04	NA
	5	3.58	4.36	5.27	4.33	4.24
	10	6.29	3.99	3.76	5.75	3.6
Right Leg						
Flexion °						
		0	7.5	15	22.5	30
Adduction °	-10	4.22	5.9	5.94	3.23	NA
	-5	4.09	4.38	5.09	4.79	5.18
	0	4.83	4.14	3.44	4.42	3.05
	5	5	NA	4.46	4.71	4.76
	10	5	3.67	NA	4.16	2.85

Cells marked with an “NA” indicate that fracture did not occur to the acetabulum for the pre-crash hip posture described. This holds true for all future explanations of injury tolerance. The average force required to cause initial fracture to the acetabulum was 4.65 kN on the left leg and 4.31 kN on the right leg. The maximum femur force required to initiate fracture was 6.29 kN on the left leg and 5.94 kN on the right leg. The minimum force was 2.61 kN on the left leg and 2.85 kN on the right leg. Figure 37 shows the distribution of femur axial force required to cause initial fracture of the acetabulum for the left and right legs.

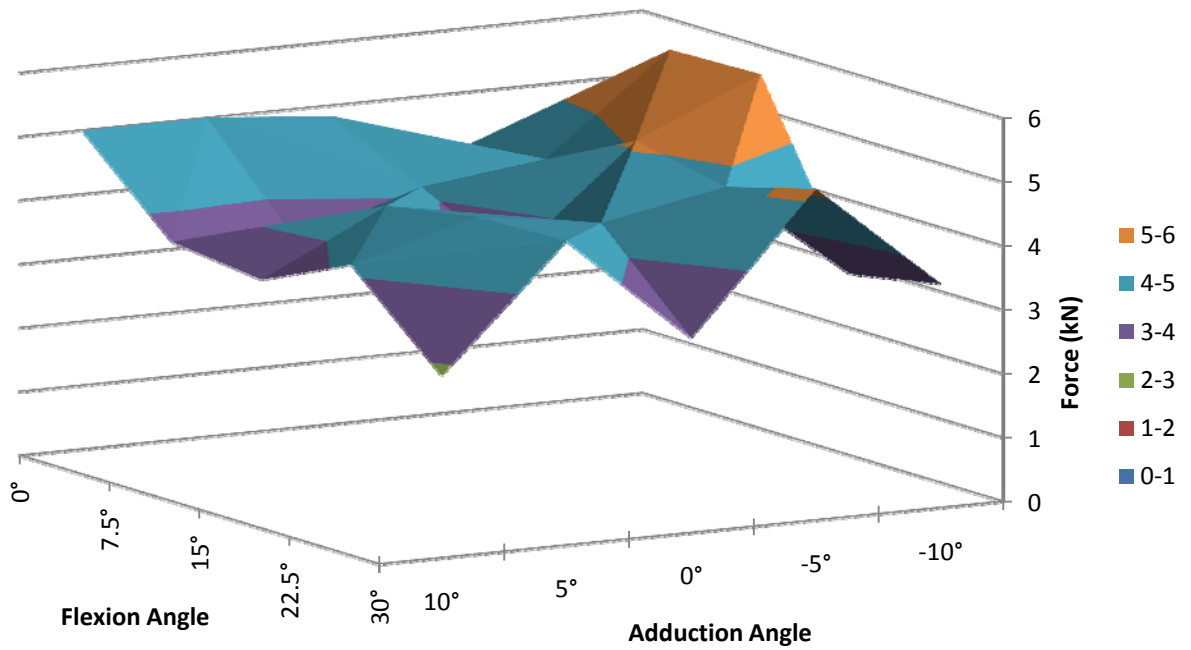
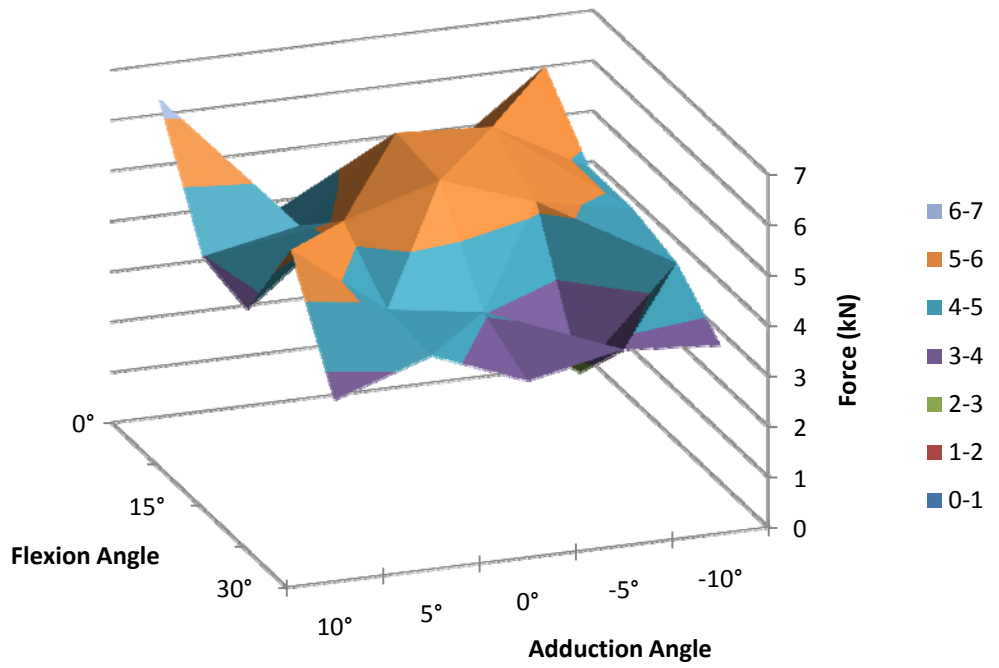


Figure 37: Distribution of Femur Axial Force Required to Cause Acetabulum Injury, in the Left Leg (top), and Right Leg (bottom)

It should be noted that in four pre-crash hip postures (denoted by “NA” in Table 5), the acetabulum did not experience injury. In these hip postures, a “dummy” injury force of 3.5 kN was used to facilitate the generation of a smooth curve in Figure 37. These results seem to indicate that flexion angle plays a larger role in determining acetabulum injury tolerance than adduction angle, as the “valley” or “peak” of the curves seems to span an axis perpendicular to the flexion axis. This is consistent with the results reported by Rupp (2003). Also, based on the results reported by Rupp, one would expect to see a symmetric force distribution in the left leg because the left leg was not ever adducted (it was abducted while the right was adducted). Finally, one would expect to see similar results for the left leg and the right leg in the abducted hip postures. The differences shown in Figure 37 further suggest that occupant kinematics may play a large role in determining injury tolerance.

Femoral Head Injury Tolerance

Table 6 gives the femur axial force at the time of initial fracture to the femoral head.

Table 6: Femur Axial Force at Time of Initial Femoral Head Fracture (kN)

Left Leg						
		Flexion °				
		0	7.5	15	22.5	30
Adduction °	-10	9.74	8.28	6.86	9.3	7.06
	-5	9.05	6.4	NA	NA	NA
	0	NA	NA	NA	NA	NA
	5	NA	8.1	NA	5.69	NA
	10	8.57	NA	7.22	7.59	3.98
	15	7.22	7.59	3.98	NA	NA
Right Leg						
		Flexion °				
		0	7.5	15	22.5	30
Adduction °	-10	NA	NA	NA	NA	NA
	-5	8.14	8.67	9.24	7.33	NA
	0	9.19	NA	NA	NA	NA
	5	NA	NA	NA	NA	NA
	10	6.11	NA	NA	6.39	NA
	15	6.39	NA	NA	NA	NA

The average force required to cause initial fracture of the femoral head was 7.53 kN on the left leg and 7.87 kN on the right leg. The maximum force was 9.74 kN on the left leg and 9.24 kN on the right leg.

The minimum force was 3.98 kN on the left leg and 6.11 kN on the right leg. Figure 38 shows the distribution of femur axial forces at the time of initial femoral head fracture.

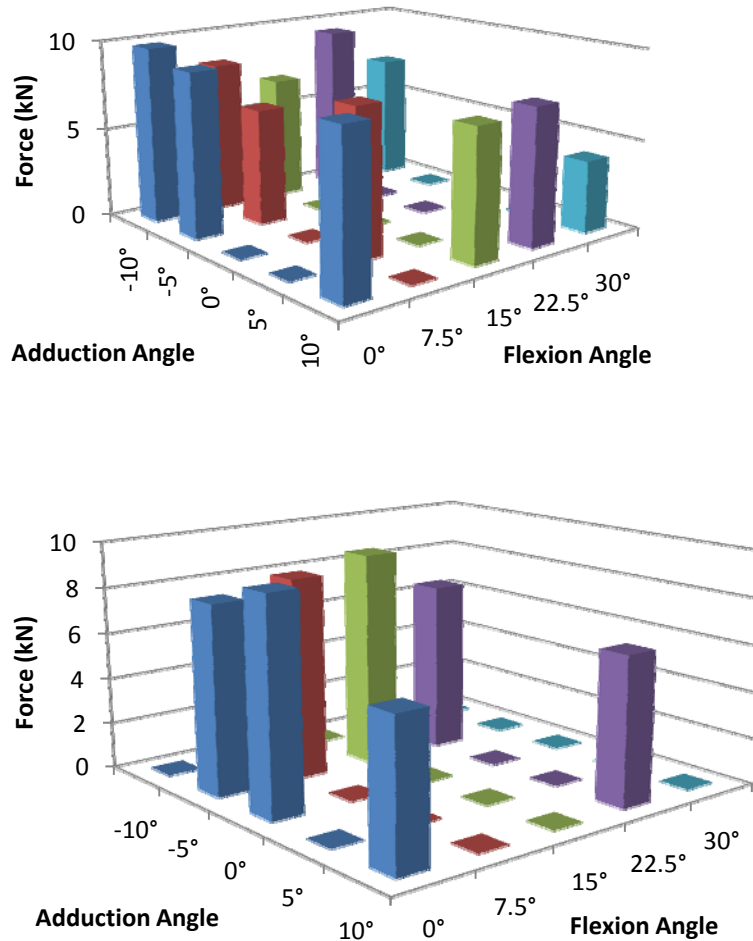


Figure 38: Distribution of Femur Axial Force at the Time of Initial Femoral Head Fracture, Left Leg (top) and Right Leg (bottom)

The results for the left leg shown in Figure 38 show a fairly symmetric distribution of a femur axial force about the zero degrees adduction posture. It also shows a decreasing force trend as flexion angle increases. The results for the right leg have very few data points, making it difficult to identify trends. The results however do seem to show an increasing femur force with increasing flexion angle. This

difference in result between the left and right legs reinforces the idea that occupant kinematics directly influences injury tolerance.

Femoral Neck Injury Tolerance

Table 7 shows the femur axial force at the time of initial fracture in the femoral neck.

Table 7: Femur Axial Force at the Time of Initial Femoral Neck Fracture (kN)

Left Leg						
Flexion °						
Adduction °		0	7.5	15	22.5	30
	-10	9.74	8.28	8.5	9.3	7.06
	-5	NA	NA	NA	NA	NA
	0	NA	NA	NA	NA	NA
	5	NA	8.96	NA	NA	NA
	10	9.28	8.11	NA	NA	NA
Right Leg						
Flexion °						
Adduction °		0	7.5	15	22.5	30
	-10	NA	NA	NA	NA	NA
	-5	NA	7.25	7.6	7.33	NA
	0	9.22	NA	NA	NA	NA
	5	NA	NA	NA	NA	NA
	10	6.11	NA	NA	7.35	NA

The average femur axial force required to cause initial fracture to the femoral neck was 8.65 kN on the left leg and 7.48 kN on the right leg. The maximum force was 9.74 kN on the left leg and 9.22 kN on the right leg. The minimum force was 7.06 kN on the left leg and 6.11 kN on the right leg. Figure 39 shows the distribution of femur axial force at the time of initial femoral neck fracture.

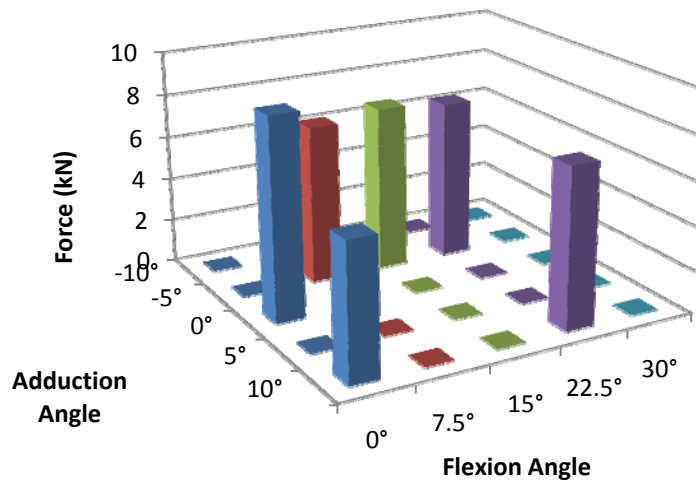
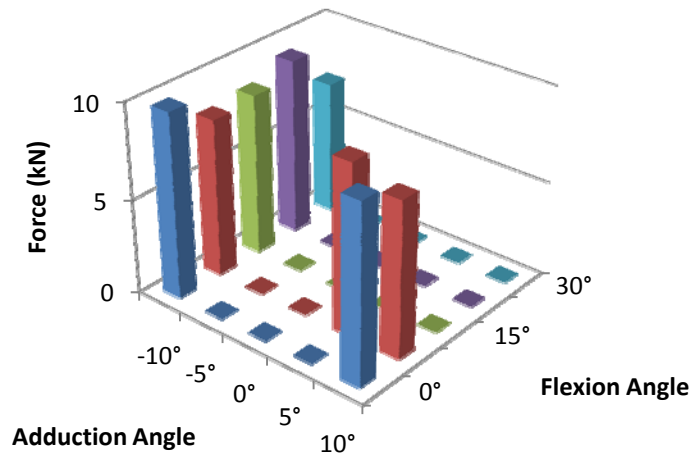


Figure 39: Distribution of Femur Axial Force at the Time of Initial Femoral Neck Fracture, Left Leg (top) and Right Leg (bottom)

A limited number of data points available in Figure 39 make it difficult to identify trends. However, based on the data shown, the distribution of force seems somewhat constant across the flexion angles considered in both the left and right legs. The right leg generally experienced fracture at lower levels of axial force.

Proximal Femoral Shaft Injury

Table 8 shows the femur axial force at the time of initial fracture in the proximal femoral shaft.

Table 8: Femur Axial Forces at the Time of Initial Fracture of the Proximal Femoral Shaft (kN)

Left Leg						
Flexion °						
Adduction °		0	7.5	15	22.5	30
	-10	9.74	7.76	6.86	9.02	7.06
	-5	8.09	6.57	NA	NA	NA
	0	NA	NA	NA	NA	NA
	5	NA	8.1	NA	6.45	7.42
	10	8.57	7.46	7.22	7.23	7.83
Right Leg						
Flexion °						
Adduction °		0	7.5	15	22.5	30
	-10	NA	5.29	NA	NA	NA
	-5	8.56	8.67	7.6	7.33	NA
	0	9.22	NA	NA	NA	NA
	5	NA	NA	NA	NA	NA
	10	8.57	NA	NA	7.35	NA

The average femur axial force required to cause initial fracture of the proximal femoral shaft was 7.69 kN on the left leg and 7.82 kN on the right leg. The maximum force was 9.74 kN on the left leg and 9.22 kN on the right leg. The minimum force was 6.45 kN on the left leg and 5.29 kN on the right leg. Figure 40 shows the distribution of femur axial forces at the time of initial proximal femoral shaft fracture.

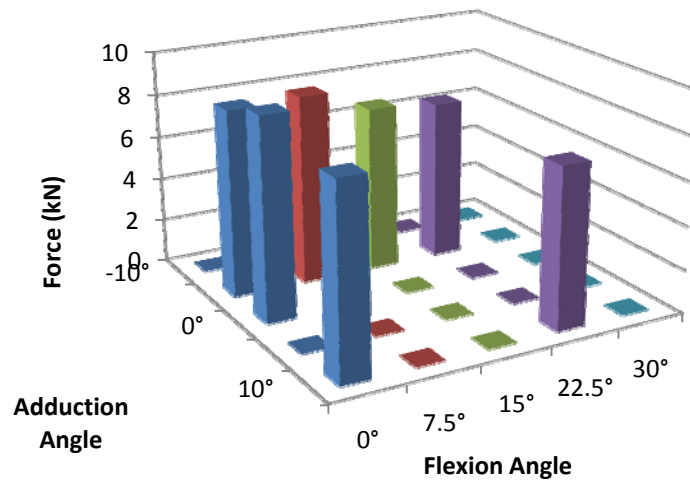
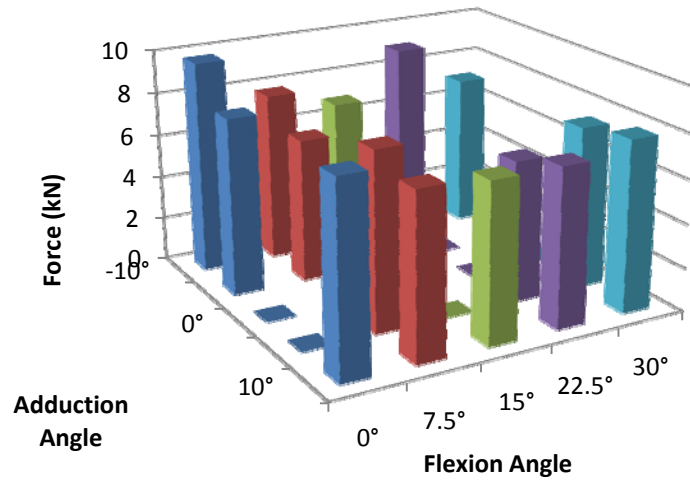


Figure 40: Distribution of Femur Axial Force at the Time of Initial Proximal Femoral Shaft Fracture, Left Leg (top) and Right Leg (bottom)

The results shown in Figure 40 indicate that there is decreased injury tolerance with increasing flexion angle. Also, the results for the left leg indicate that there is increased tolerance with increasing adduction or abduction angle. The results for the right leg however seem to show the opposite trend, with the zero degree adduction posture being the strongest. This again indicates that occupant kinematics may be the main contributor to KTH injury tolerance.

Mid Femoral Shaft Injury

Table 9 gives the femur axial force in the left and right legs at the time of mid femoral shaft fracture.

Table 9: Femur Axial Force at the Time of Initial Fracture to the Mid Femoral Shaft (kN)

Left Leg						
		Flexion °				
		0	7.5	15	22.5	30
Adduction °	-10	9.2	8.27	8.04	9.3	9.15
	-5	8.98	6.83	NA	NA	NA
	0	NA	NA	NA	NA	NA
	5	NA	8.96	NA	NA	NA
	10	NA	NA	NA	7.32	NA
	15	NA	NA	NA	NA	NA
Right Leg						
		Flexion °				
		0	7.5	15	22.5	30
Adduction °	-10	NA	6.54	NA	NA	NA
	-5	NA	NA	10.9	NA	NA
	0	NA	NA	NA	NA	NA
	5	NA	NA	NA	NA	NA
	10	8.68	NA	NA	9.03	NA
	15	NA	NA	NA	NA	NA

The average femur axial force at the time of initial fracture of the mid-femoral shaft was 8.45 kN on the left leg and 8.79 kN on the right leg. The maximum force was 9.30 kN on the left leg and 10.90 kN on the right leg. The minimum force was 6.54 kN on the left leg and 8.45 kN on the right leg. Figure 41 gives the distribution of femur axial forces in the left and right legs at the time of mid femoral shaft fracture.

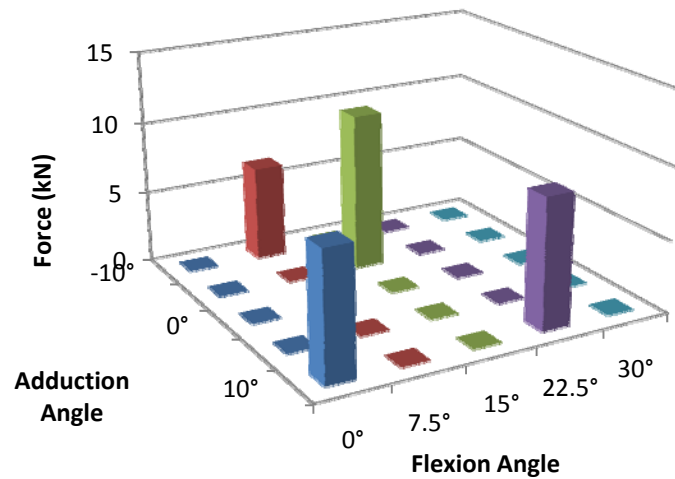
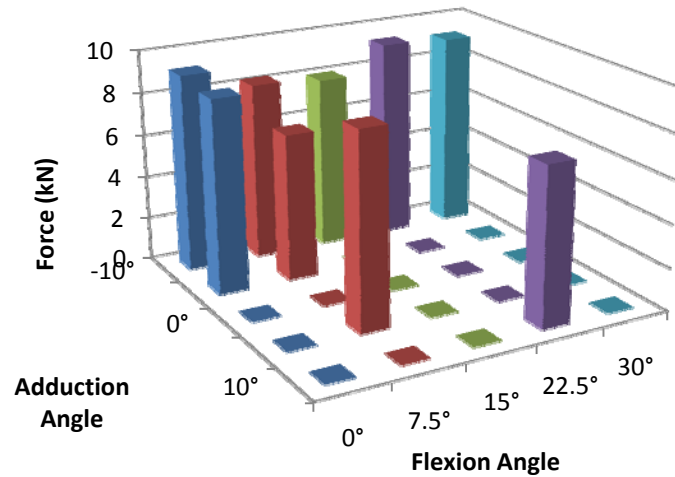


Figure 41: Femur Axial Force Distribution at the Time of Initial Mid Femoral Shaft Fracture, Left Leg (top) and Right Leg (bottom)

A limited number of data points make it difficult to identify trends in Figure 41. The results for the left leg indicate that the mid-femoral shaft may be weakest in the 10° abducted posture, as injury occurred to the shaft at this posture for all angle of flexion.

Femoral Condyles Injury

Table 10 shows the femur axial forces at the time of initial fracture to the femoral condyles.

Table 10: Femur Axial Force at the Time of Initial Femoral Condyle Fracture (kN)

Left Leg						
Flexion °						
Adduction °		0	7.5	15	22.5	30
	-10	NA	NA	NA	NA	NA
	-5	NA	NA	8.37	NA	6.79
	0	NA	NA	NA	NA	NA
	5	3.5	NA	NA	7.49	NA
	10	NA	4.86	NA	NA	NA
Right Leg						
Flexion °						
Adduction °		0	7.5	15	22.5	30
	-10	NA	NA	NA	NA	NA
	-5	NA	NA	10.7	NA	NA
	0	NA	NA	NA	NA	NA
	5	NA	NA	NA	NA	NA
	10	6.62	NA	NA	7.35	NA

The average femur axial force at the time of initial fracture of the femoral condyles was 6.20 kN on the left leg and 8.22 kN on the right leg. The maximum force was 8.37 kN on the left leg and 10.7 kN on the right leg. The minimum force was 3.5 kN on the left leg and 6.62 kN on the left leg. Figure 42 shows the distribution of femur axial forces at the time of initial femoral condyle fracture.

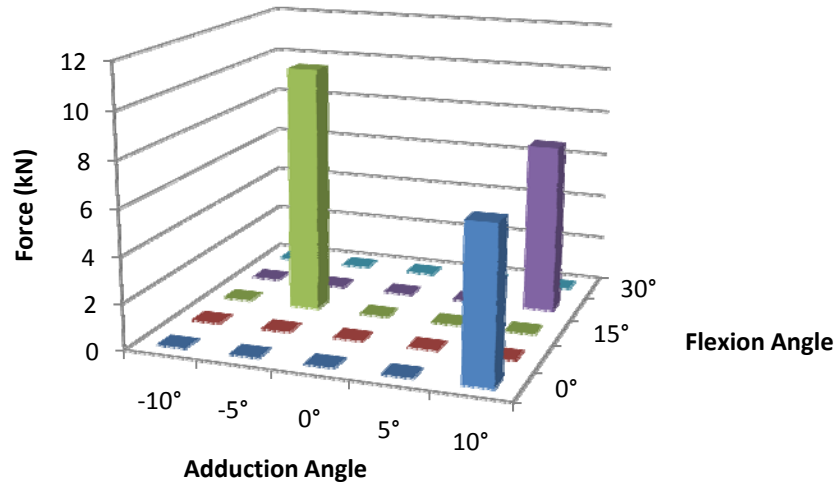
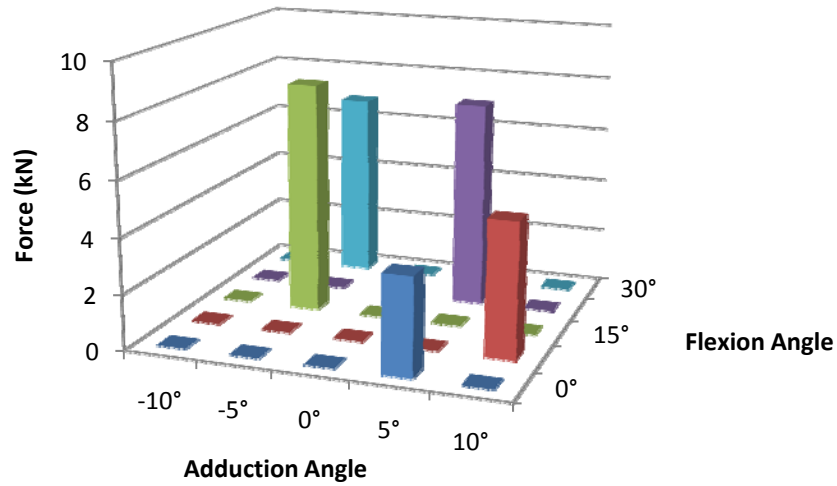


Figure 42: Distribution of Femur Axial Forces at the Time of Initial Fracture to the Femoral Condyles, Left Leg (top) and Right Leg (bottom)

A limited number of data points in Figure 42 make it difficult to identify any trends. It can be seen however that the condyles generally only fractured at high levels of femur force.

Trends in Injury Tolerance Data

Several interesting trends can be identified by synthesizing the data presented in the previous sections. First, consider the plot of number of injuries sustained by the various KTH components shown in Figure 43.

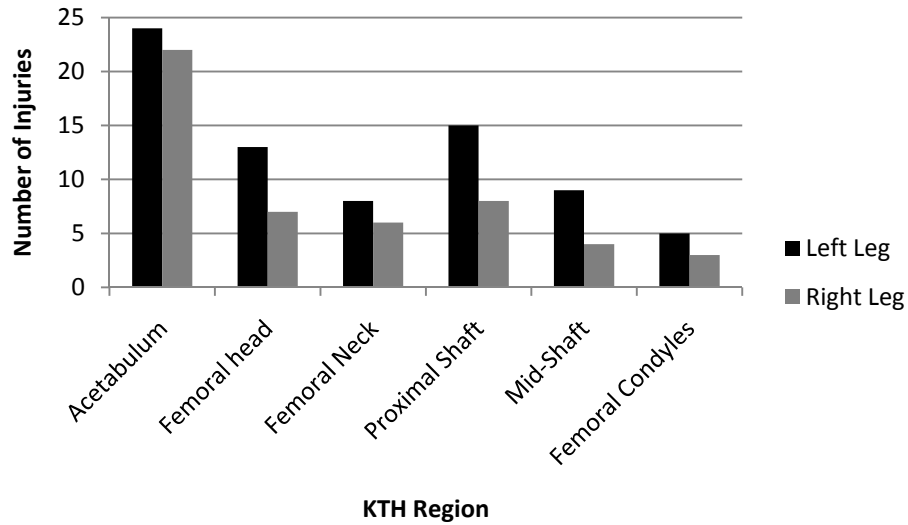


Figure 43: Distribution of Injuries by KTH Region

These results show that the hip is the most injury prone region of the KTH complex, followed by the proximal shaft, the femoral head, the femoral neck and mid-shaft, and the femoral condyles. The femoral neck and mid-shaft had very similar injury distributions, indicating that they are approximately equally injury prone. These results are somewhat different than what was reported by Kuppaa (2003), who showed that the hip is at greatest risk for AIS2+ injury, followed by the knee, then the thigh. Kuppaa’s results are for seatbelt only constraint. The difference between Kuppaa’s results and the results presented in Figure 43 may indicate that the use of seatbelts disproportionately decreases risk to the thigh (mid-shaft) or increases risk to the knee (femoral condyles).

Next, consider the plots shown in Figures 44-53, which compare the maximum femur axial force to the femur axial force required to cause injury to various KTH components.

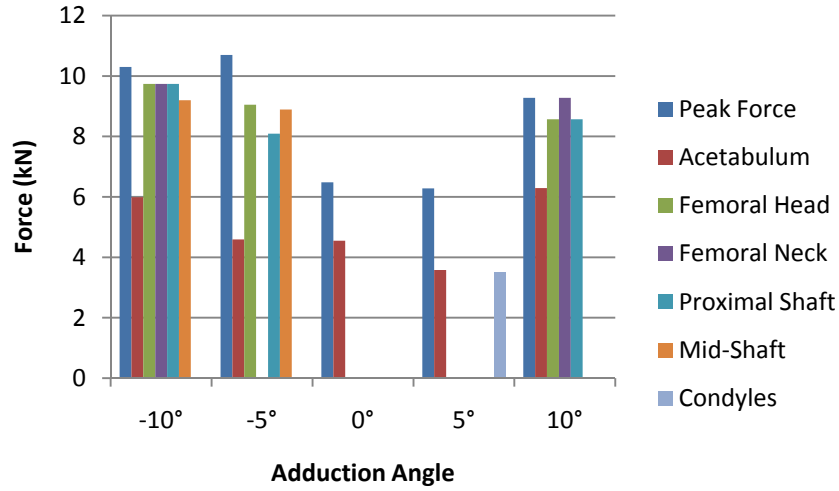


Figure 44: Comparison of Maximum Femur Axial Force to Axial Force at time of Initial KTH Component Fracture, Left Leg, 0° Flexion

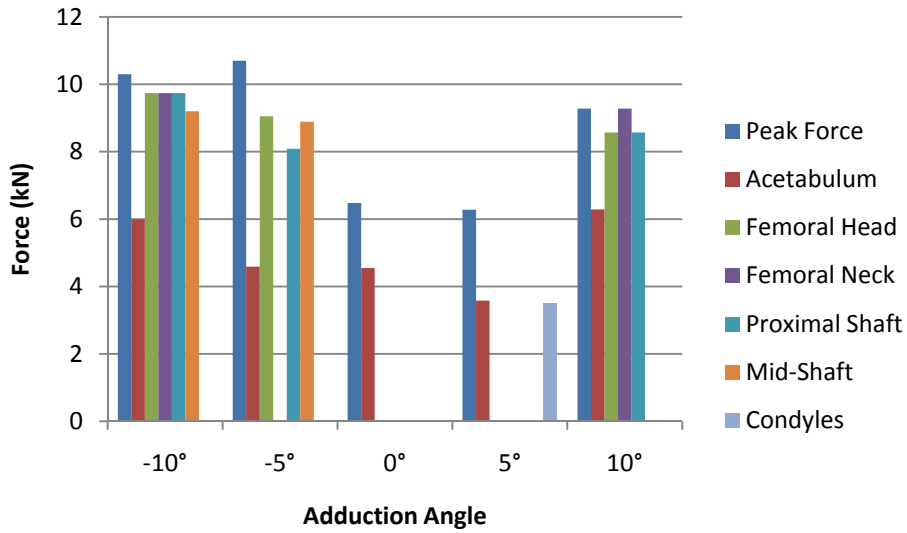


Figure 45: Comparison of Maximum Femur Axial Force to Axial Force at time of Initial KTH Component Fracture, Left Leg, 7.5° Flexion

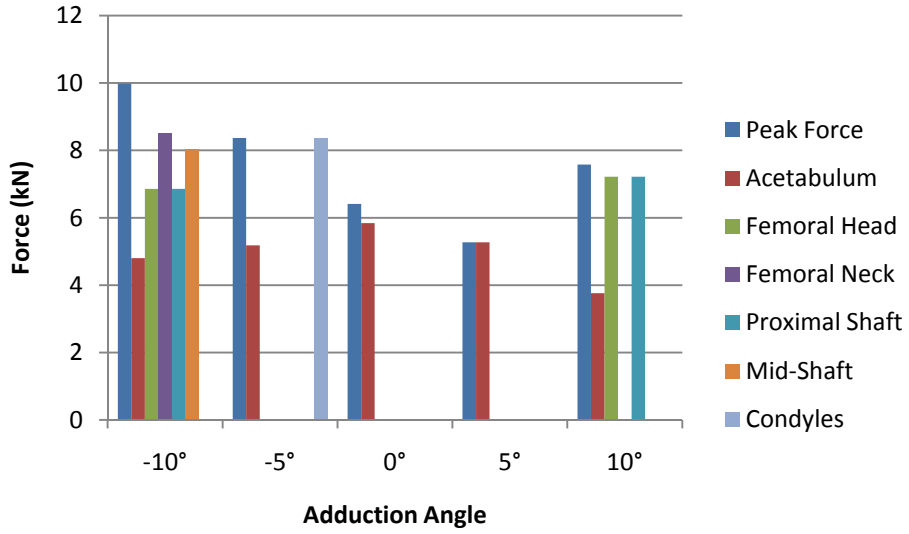


Figure 46: Comparison of Maximum Femur Axial Force to Axial Force at time of Initial KTH Component Fracture, Left Leg, 15° Flexion

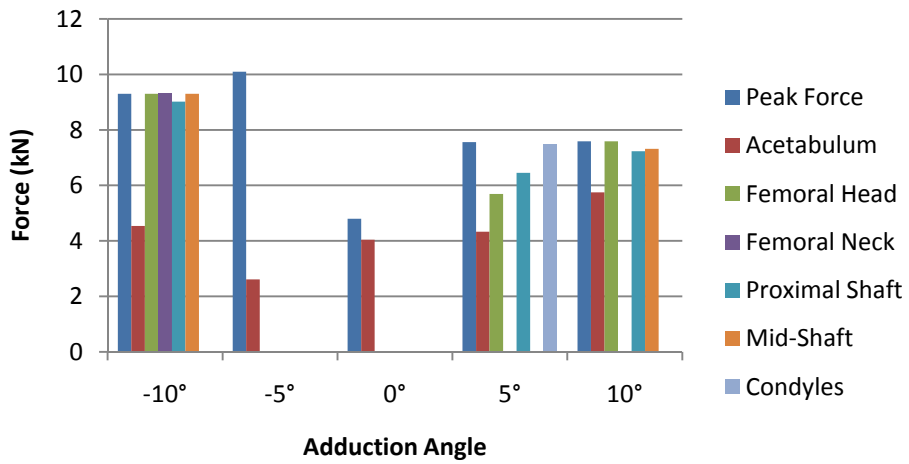


Figure 47: Comparison of Maximum Femur Axial Force to Axial Force at time of Initial KTH Component Fracture, Left Leg, 22.5° Flexion

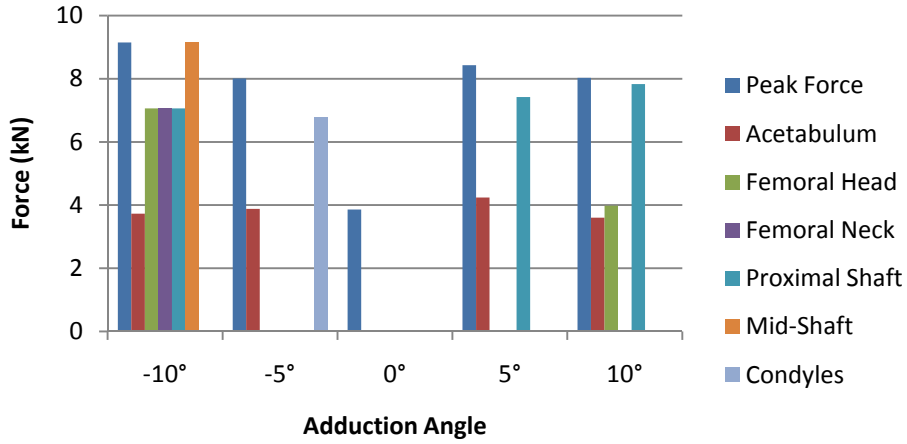


Figure 48: Comparison of Maximum Femur Axial Force to Axial Force at time of Initial KTH Component Fracture, Left Leg, 30° Flexion

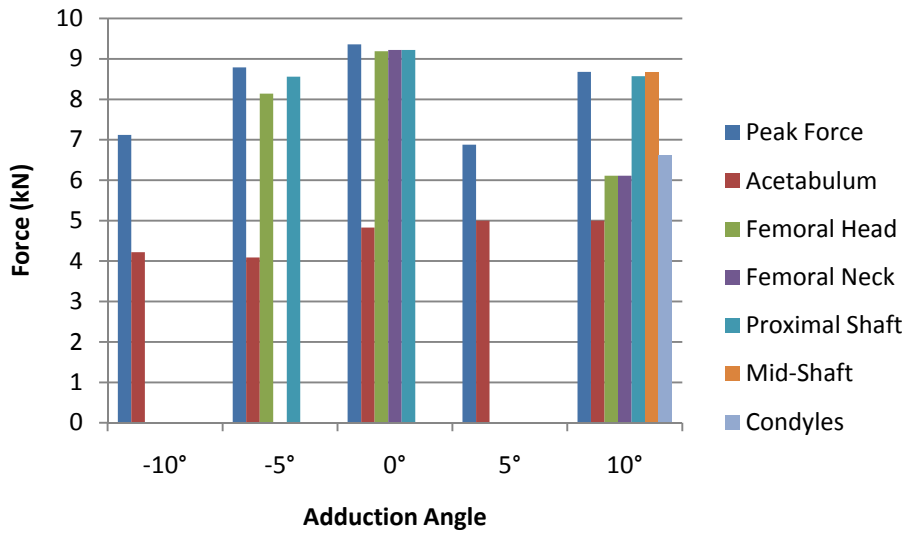


Figure 49: Comparison of Maximum Femur Axial Force to Axial Force at time of Initial KTH Component Fracture, Right Leg, 0° Flexion

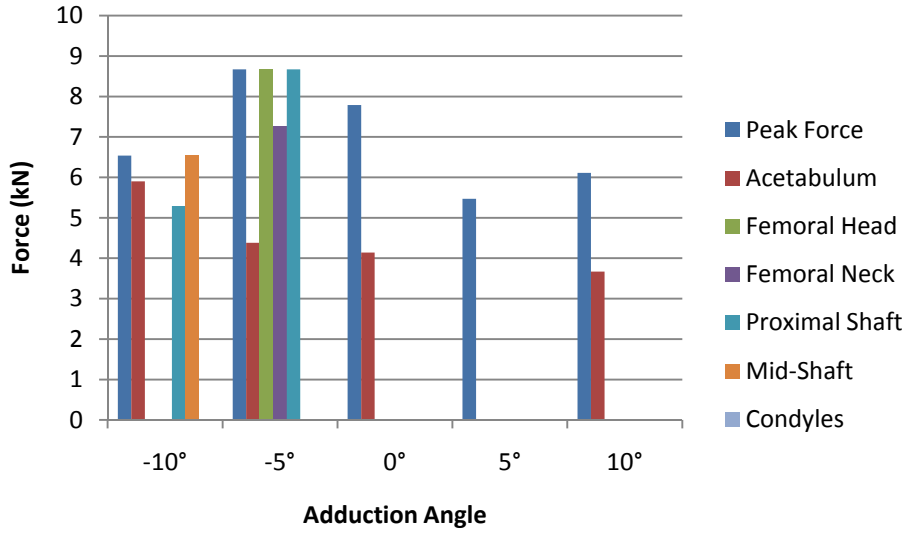


Figure 50: Comparison of Maximum Femur Axial Force to Axial Force at time of Initial KTH Component Fracture, Right Leg, 7.5° Flexion

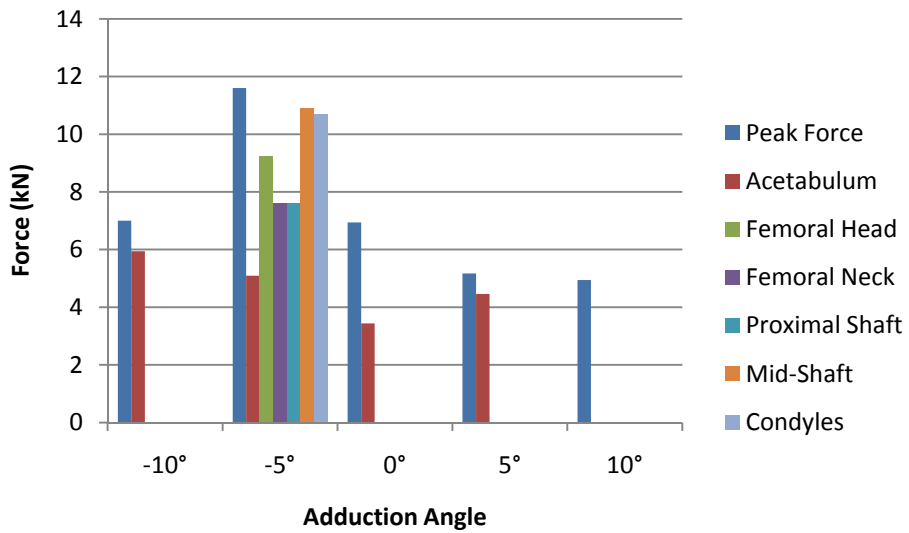


Figure 51: Comparison of Maximum Femur Axial Force to Axial Force at time of Initial KTH Component Fracture, Right Leg, 15° Flexion

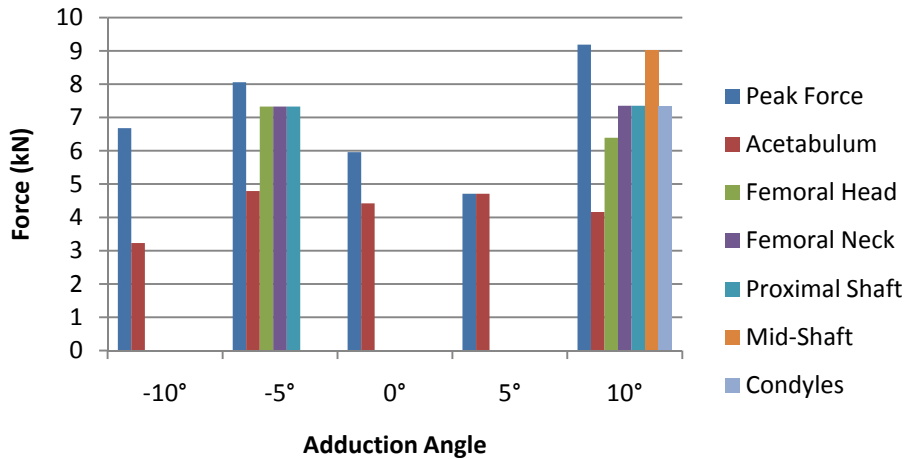


Figure 52: Comparison of Maximum Femur Axial Force to Axial Force at time of Initial KTH Component Fracture, Right Leg, 22.5° Flexion

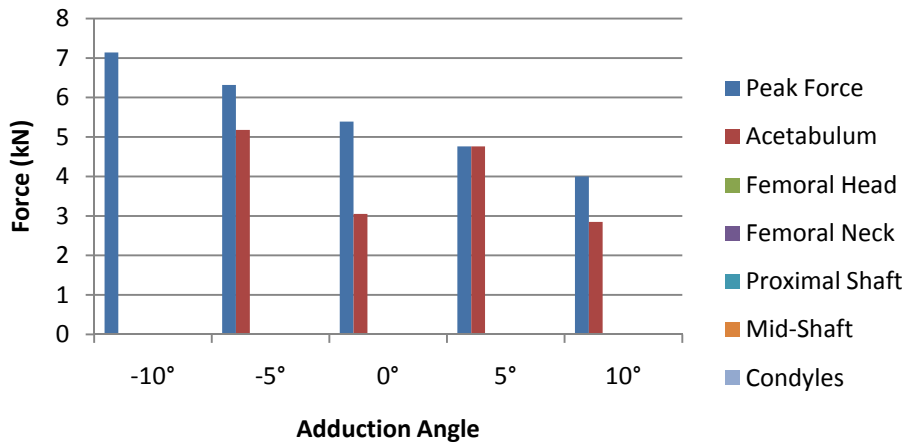


Figure 53: Comparison of Maximum Femur Axial Force to Axial Force at time of Initial KTH Component Fracture, Right Leg, 30° Flexion

Comparing the results shown in Figures 44-53 shows that there is no obvious trend showing a maximum or minimum axial force at the time of initial fracture for the various KTH components. Furthermore, there is no trend showing at what percentage of maximum femur axial force the various KTH components fractured at over the range of hip postures considered. This indicates that pre-crash hip posture does not play a direct role in determining risk to injury of the KTH region. This is possibly because the occupant's hip posture is changed significantly during the time immediately leading up to the knee bolster impact. This would explain why this project did not observe the same kinds of trends as Rupp (2003).

One possible parameter that may play a more direct role in determining an occupant's risk to injury of the KTH region is occupant kinematics during the crash event. Recall that there were two main impact scenarios observed in this project: a direct impact when both of the occupant's knees impacted the bolster directly and pushed upward on it, and an indirect impact when the occupant's left knee behaved the same as in the direct impact but, the right knee slid downward long the plane of the bolster. A review of the maximum axial force data and the axial force at time of initial fracture data shows that maximum axial force and occurrence of fracture is significantly decreased in the indirect impact scenarios. Tables 11 and 12 summarize these findings.

Table 11: Comparison of Maximum Femur Axial Forces in Direct and Indirect Impacts

Left Leg	Average Maximum Femur Force (kN)	Standard Deviation (kN)
Direct Impact	7.12	1.94
Indirect Impact	8.89	1.03
Right Leg	Average Maximum Femur Force (kN)	Standard Deviation (kN)
Direct Impact	7.81	1.86
Indirect Impact	6.12	1.31

Table 12: Percent Occurrence of Right Leg Fracture in Direct and Indirect Impacts

	Acetabulum	Femoral Head	Femoral Neck	Proximal Shaft	Mid-Shaft	Femoral Condyles
Direct Impact	100	50	50	50	23	23
Indirect Impact	77	7.7	0	15	7.7	0

The results in Tables 11 and 12 show that indirect impacts result in smaller axial forces in the right leg, and decreased occurrence of fracture in the right leg compared to direct impacts. Furthermore, the indirect impacts result in less variability in maximum femur axial force for all the hip postures considered compared to the direct impacts. Finally, the results indicate that the decrease in femur axial force in the right leg during an indirect impact leads to an increase in force in the left leg. These results suggest that occupant kinematics, particularly the interaction between the knee and the knee bolster, play a direct role in determining risk of injury to the KTH region.

The reason that some impact scenarios were direct while others were indirect may be explained by looking at the time histories for the resultant contact force between the feet and the floor. Figure 54 and 55 compare the time histories for the neutral impact (direct) and the 10° abduction impact (indirect).

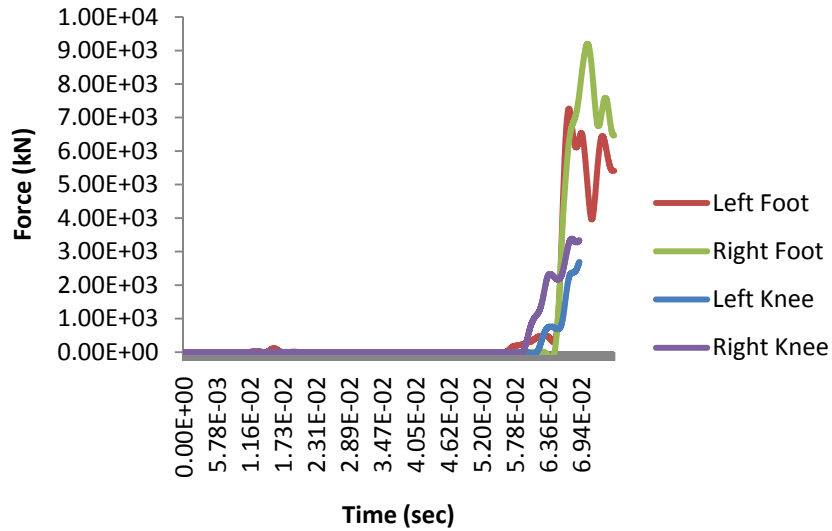


Figure 54: Resultant Foot Contact Force for Neutral Posture Impact (Direct)

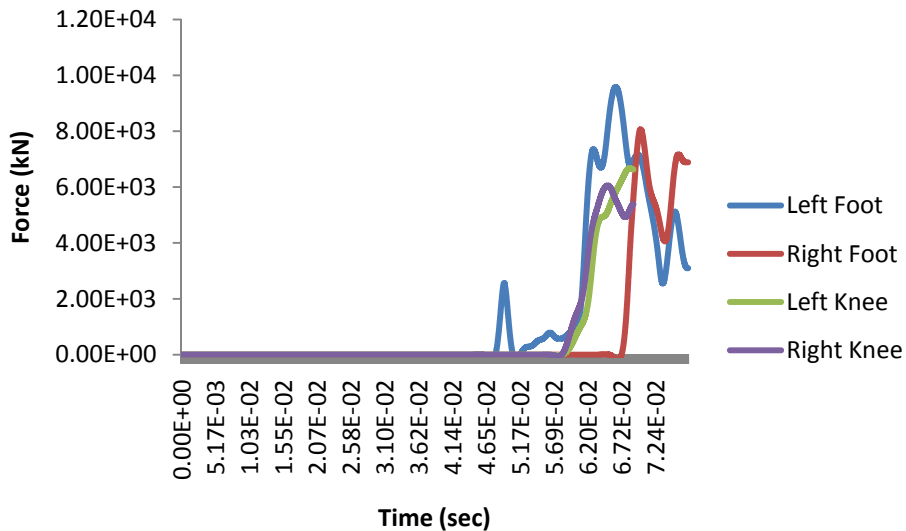


Figure 55: Resultant Foot Contact Force for 10° Abduction Posture Impact (Indirect)

Note that in Figure 54, the feet contact the floor and the knees contact the bolster all at nearly the same time, while in Figure 55, the left foot contacts the floor much earlier than the right and the knees contact the bolster at nearly the same time that the left foot contacts the floor. Because the right foot has not contacted the floor when the right knee impacts the bolster, the right leg is able to move downward along

the bolster upon impact. The left foot on the other hand impacts the floor earlier, so when the left knee impacts the bolster, it cannot slide downwards and must more directly impact it, absorbing more force. In general, this trend was observed for all direct and indirect impact scenarios. The foot contact force time histories for all the simulations are provided in Appendix A.

Comparison of Sled Test and Vehicle Simulations

The results of the parametric investigation indicate the occupant kinematics during impact play a large role in determining an occupant's risk to injury during a frontal impact. Because of this, the kinematics experienced by the FE KTH was compared in the sled test and vehicle simulations. A detailed explanation of the injuries resulting from the sled test simulations is provided by Silvestri (2009). In general, the FE KTH experienced more widespread injury in the vehicle simulations than in the sled test simulations.

The main difference between occupant kinematics in the sled test and vehicle simulations involves the foot contact force with the floor. In the sled test, both feet are positioned on the floor surface that they are to impact, resulting in a direct impact scenario. Figure 56 compares the positioning of the feet in the sled test and the vehicle simulations.

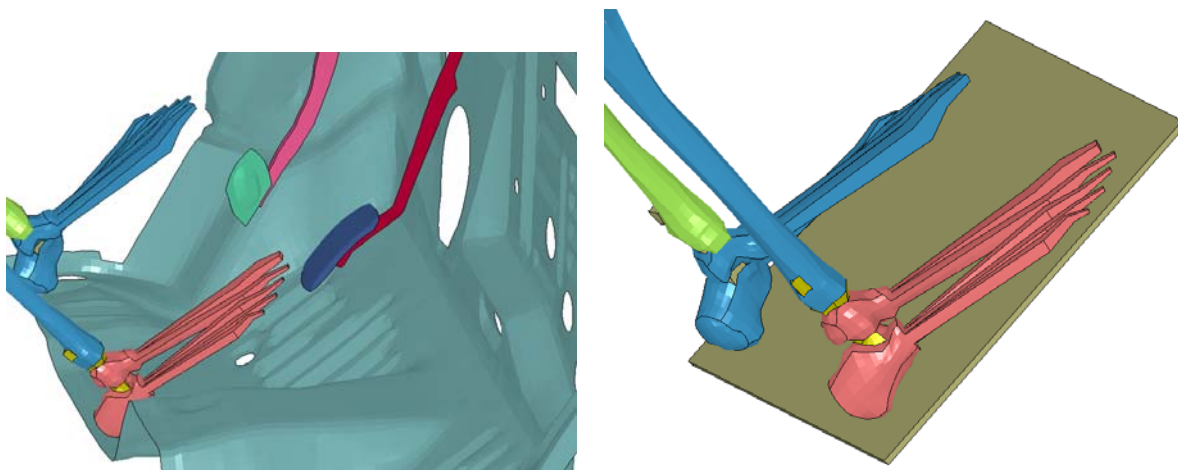


Figure 56: Comparison of Floor Placement in Vehicle Simulation (left) and Sled Test Simulation (right)

Note the extra horizontal distance the right foot can travel in the vehicle simulation compared to the sled test simulation. This difference in occupant kinematics suggests that sled tests provide conservative

results compared to full vehicle simulations because an indirect impact is less likely in the sled test environment.

Remarks

This section has shown the results obtained in this project. First, it was shown that the vehicle-occupant simulation modeling methodology was appropriate because the femur axial forces obtained in the simulations were comparable to what has been observed in physical tests (approximately seven kN). Next, the results of the parametric study were presented. The results indicate that there is not a strong trend between injury tolerance and pre-crash hip posture. They do however suggest that contact force time histories between the feet and the floor may influence risk to injury by affecting the impact mechanism between the knee and the knee bolster (direct or indirect). Finally, it was shown that sled tests differ from vehicle collisions in the manner in which the test subject is positioned at the start of the test. This affects the impact scenario between the knee and the knee bolster (direct or indirect), and can affect measured femur axial force and likelihood of injury.

Conclusions and Discussion

This project studied injury to the KTH region by simulating a FE KTH model as an occupant in a FE Ford Taurus model during a frontal impact event. A range of pre-crash hip postures was investigated. Also, differences in occupant kinematics were noted in the vehicle simulations and in a standard laboratory sled test simulation.

The results of this study do not show a strong correlation between injury tolerance and pre-crash hip posture. Rupp (2003) showed that hip posture affects injury tolerance by testing the injury tolerance of cadavers positioned with a neutral, adducted, or flexed hip posture. The results of this study indicate that an occupant's posture is changed drastically enough during the impact event to make the effects described by Rupp negligible. The study did find that the impact scenario (direct or indirect) does affect risk of KTH injury. When the feet contact the floor at a similar time as the knees impact the bolster, a direct impact scenario results, which involves higher femur axial forces and injury rates. If there is lag time between when the knees impact the bolster and the feet impact the floor, the leg is able to slide downward along the bolster, and an indirect impact scenario occurs, which results in lower femur forces and injury occurrences. It should be noted that having this lag time is not necessarily desirable as it can lead to increased risk to ligament injuries (Meyer, 2003). This phenomenon should be studied in the future. Silvestri and Heath (2010) provide a framework for revising the FE KTH to capture these effects. Additionally, increased lag time between foot-floor and knee-bolster impacts may affect the load distribution in the tibia. This is another phenomenon that should be studied in future work.

The phenomenon of direct or indirect impact scenarios should be investigated in greater detail. Research in this area could involve studying the effects of making the floor deeper so that the feet contact it at a later time during the impact event. Alternatively, a highly deformable material could be placed over the floor, which would decrease the rate at which the foot-floor contact force increases. This may provide a means for the knee to move downward along the knee bolster upon initial impact.

Future work could also consist of studying occupant kinematics in more detail. Topics may include studying the effect of different restraint conditions (airbags, seatbelts, etc.), seating location (driver's seat, passenger's seat, back seat), vehicle type (sedan, utility vehicle, truck, etc.), or occupant size. Because the initial conditions of an impact event are very difficult to predict, a good understanding of occupant kinematics must be developed across a wide range of parameters that affect response. Fortunately, occupant kinematics studies could most likely be carried out with a less detailed occupant model, which would facilitate studying a wide range of parameters by decreasing required computation time.

Hip dislocation was not observed in this study. Because hip dislocation is a common KTH injury during frontal crashes, it is likely that the FE KTH needs to be improved to capture this type of injury. Improvements may need to be made to the hip ligament modeling or cartilage may need to be included at the hip joint.

The results of this project indicate that sled tests result in conservative impact scenarios compared to actual vehicle collisions. This is because sled tests are more likely to result in a direct impact scenario because the test specimen is positioned with its feet already resting on the impact surface. In contrast, in a vehicle crash, the occupant's feet are likely to be able to travel some distance along the floor before reaching the impacting surface, increasing the likelihood of an indirect impact. The conservative results inherent in a sled test are likely to be acceptable from a regulatory point of view.

Additional experimental work would be very beneficial in continuing analytical research in injury studies. Additional physical tests are needed to improve the validation process for numerical models. One motivation for the additional physical tests is that analysts do not have a way of determining different parameters at the moment when fracture initiates in a test (e.g. forces, displacements, etc.). The results of the physical tests usually consist of a single curve, showing for example a force time history, that the analytical model can be validated against. If the analyst however wants to determine at what time fracture initiated, there is no way of validating the time predicted in the model with observations from a physical test. Methods of recording this kind of information in physical tests, such as high speed cameras or x-ray

technology, should be investigated in the future. Also, physical tests should have better documentation of their initial setups (e.g. distances from impacting surfaces). Finally, availability of the results of physical tests should be increased so that analysts can validate their models against more tests.

Researchers should continue to try to mitigate risk to KTH injuries. This can be done by making necessary improvements to vehicle safety regulatory policy, providing guidelines to vehicle manufacturers for designing safer occupant compartments, and educating the public on the risks of various driving behaviors. Although the high variability associated with possible impact scenarios and the corresponding risk to injury makes this an arduous task, it is an achievable one. This is evident from the improvements in occupant restraint technology in reducing head and chest injuries, which had typically resulted in death. Continued research in the field of lower extremity injuries could drastically reduce their occurrence in a similar way. This would not only reduce the economic burden on society in providing medical care to victims, but also improve the lives of would be victims by decreasing the prevalence and severity of injury.

References

Agarwal, Shefalika. *Final Report of New Car Assessment Program Testing of a 2004 Ford Taurus SE*.

Rep. no. NCAP-MGA-2004-001. Burlington, WI: MGA Research Corporation, 2003. Print.

Bidewi, Paul G., and Kennerly H. Digges. "Investigating Ankle Injury Mechanisms in Offset Frontal Collisions Utilizing Computer Modeling and Case-Study Data." *43rd Stapp Car Crash*

Conference Proceedings (1999): 217-42. Web.

BioMed Central | The Open Access Publisher. Web. 15 Mar. 2010. <<http://biomedcentral.com>>.

Blincoe, L., A. Seay, E. Zaloshnja, T. Miller, E. Romano, S. Luchter, and R. Spicer. *The Economic Impact of Motor Vehicle Crashes 2000*. Tech. no. DOT HS 809 446. Washington D.C.: U.S. Department of Transportation, 2002. Print.

"File:Knee Diagram.svg - Wikipedia, the Free Encyclopedia." *Main Page - Wikipedia, the Free Encyclopedia*. Web. 15 Mar. 2010. <http://en.wikipedia.org/wiki/File:Knee_diagram.svg>.

"Finite Element Model Archive." National Crash Analysis Center. Web. 06 May 2009.

Finite Element Model of Ford Taurus. Rep. FHWA/NHTSA/NCAC. Print.

Gabauer, Douglas, and Robert Thomson. "Correlation of Vehicle and Roadside Crash Test Injury Criteria." *Proceedings of the 19th Enhanced Safety Vehicles Conference* (2005). Web.

Gray, Henry, and Warren H. Lewis. *Anatomy of the Human Body*. Philadelphia: Lea & Febiger, 1918. Print.

Guha, Sarba, Dilip Bhalsod, and Jacob Krebs. *LSTC Hybrid III Dummies Positioning and Post Processing*. Rep. 2008. Print.

"HIP AND KNEE INFLAMMATIONS CHART FLEXIBLE LAMINATION [AN-9781587792625] - \$11.95 : Skeletons And More!" *Skeletons And More, Halloween Props Anatomical Models*. Web.

15 Mar. 2010.

<http://skeletonsandmore.com/cart/index.php?main_page=product_info&products_id=331>.

Jayaraman, Vijay M., Eric T. Sevensma, Masaya Kitagawa, and Roger C. Haut. "Effects of Anterior Posterior Constraint on Injury Patterns in the Human Knee During Tibial-Femoral Joint Loading from Axial Forces through the Tibia." *Stapp Car Crash Journal* 45 (2001): 449-68. Print.

Koch, J. C. "The Laws of Bone Architecture." *The American Journal of Anatomy* 21 (1917): 177-298. Web.

Kuppa, Shashi, Fessahaie, Osvaldo. "An Overview of Knee-Thigh-Hip Injuries in Frontal Crashes in the United States." Proc. of 18th International Technical Conference on Enhanced Safety of Washington D.C.: National Highway Traffic Safety Administration, 2003. 1-15. Print.

Kuppa, Shashi, Jing Wang, Mark Haffner, and Rolf Eppinger. "Lower Extremity Injuries and Associated Injury Criteria." Proc. of 17th International Technical Conference on Enhanced Safety of Vehicles in Amsterdam, The Netherlands. Washington D.C.: National Highway Traffic Safety Administration, 2001. 1-15. Print.

"Ligament and Tendon Structure and Function." *Michigan Engineering / College of Engineering - Home*. Web. 15 Mar. 2010. <<http://www.engin.umich.edu/class/bme456/ligten/ligten.htm>>.

"LS-PrePost Online Documentation." Livermore Software Technology Corporation. Web. 06 May 2009.

Martinon-Torres, Maria. "Quantifying Trabecular Orientation in the Pelvic Cancellous of Modern Humans, Chimpanzees, and the Kebara 2 Neanderthal." *American Journal of Human Biology* 15.5 (2003): 647-61. Web.

"Mechanical Properties of Bone." *FEPPD - Federation of European and International Dental Technicians*. Web. 15 Mar. 2010. <http://www.feppd.org/ICB-Dent/campus/biomechanics_in_dentistry/ldv_data/mech/basic_bone.htm>.

- Meyer, Eric G., Michael T. Sinnott, and Roger C. Haut. "The Effect of Axial Load in the Tibia on the Response of the 90 Degree Flexed Knee to Blunt Impacts with a Deformable Interface." *Stapp Car Crash Journal* 48 (2004): 53-70. Print.
- Perfect, S. A., J. A. Weiss, and D. A. Schauer. "Finite Element Modeling of the Human Anatomic Pelvis and Leg." *NHTSA* (1997). Web.
- Silvestri, C., Heath, D., Ray, M. "An LS-DYNA® Model for the Investigation of the Human Knee Joint Response to Axial Tibial Loadings." *Proc. 11th International LS-DYNA Users Conference*, Detroit, MI (2010).
- Silvestri, C., Heath, D., Ruparel, T., Ray, M. "Validation of a Biofidelic LS-DYNA Model and comparison versus a traditional ATD Finite Element Model for Assessing Knee-Thigh-Hip Injuries." *International Journal of Vehicle Safety* [In Review].
- C. Silvestri, and Ray, M. H. "Development of a Finite Element Model of the Knee-Thigh-Hip of a 50th Percentile Male Including Ligaments and Muscles." *International Journal of Crashworthiness* 14.2 (2009): 215-29. Print.
- Silvestri, Chiara. "Development and Validation of a Knee-Thigh-Hip LSDYNA Model of a 50th Percentile Male." Diss. Worcester Polytechnic Institute, 2008. Print.
- Rupp, J. A. *Discretionary Cooperative Agreement in Support of Biomechanical Research - KTH Injury Investigations*. Rep. no. NB0221. Ann Arbor: University of Michigan Transportation Research Institute (UMTRI), 2002. Print.
- Rupp, J. D., M. P. Reed, C. A. Van Ee, S. Kuppa, S. C. Wang, J. A. Goulet, and L. W. Schneider. "The Tolerance of the Human Hip to Dynamic Knee Loading." *Stapp Car Crash Journal* 45 (2002): 211-28. Print.

Rupp, Jonathan D., Matthew P. Reed, Thomas A. Jeffreys, and Lawrence W. Schneider. "Effects of Hip Posture on the Frontal Impact Tolerance of the Human Hip Joint." *Stapp Car Crash Journal* 47 (2003): 21-33. Print.

Trauma.org / Home. Web. 15 Mar. 2010. <<http://trauma.org>>.

Viano, D. C. "Bolster Impacts to the Knee and Tibia in Human Cadavers and an Anthropomorphic Dummy." *Proceedings of the 22nd Stapp Car Crash Conference* (1978). Web.

Appendix A: Raw Data from Parametric Simulations

This appendix provides all the raw data from the parametric simulations. It provides all of the data used to develop the conclusions presented in this chapter, and to identify the trends presented in the results chapter. When reviewing the data, keep the following contact and femur axial force definitions in mind:

Contact Definitions:

I.D.=99100: Left patella - Dash
I.D.=9100: Left patella - Dash
I.D.=99101: Right patella- Knee bolster
I.D.=99102: Left tibia – Dash
I.D.=9101: Right patella – Knee bolster
I.D.=99103: Right tibia - Dash
I.D.=99104: Right tibia – Knee bolster
I.D.=9102: Left tibia – Knee bolster
I.D.=9103: Right tibia – Knee bolster
I.D.=9111: Left foot - floor
I.D.=9114: Right foot floor

Femur Forces:

I.D.=9100

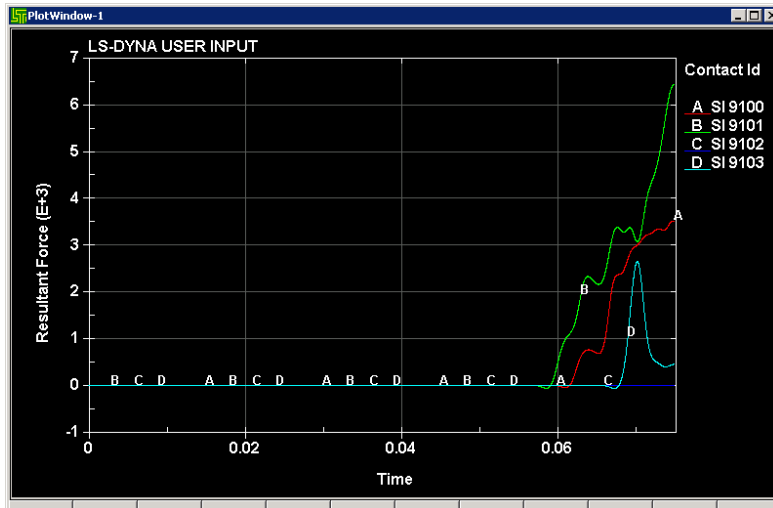


The femur axial forces were measured at the highlighted sections in the above figure. I.D.s 5-8 are on the left leg and start at the knee and move towards the hip. I.D.s 9-12 are on the right leg and move from the hip towards the knee.

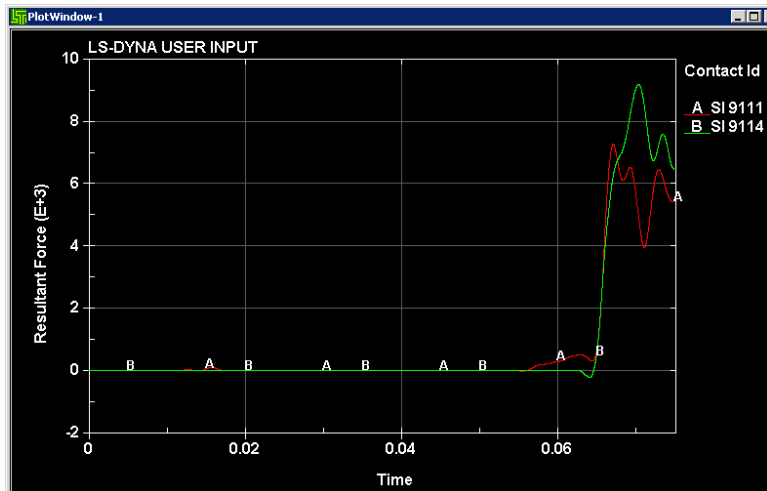
Neutral Results Summary

Summary: Patella fracture occurred shortly after contact with knee bolster. Little correlation between maximum femur forces and foot contact forces. Right leg experienced higher force and more serious injury. Upon contact with the bolster, the knee flexion angle decreased (approached 90°). The feet and knee bolster contacted the vehicle while the buttocks and torso continued moving forward; little change in flexion angle occurred. The femurs appeared to rotate in the acetabulum as a result of the knees moving upward along the bolster. Upon initial contact with the bolster, the knees slid down along it. As the impact force increased, the knees pushed the bolster upwards, fracture occurred when the knees began moving up.

Contact Forces:

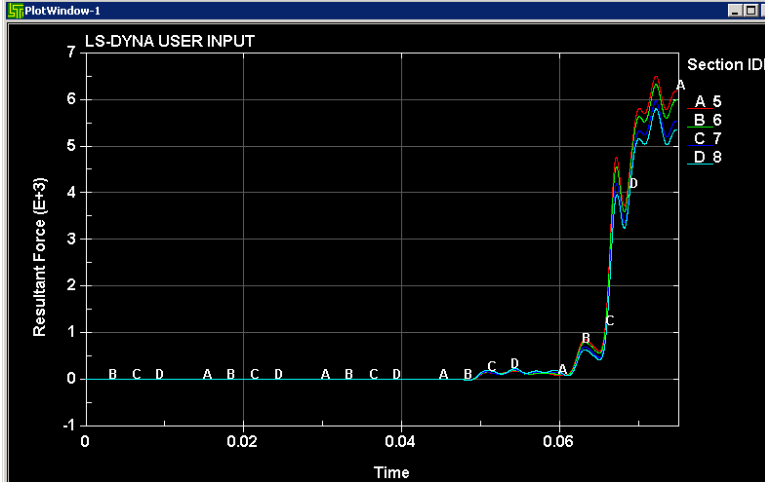


Knee – Bolster Contact



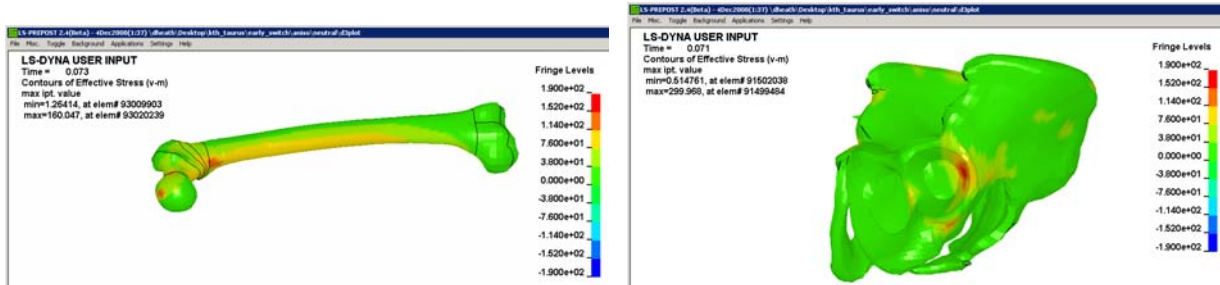
Foot – Floor Contact

Femur Axial Forces

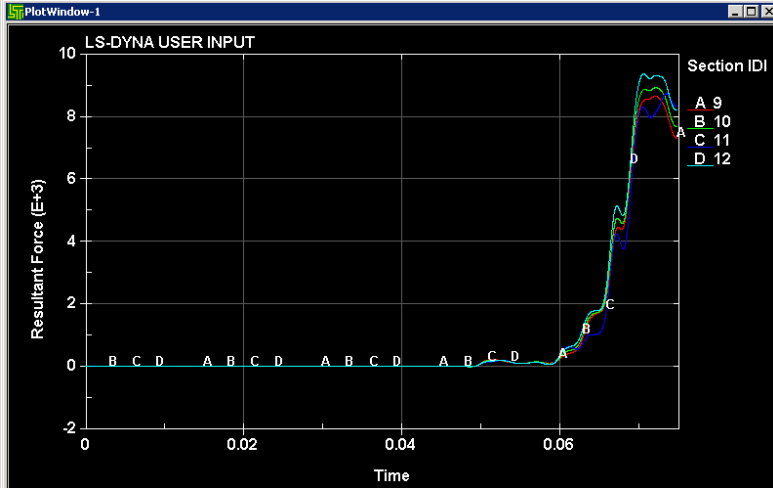


Left Femur Axial Forces

Fracture Force Summary: Left Acetabular Cup Fracture at t=0.069 sec, femur axial force = 4.55 kN; fracture spread to femur, maximum stresses occurred at the femoral head and proximal femoral shaft (~160 MPa) at t=0.073 sec. Peak force=6.48 kN, time=0.072

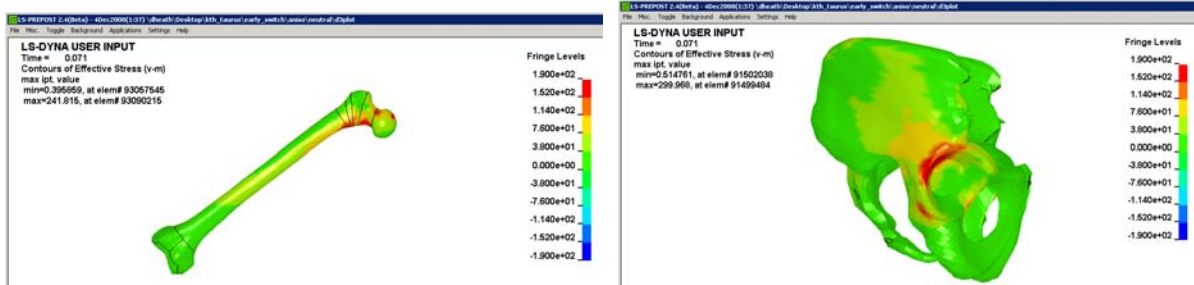


Left KTH Fracture States at Max. Stress



Right Femur Axial Forces

Fracture Forces Summary: Right acetabular cup fracture at t=0.068 sec, femur axial force = 4.83 kN; fracture spread to acetabular rim. Fracture occurred to the femoral head at time=0.07 sec, force = 9.19 kN. Fracture occurred to the anterior and posterior femoral neck and proximal femoral shaft at time=0.071 sec, force=9.22 kN. Peak force=9.36 kN, time=0.071

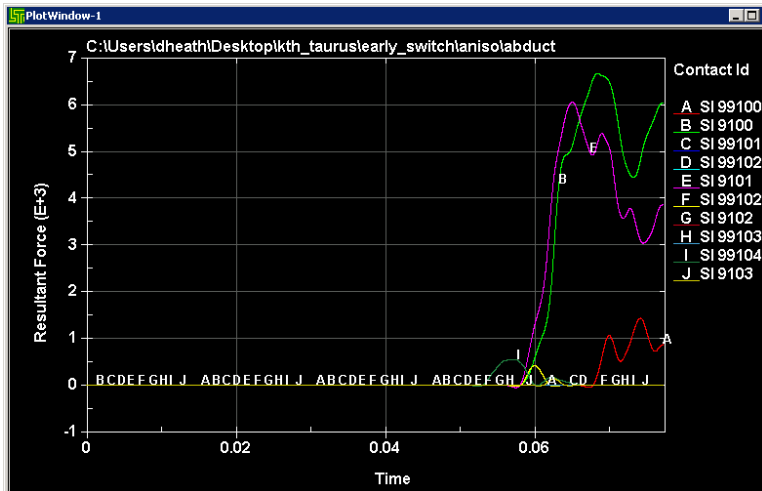


Right KTH Fracture State at Max. Stress

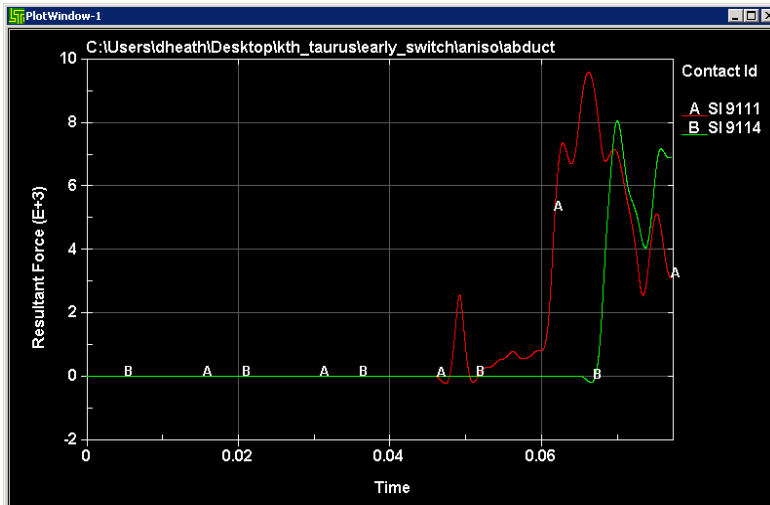
Abduct10° Results Summary

Summary: Patella fracture occurred shortly after contact with knee bolster. Little correlation between maximum femur forces and foot contact forces, but there is correlation between knee contact forces and foot contact force. Left leg experienced higher force and more serious injury, though the right acetabulum experienced fracture first. Upon contact with the knee bolster, the right knee slid under it, causing it to be “trapped” between the bolster and the floor; the right femur appeared to rotate downward in the acetabulum as a result of the knees moving downward along the bolster. The left knee had a more direct impact with the bolster and did not slide along it as much as the right; some upward rotation occurred. The time of left femoral fracture corresponded to the knee moving up.

Contact Forces

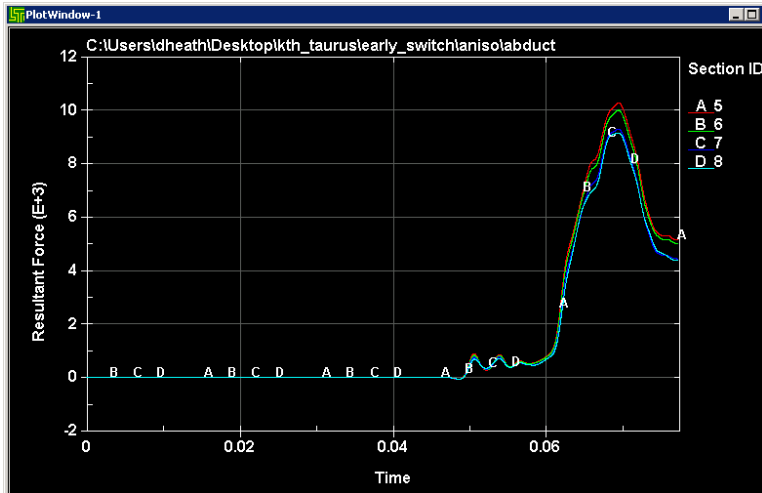


Knee Bolster Contact Forces



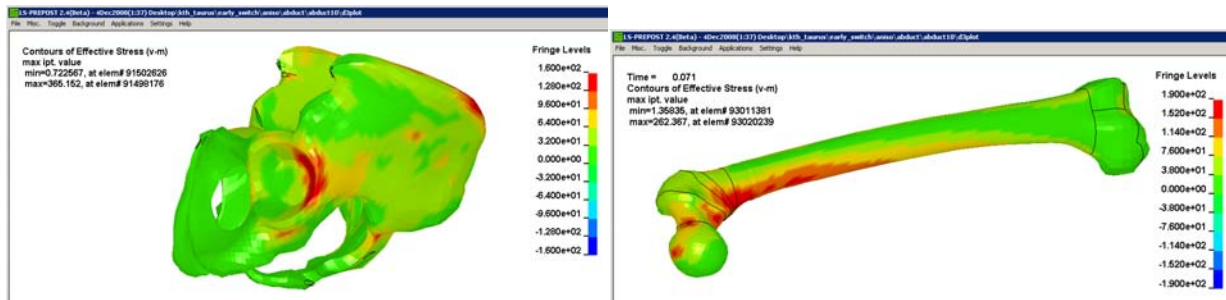
Foot Contact Forces

Femur Forces

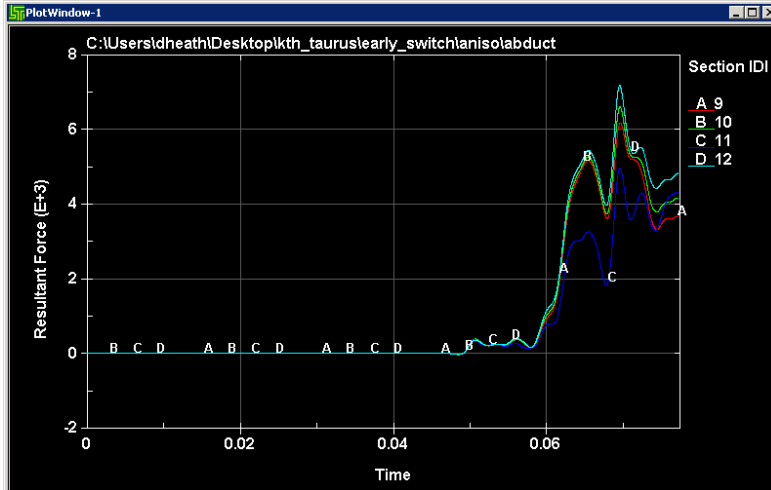


Left Leg Femur Axial Forces

Fracture Force Summary: Left Acetabular Cup Fracture at $t=0.064$ sec, femur axial force = 5.99 kN; fracture spread to acetabular rim. Fracture occurred to the femoral head, anterior and posterior femoral neck and proximal femoral shaft at time= 0.068 sec, force = 9.74 kN. Fracture occurred to the fifth point of the femoral shaft (measured from the hip) at time= 0.071 sec, force= 9.20 kN (this occurred after the peak force). Peak force= 10.3 , time= 0.070 .

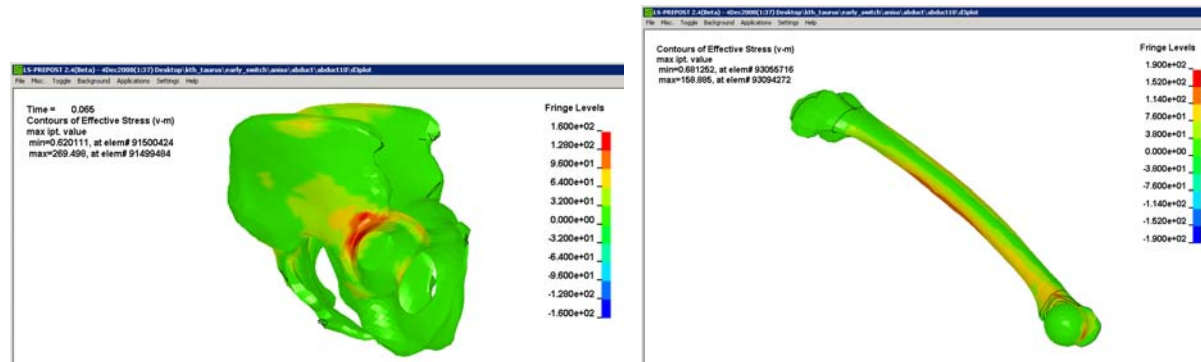


Left Leg Stresses at time of Max. Stress (t=0.72 sec pelvis)



Right Leg Femur Axial Forces

Fracture Force Summary: Right Acetabular Cup Fracture at $t=0.063$ sec, femur axial force = 4.22 kN; fracture spread to acetabular rim. Fracture did not occur to the femur. Maximum stress occurred to the femoral head, proximal shaft, and midshaft at $t=0.071$, stress ~ 160 MPa, force=5.49 kN (post peak). Peak force=7.12 kN, time=0.070.

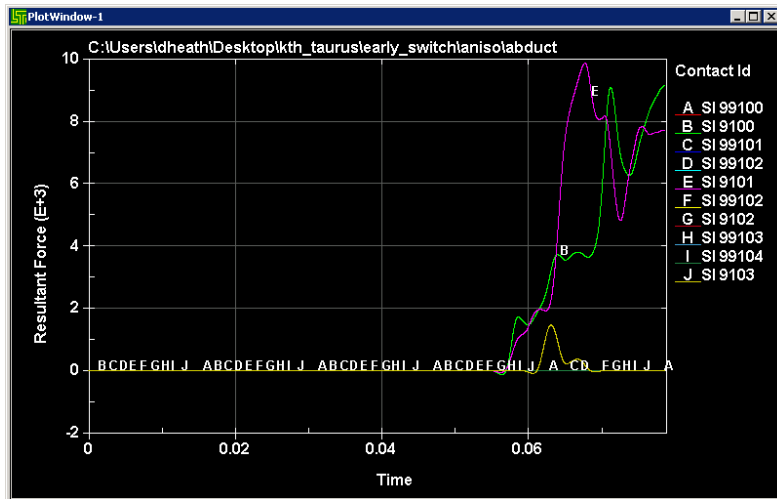


Right Leg Stresses at time of Max. Stress (t=0.71 sec femur)

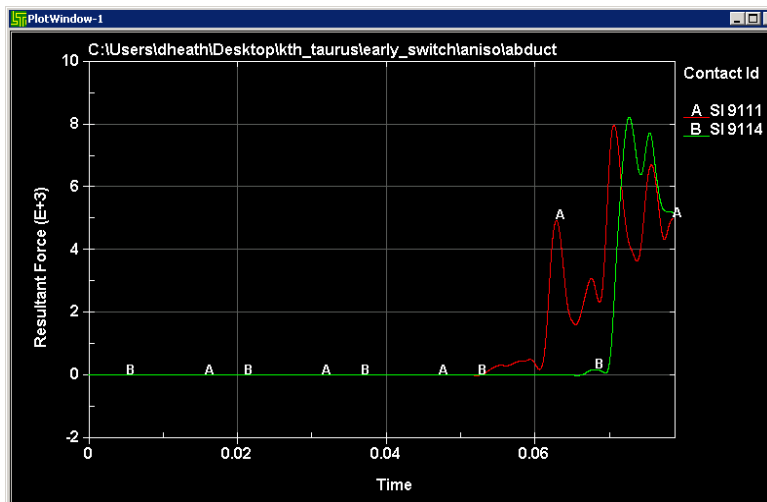
Abduct5° Results Summary

Summary: Patella fracture occurred shortly after contact with knee bolster. Signs of correlation between maximum femur forces and foot contact forces (both occurred t~0.07 sec). Left leg experienced higher force and more serious injury, though the right leg experienced fracture first both in the femur and the pelvis. Upon contact with the knee bolster, the right knee slid under it, causing it to be “trapped” between the bolster and the floor, though this was less pronounced than in the 10° case. The left knee had a more direct impact with the bolster and did not slide along it as much as the right; some upward rotation occurred. The time of left femoral fracture corresponded to the knee moving up.

Contact Forces

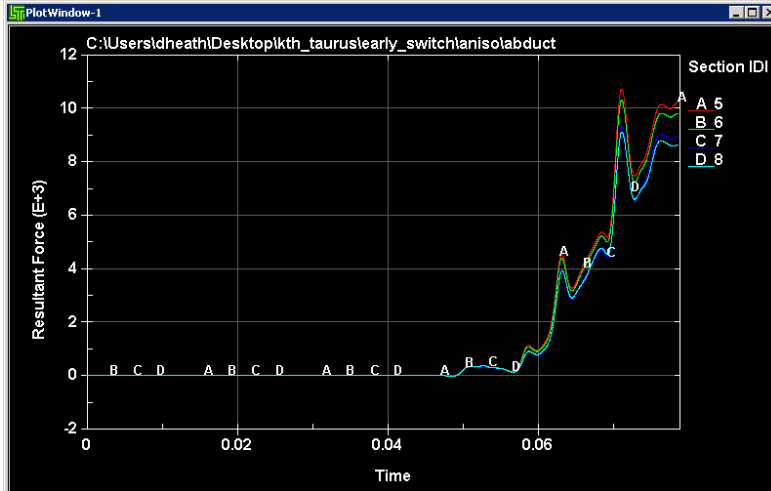


Knee Bolster Contact Forces



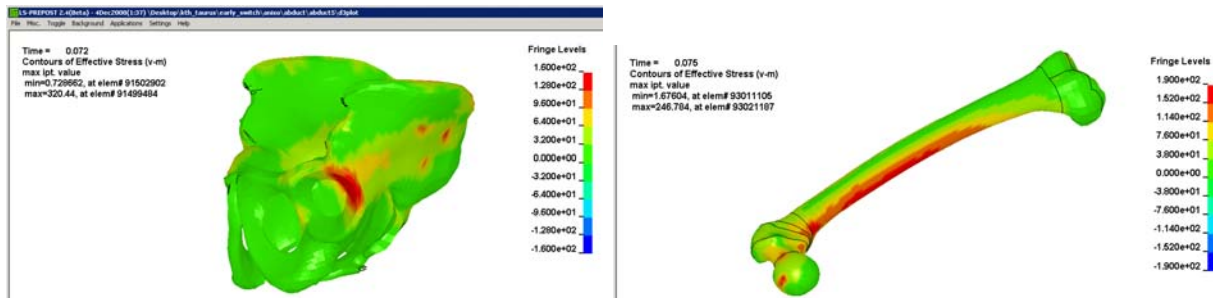
Foot Contact Forces

Femur Forces



Left Leg Femur Axial Forces

Fracture Force Summary: Left Acetabular Cup Fracture at $t=0.067$ sec, femur axial force = 4.59 kN; fracture spread to acetabular rim. Fracture occurred to the femoral head at time= 0.072 sec, force = 9.05 kN (after peak). Fracture occurred to the proximal femoral shaft at time= 0.074 sec, force= 8.09 kN (after peak). The midsection of the femoral shaft fractured at $t=0.75$ sec, force= 8.98 kN (after peak). Peak force= 10.5 , time= 0.071 sec. Peak force= 10.7 , time= 0.071 .

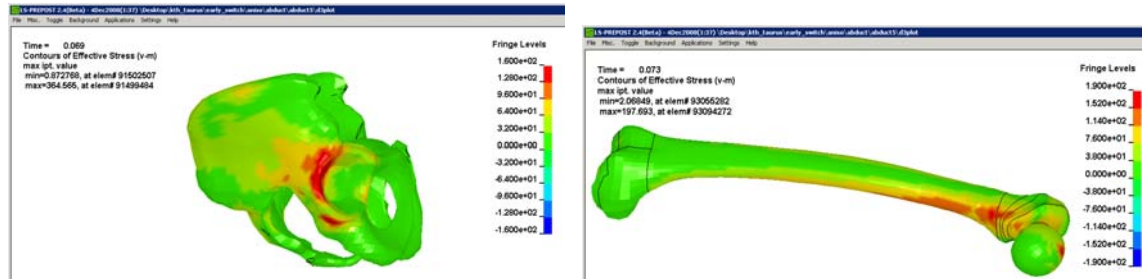


Left Leg Stresses at time of Max. Stress



Right Leg Femur Axial Forces

Fracture Force Summary: Right Acetabular Cup Fracture at $t=0.064$ sec, femur axial force = 4.09 kN; fracture spread to acetabular rim. Fracture occurred to the femoral head at time= 0.067 sec, force = 8.14 kN. Fracture occurred to the proximal femoral shaft at time= 0.72 sec, force= 8.56 (after peak). Peak force= 8.76 kN, time= 0.068 sec. Peak force= 8.79 , time= 0.068 .



Right Leg Stresses at time of Max. Stress (t=0.71 sec femur)

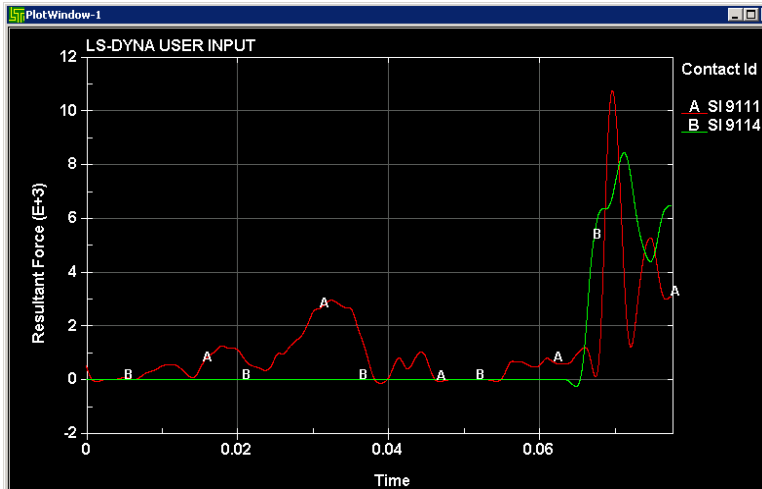
Adduct5° Results Summary

Summary: Patella fracture occurred shortly after contact with knee bolster. Signs of correlation between maximum femur forces and foot contact forces (both occurred t~0.07 sec). The right leg experienced higher force, however the left experienced more serious injury (pelvis and femur fracture). Upon contact with the knee bolster, both knees had a direct impact with the bolster and pushed it upward, causing some upward rotation. The time of left femoral fracture corresponded to the knee moving up. This was more pronounced in the right leg.

Contact Forces

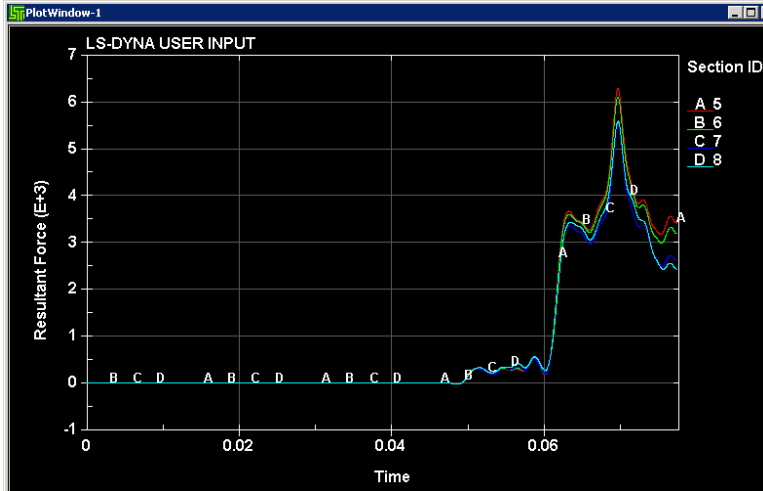


Knee Bolster Contact Forces



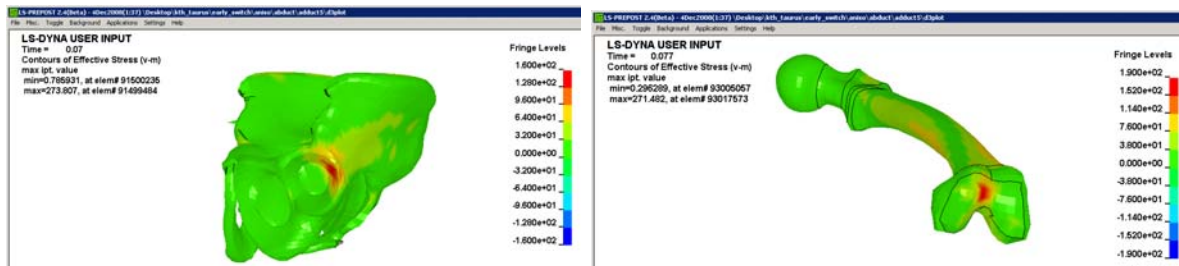
Foot Contact Forces

Femur Forces

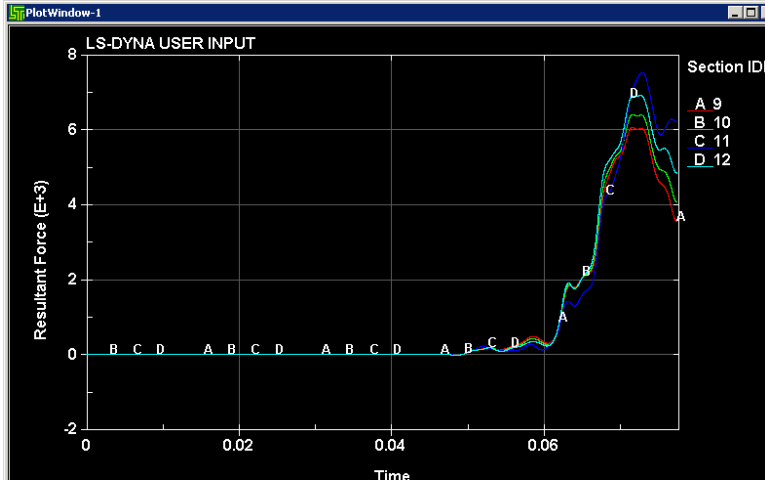


Left Leg Femur Axial Forces

Fracture Force Summary: Left Acetabular Cup Fracture at $t=0.064$ sec, femur axial force = 3.58 kN; fracture **did not** spread to acetabular rim. Fracture occurred to the medial femoral condyle at $t=0.078$ sec, force = 3.50 kN (after peak). Maximum stress in the proximal femoral shaft and greater trochanter occurred at $t=0.074$ sec, force=8.09 kN (after peak). Peak force=6.20 kN, time=0.070 sec.

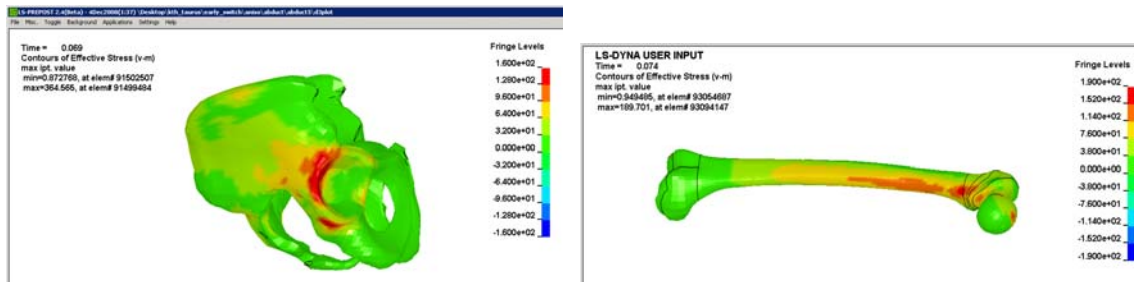


Left Leg Stresses at time of Max. Stress



Right Leg Femur Axial Forces

Fracture Force Summary: Right Acetabular Cup Fracture at t=0.068 sec, femur axial force = 5.00 kN; fracture spread to acetabular rim. Fracture did not occur to the femur however, the stresses approach the threshold (Max. Stress=189.7 MPA). Stresses of this magnitude were observed on the femoral head and proximal shaft at time =0.074 sec, force=6.25 kN (after peak). Peak force=6.88 kN, time=0.072 sec.

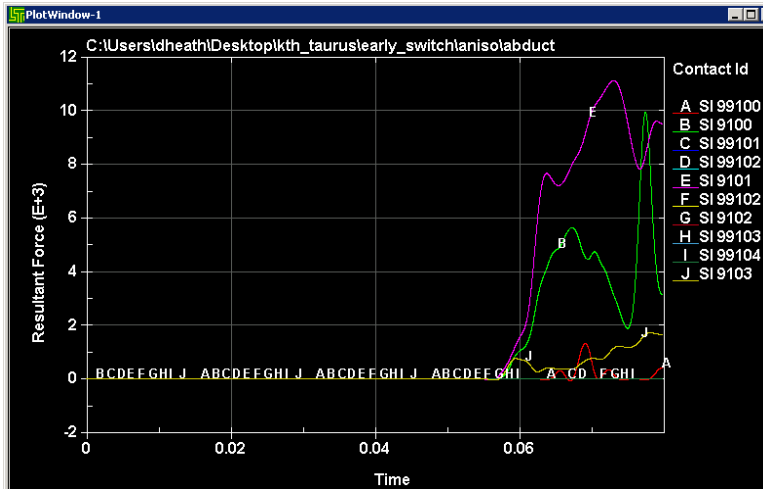


Right Leg Stresses at time of Max. Stress (t=0.71 sec femur)

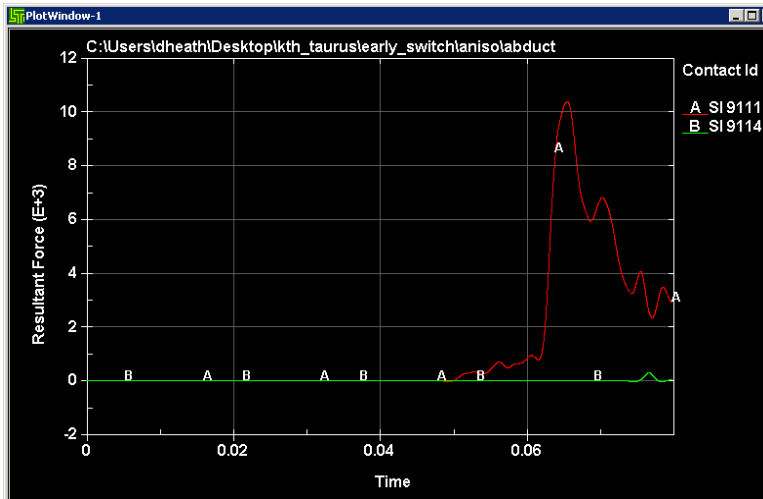
Adduct10° Results Summary

Summary: Patella fracture occurred shortly after contact with knee bolster. No sign of correlation between maximum femur forces and foot contact forces. The left leg experienced higher force, however the right experienced more serious injury (pelvis and femur fracture). Upon contact with the knee bolster, both knees had a direct impact with the bolster and pushed it upward, causing some upward rotation. The time of left femoral fracture corresponded to the knee moving up. They right foot did not contact the floor, and large relative displacements of the tibia and femur resulted, demonstrating the phenomenon described by Meyer.

Contact Forces

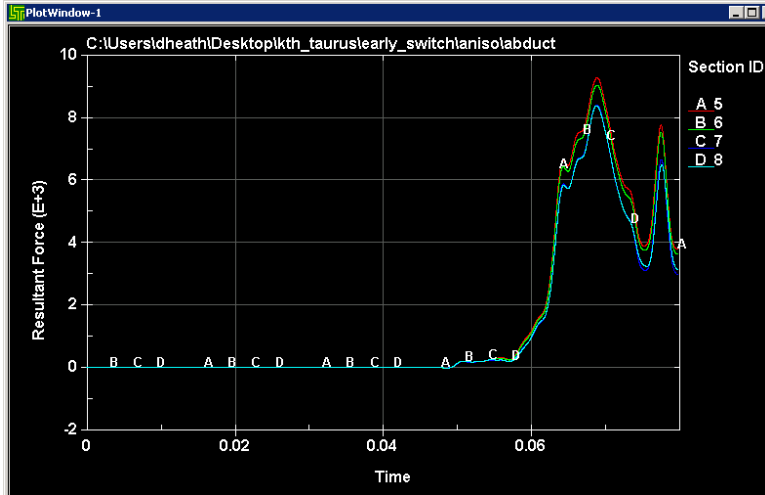


Knee Bolster Contact Forces



Foot Contact Forces

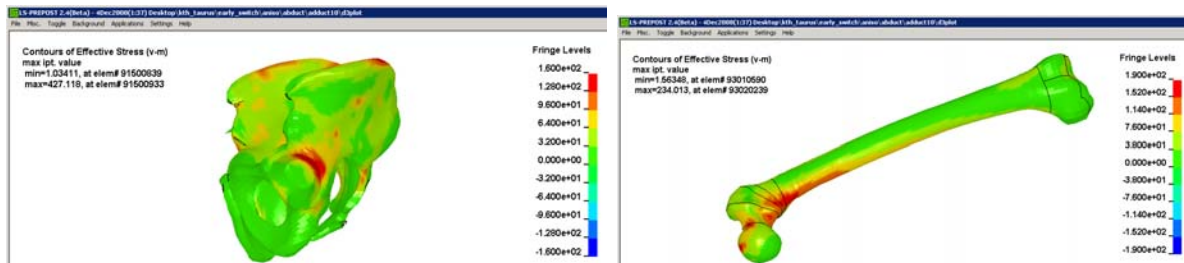
Femur Forces



Left Leg Femur Axial Forces

Fracture Force Summary:

Parameter	Time (sec)	Force (kN)	Notes
Peak Force	0.069	9.28	
Acetabulum	0.064	6.29	Spread to rim
Femoral Head	0.068	8.57	
Femoral Neck	0.069	9.28	
Trochanter			
Proximal Femur	0.068	8.57	
Femoral Shaft			
Femoral Condyle			



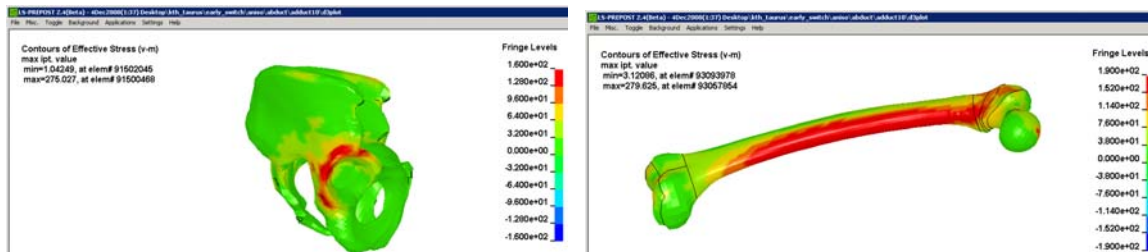
Left Leg Stresses at time of Max. Stress (t=0.069 for both)



Right Leg Femur Axial Forces

Fracture Force Summary: Right

Parameter	Time (sec)	Force (kN)	Notes
Peak Force	0.071	8.68	
Acetabulum	0.063	5.00	Spread to rim
Femoral Head	0.065	6.11	
Femoral Neck	0.065	6.11	
Trochanter			
Proximal Femur	0.068	8.57	
Femoral Shaft	0.071	8.68	
Femoral Condyle	0.066	6.62	Medial Condyle

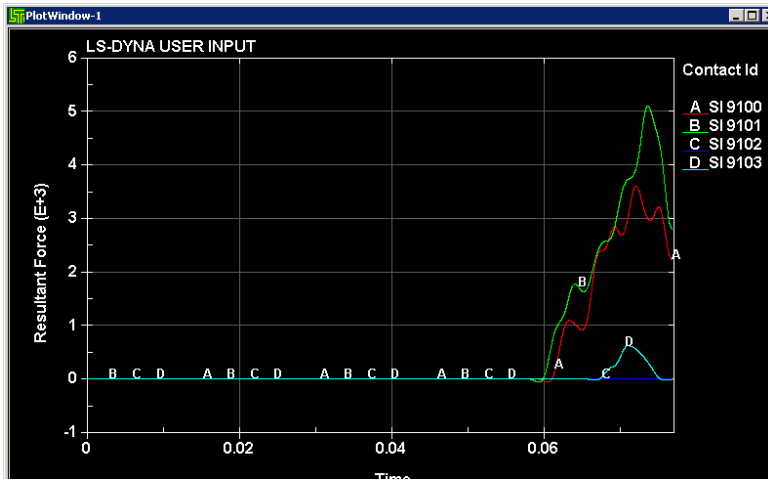


Right Leg Stresses at time of Max. Stress (t=0.77 sec pelvis and femur)

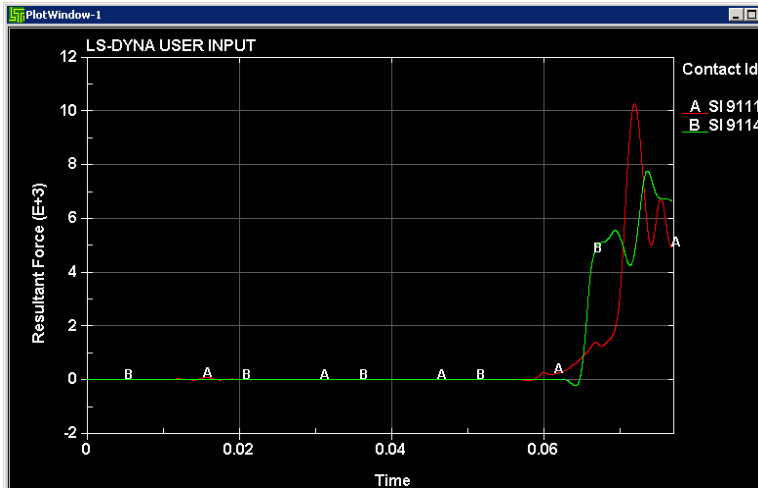
Flex7.5° Results Summary

Summary: Patella fracture occurred shortly after contact with knee bolster. Signs of correlation between maximum femur forces and foot contact forces (~0.07 sec). The left leg experienced higher force. Upon contact with the knee bolster, both knees had a direct impact with the bolster and pushed it upward, causing some upward rotation.

Contact Forces



Knee Bolster Contact Forces



Foot Contact Forces

Femur Forces



Left Leg Femur Axial Forces

Fracture Force Summary:

Parameter	Time (sec)	Force (kN)	Notes
Peak Force	0.071	7.76	
Acetabulum	0.073	5.97	After peak; spread to rim

Femoral Head

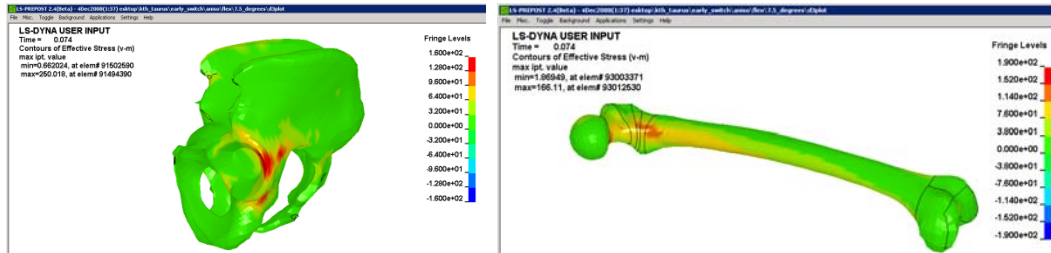
Femoral Neck

Trochanter

Proximal Femur

Femoral Shaft

Femoral Condyle



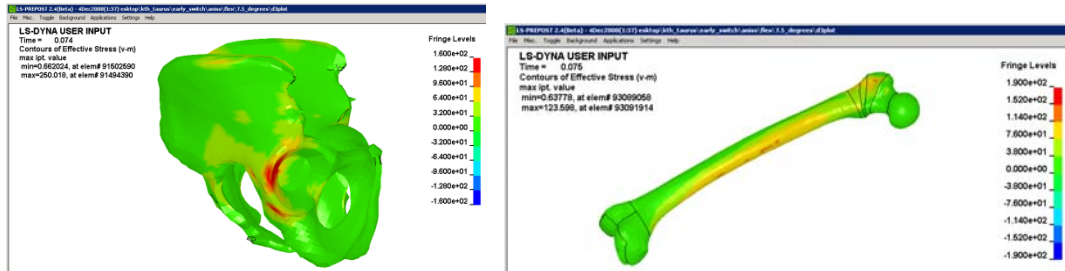
Left Leg Stresses at time of Max. Stress (t=0.069 for both)



Right Leg Femur Axial Forces

Fracture Force Summary: Right

Parameter	Time (sec)	Force (kN)	Notes
Peak Force	0.074	7.79	
Acetabulum	0.069	4.14	
Femoral Head			
Femoral Neck			
Trochanter			
Proximal Femur			
Femoral Shaft			
Femoral Condyle			

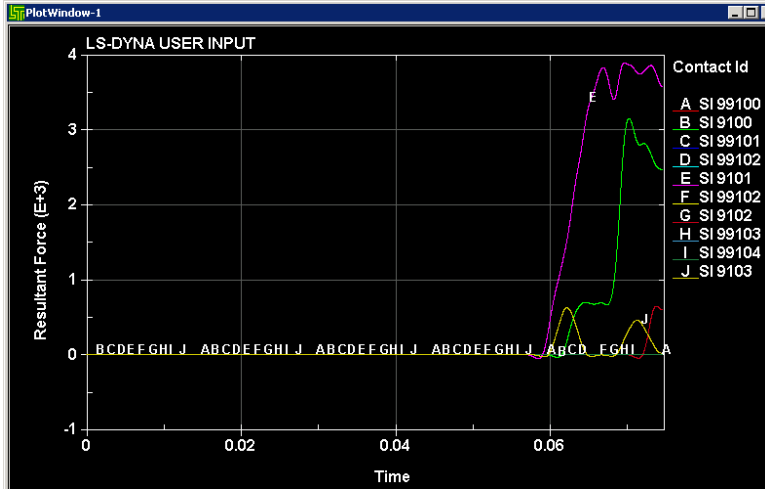


Right Leg Stresses at time of Max. Stress (t=0.77 sec pelvis and femur)

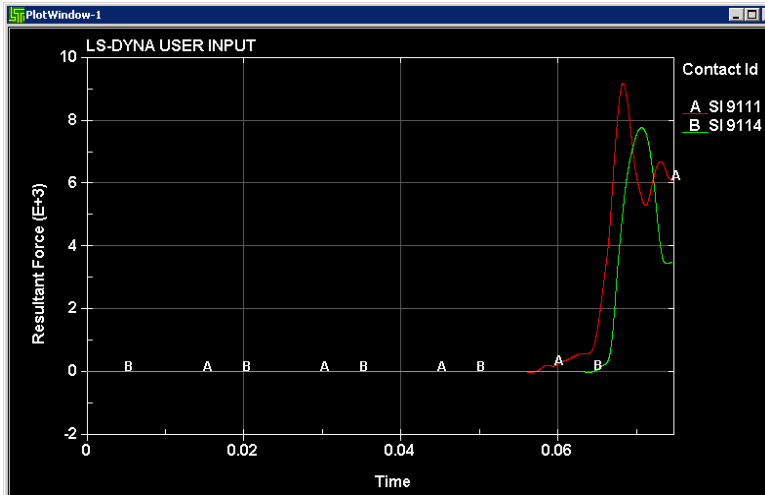
Flex15° Results Summary

Summary: Patella fracture occurred shortly after contact with knee bolster. Signs of correlation between maximum femur forces and foot contact forces (~0.07 sec). The right leg experienced higher force. Upon contact with the knee bolster, both knees had a direct impact with the bolster and pushed it upward, causing some upward rotation.

Contact Forces

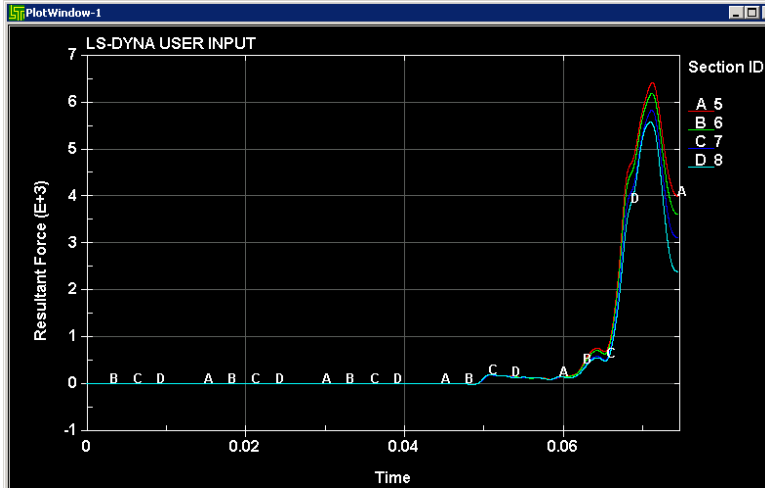


Knee Bolster Contact Forces



Foot Contact Forces

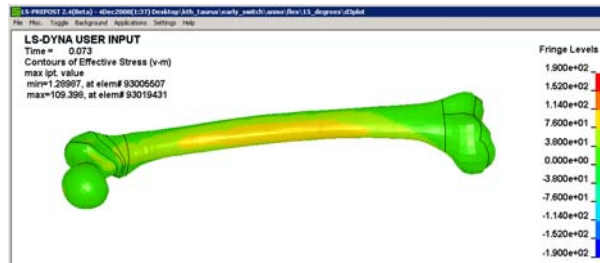
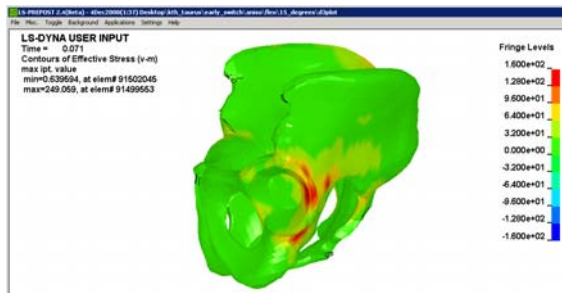
Femur Forces



Left Leg Femur Axial Forces

Fracture Force Summary:

Parameter	Time (sec)	Force (kN)	Notes
Peak Force	0.071	6.41	
Acetabulum	0.070	5.84	Spread to rim
Femoral Head			
Femoral Neck			
Trochanter			
Proximal Femur			
Femoral Shaft			
Femoral Condyle			



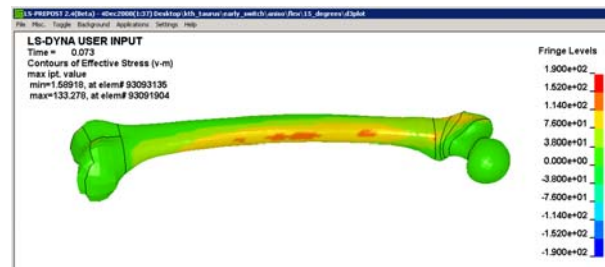
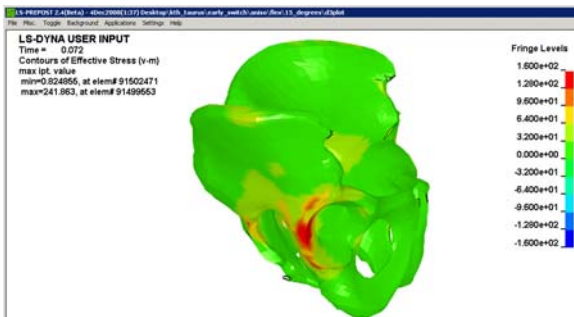
Left Leg Stresses at time of Max. Stress (t=0.069 for both)



Right Leg Femur Axial Forces

Fracture Force Summary: Right

Parameter	Time (sec)	Force (kN)	Notes
Peak Force	0.071	6.94	
Acetabulum	0.065	3.44	Spread to Rim
Femoral Head			
Femoral Neck			
Trochanter			
Proximal Femur			
Femoral Shaft			
Femoral Condyle			

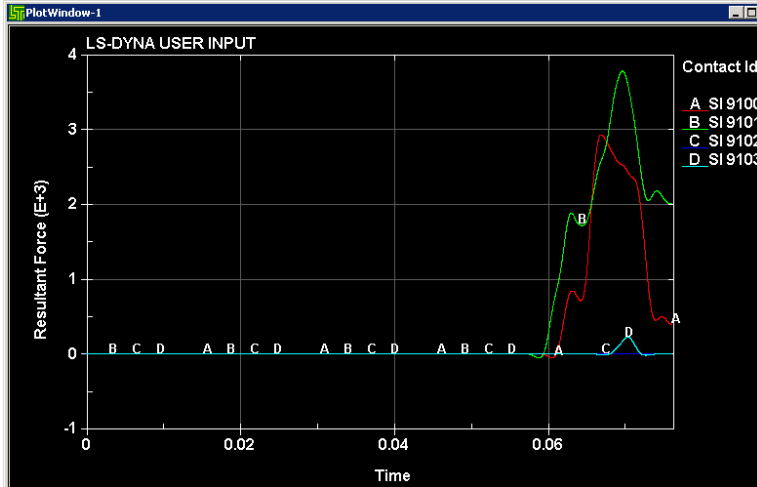


Right Leg Stresses at time of Max. Stress

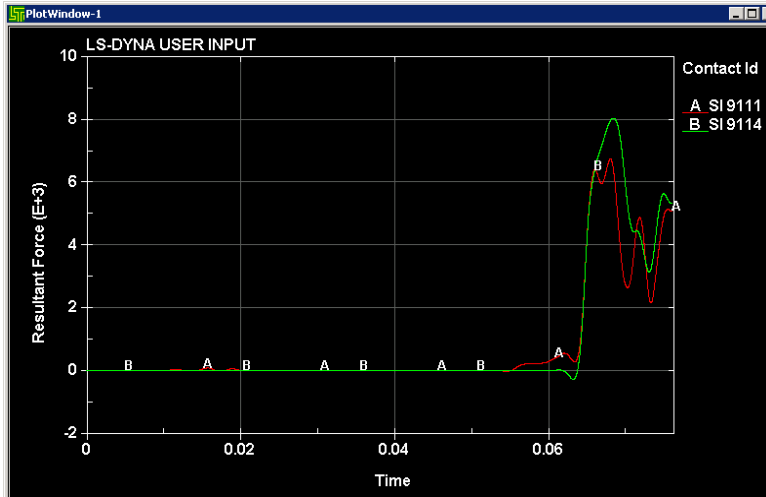
Flex22.5° Results Summary

Summary: Patella fracture occurred shortly after contact with knee bolster. Signs of correlation between maximum femur forces and foot contact forces (~0.07 sec). The right leg experienced higher force. Upon contact with the knee bolster, both knees had a direct impact with the bolster and pushed it upward, causing some upward rotation.

Contact Forces

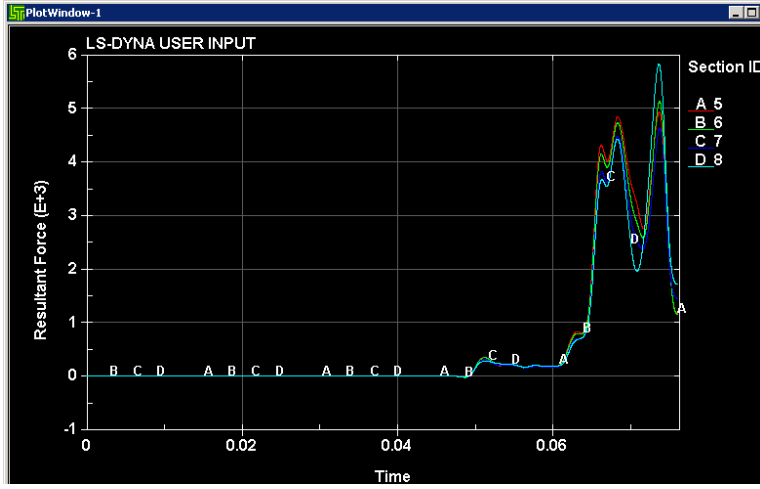


Knee Bolster Contact Forces



Foot Contact Forces

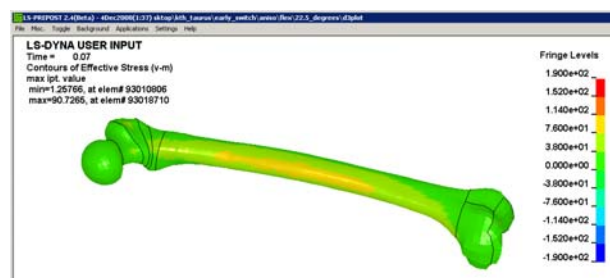
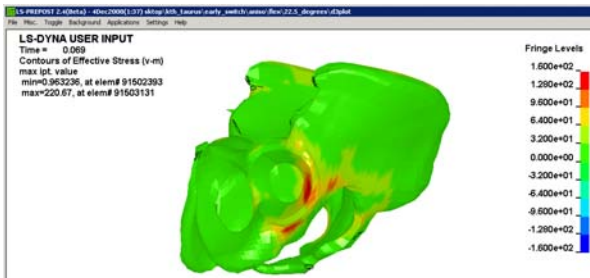
Femur Forces



Left Leg Femur Axial Forces

Fracture Force Summary:

Parameter	Time (sec)	Force (kN)	Notes
Peak Force	0.068	4.80	
Acetabulum	0.067	4.04	
Femoral Head			
Femoral Neck			
Trochanter			
Proximal Femur			
Femoral Shaft			
Femoral Condyle			



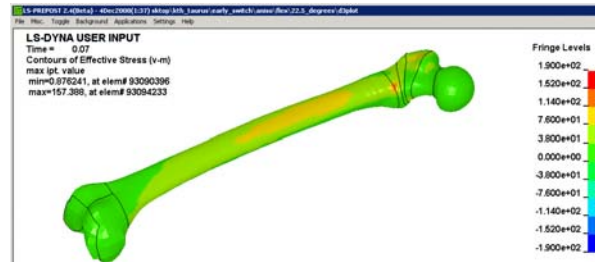
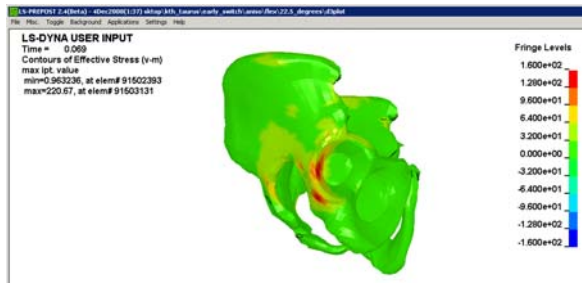
Left Leg Stresses at time of Max. Stress (t=0.069 for both)



Right Leg Femur Axial Forces

Fracture Force Summary: Right

Parameter	Time (sec)	Force (kN)	Notes
Peak Force	0.069	5.96	
Acetabulum	0.067	4.42	
Femoral Head			
Femoral Neck			
Trochanter			
Proximal Femur			
Femoral Shaft			
Femoral Condyle			

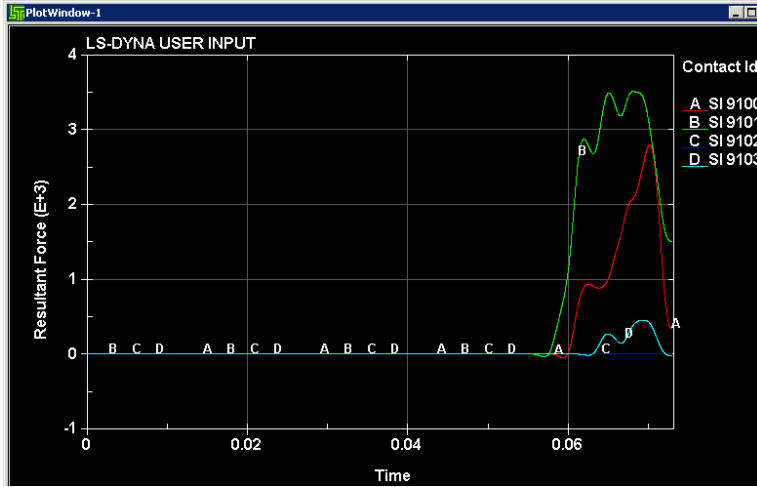


Right Leg Stresses at time of Max. Stress

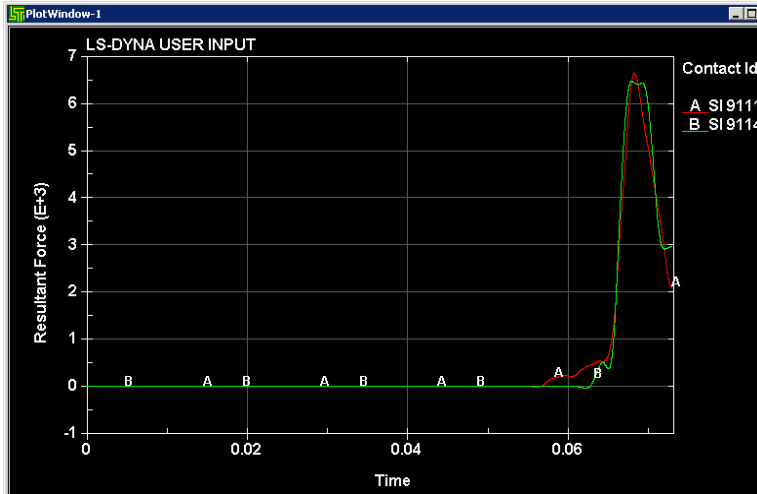
Flex30° Results Summary

Summary: Patella fracture occurred shortly after contact with knee bolster. Signs of correlation between maximum femur forces and foot contact forces (~0.07 sec). The left leg experienced higher force and was the only leg to experience injury. Upon contact with the knee bolster, both knees had a direct impact with the bolster and pushed it upward, causing some upward rotation.

Contact Forces



Knee Bolster Contact Forces



Foot Contact Forces

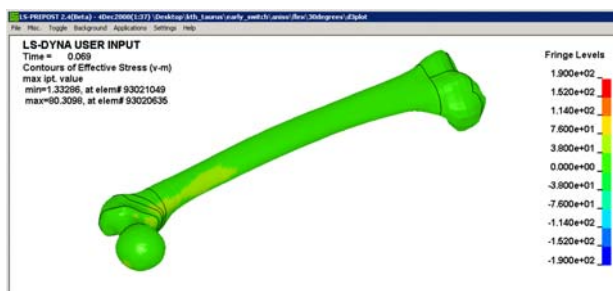
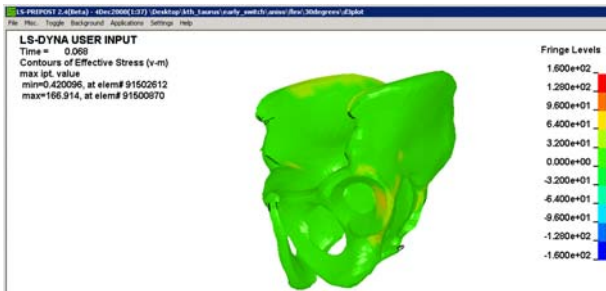
Femur Forces



Left Leg Femur Axial Forces

Fracture Force Summary:

Parameter	Time (sec)	Force (kN)	Notes
Peak Force	0.068	3.86	
Acetabulum			
Femoral Head			
Femoral Neck			
Trochanter			
Proximal Femur			
Femoral Shaft			
Femoral Condyle			



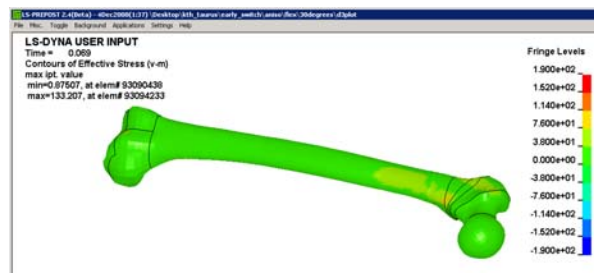
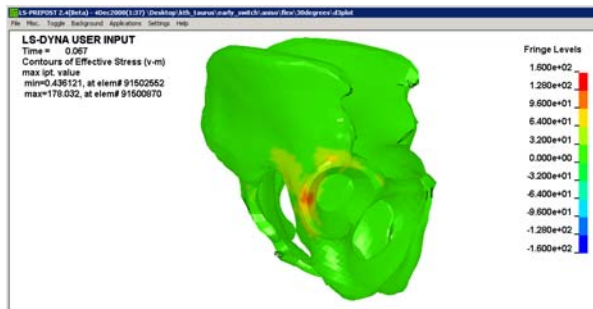
Left Leg Stresses at time of Max. Stress (t=0.069 for both)



Right Leg Femur Axial Forces

Fracture Force Summary: Right

Parameter	Time (sec)	Force (kN)	Notes
Peak Force	0.067	5.39	
Acetabulum	0.066	3.05	
Femoral Head			
Femoral Neck			
Trochanter			
Proximal Femur			
Femoral Shaft			
Femoral Condyle			

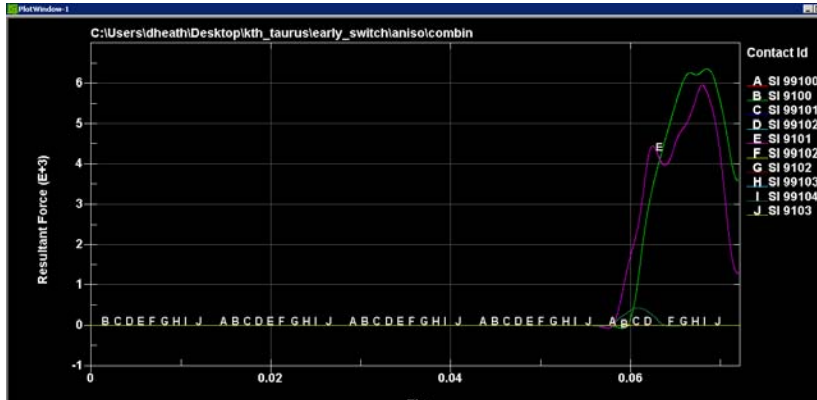


Right Leg Stresses at time of Max. Stress

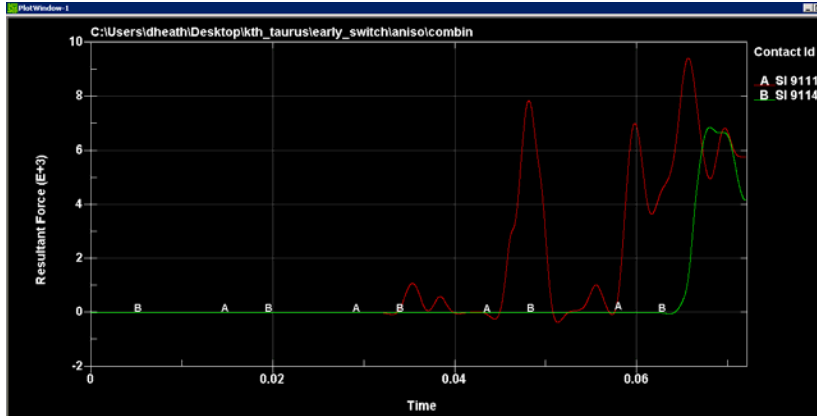
Combined Flex30° Abduct10° Results Summary

Summary: Patella fracture occurred shortly after contact with knee bolster. Little sign of correlation between maximum femur forces and foot contact forces. The right leg experienced higher force and was the only leg to experience injury. Upon contact with the knee bolster, the right leg moved downward along it, causing downwards rotation of the hip. The left leg had a more direct impact, pushing the knee bolster upward and causing upward rotation at the hip. Left femur fracture occurred at approximately the same time as the upward rotation at the hip.

Contact Forces

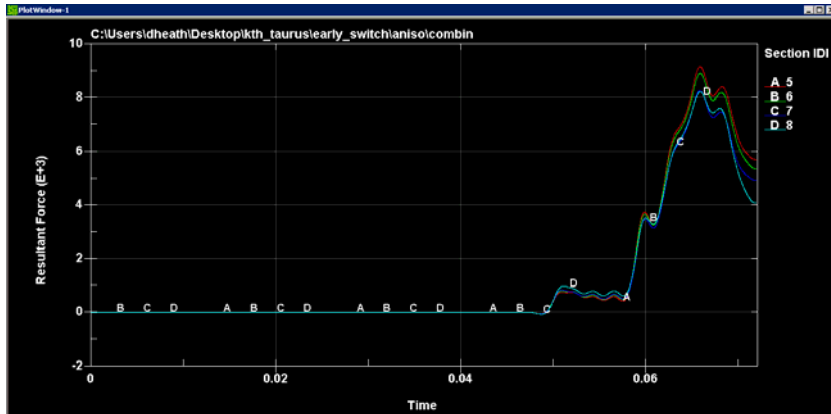


Knee Bolster Contact Forces



Foot Contact Forces

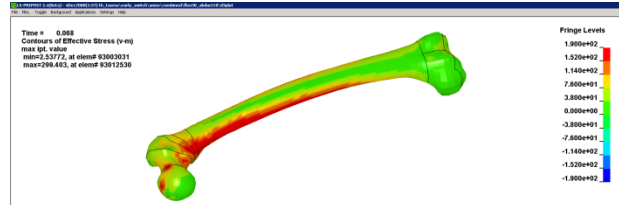
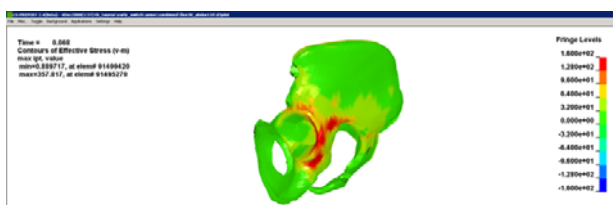
Femur Forces



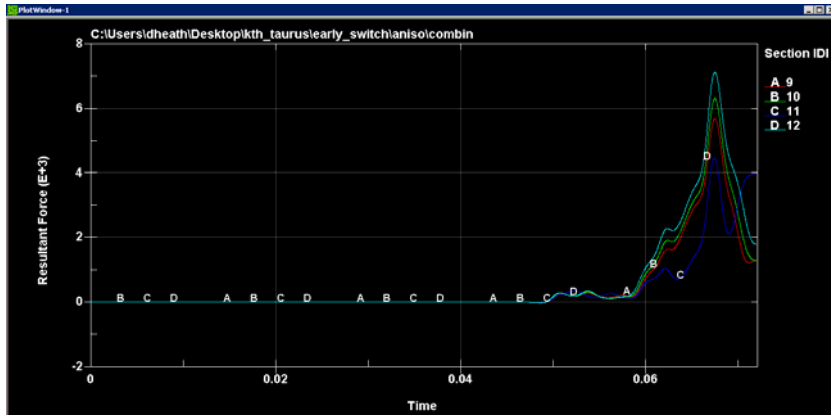
Left Leg Femur Axial Forces

Fracture Force Summary:

Parameter	Time (sec)	Force (kN)	Notes
Peak Force	0.066	9.15	
Acetabulum	0.060	3.73	Spread to rim
Femoral Head	0.064	7.06	
Femoral Neck	0.064	7.06	
Trochanter			
Proximal Femur	0.064	7.06	
Femoral Shaft	0.066	9.15	Occurs at peak force
Femoral Condyle			



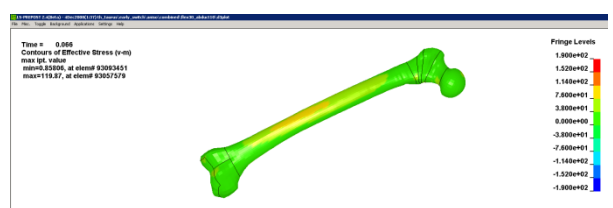
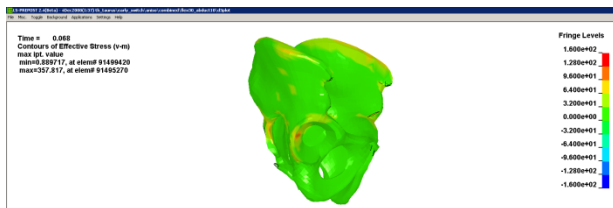
Left Leg Stresses at time of Max. Stress (t=0.069 for both)



Right Leg Femur Axial Forces

Fracture Force Summary: Right

Parameter	Time (sec)	Force (kN)	Notes
Peak Force	0.068	7.14	
Acetabulum			
Femoral Head			
Femoral Neck			
Trochanter			
Proximal Femur			
Femoral Shaft			
Femoral Condyle			

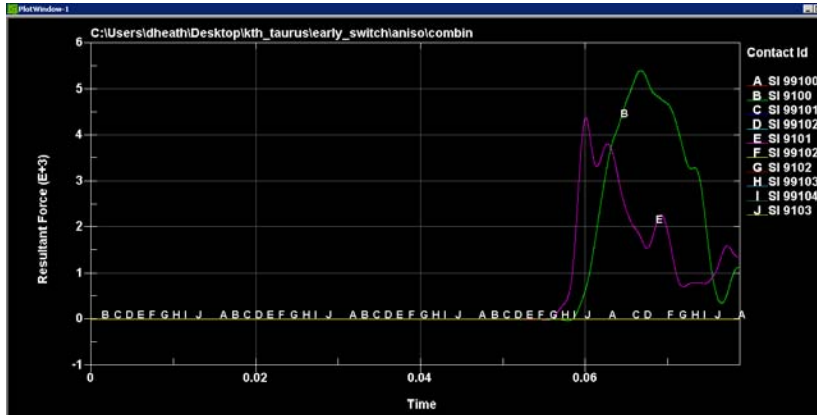


Right Leg Stresses at time of Max. Stress

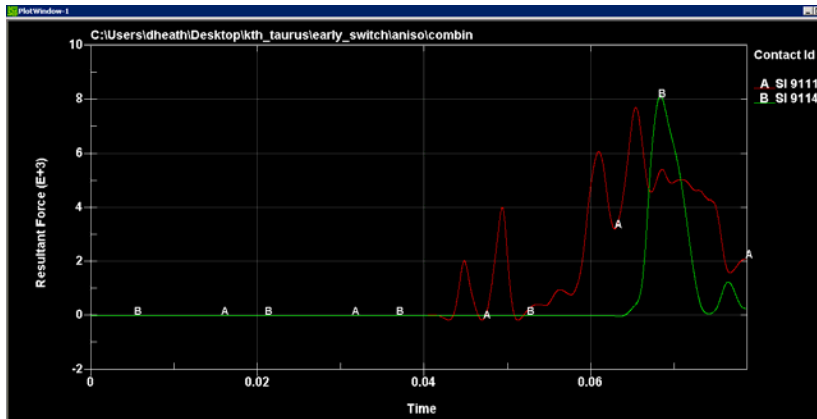
Combined Flex30° Adduct10° Results Summary

Summary: Patella fracture occurred shortly after contact with knee bolster. Little sign of correlation between maximum femur forces and foot contact forces. The right leg experienced higher force and more serious injury. Upon contact with the knee bolster, the right leg moved downward along it, causing downwards rotation of the hip. The left leg had a more direct impact, pushing the knee bolster upward and causing upward rotation at the hip. Left femoral shaft fracture occurred at approximately the same time as the upward rotation at the hip.

Contact Forces

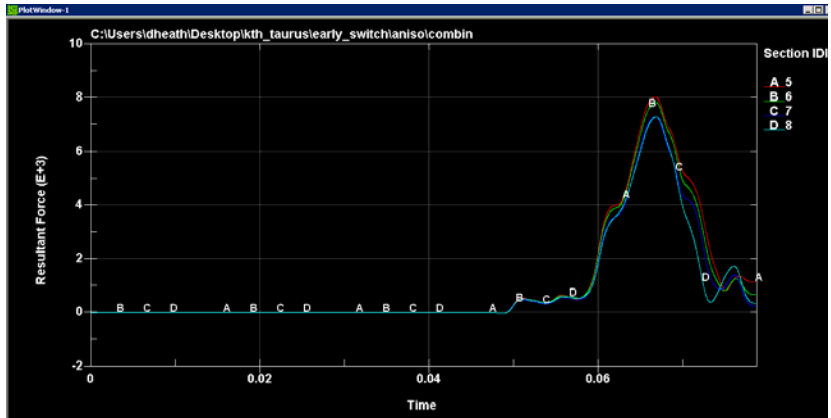


Knee Bolster Contact Forces



Foot Contact Forces

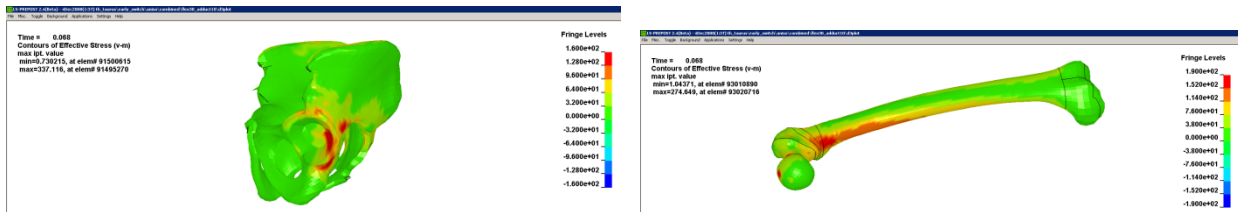
Femur Forces



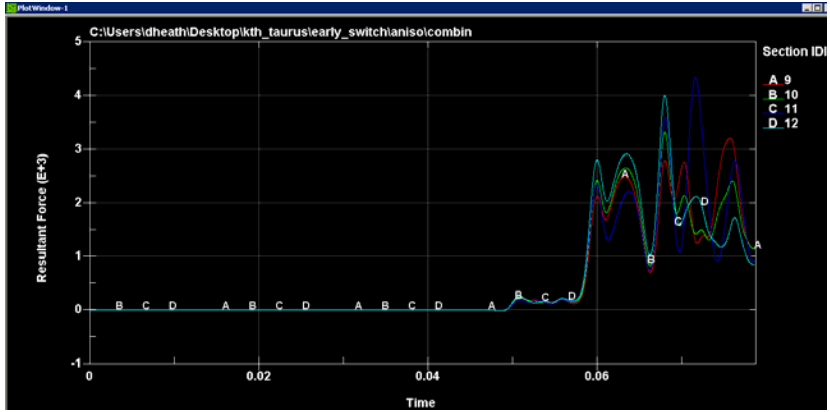
Left Leg Femur Axial Forces

Fracture Force Summary:

Parameter	Time (sec)	Force (kN)	Notes
Peak Force	0.067	8.03	
Acetabulum	0.061	3.60	
Femoral Head	0.062	3.98	
Femoral Neck			
Trochanter			
Proximal Femur	0.066	7.83	
Femoral Shaft			
Femoral Condyle			



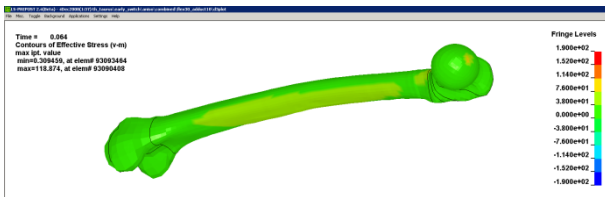
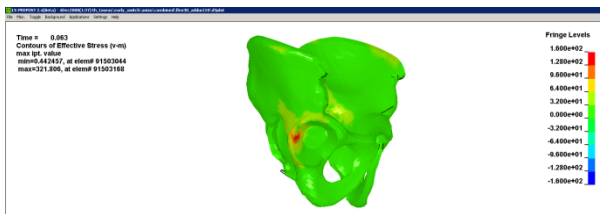
Left Leg Stresses at time of Max. Stress (t=0.069 for both)



Right Leg Femur Axial Forces

Fracture Force Summary: Right

Parameter	Time (sec)	Force (kN)	Notes
Peak Force	0.68	4.00	
Acetabulum	0.063	2.85	
Femoral Head			
Femoral Neck			
Trochanter			
Proximal Femur			
Femoral Shaft			
Femoral Condyle			

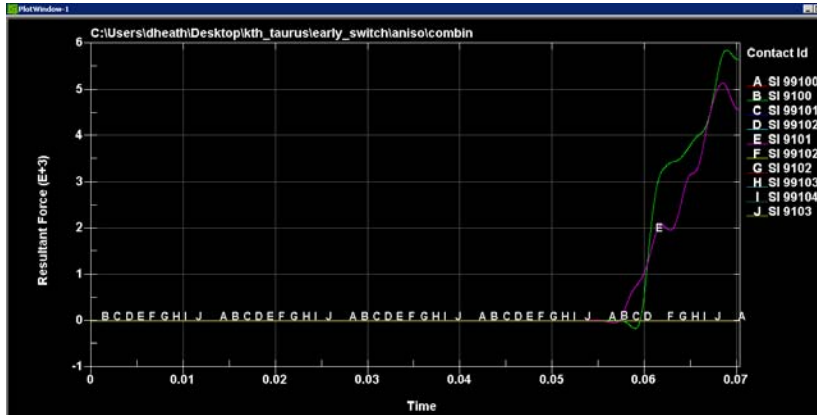


Right Leg Stresses at time of Max. Stress

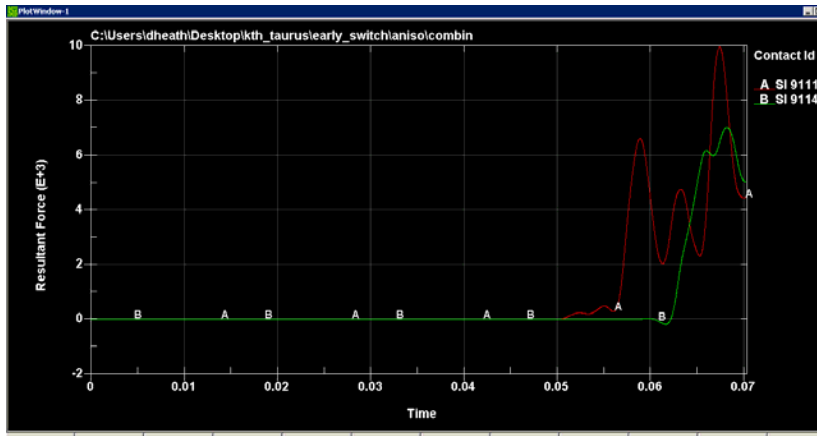
Combined Flex30° Abduct5° Results Summary

Summary: Patella fracture occurred shortly after contact with knee bolster. Little sign of correlation between maximum femur forces and foot contact forces. The left leg experienced higher force and more serious injury. Upon contact with the knee bolster, the right leg moved downward along it, causing downwards rotation of the hip. The left leg had a more direct impact, pushing the knee bolster upward and causing upward rotation at the hip. Left femoral condyle fracture occurred at approximately the same time as the upward rotation at the hip.

Contact Forces

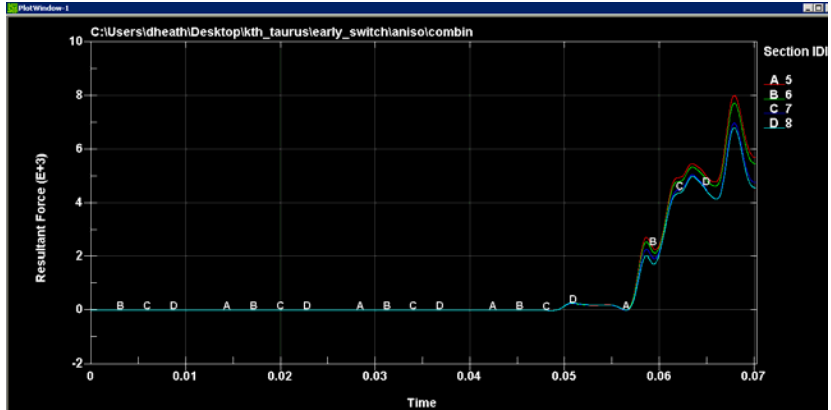


Knee Bolster Contact Forces



Foot Contact Forces

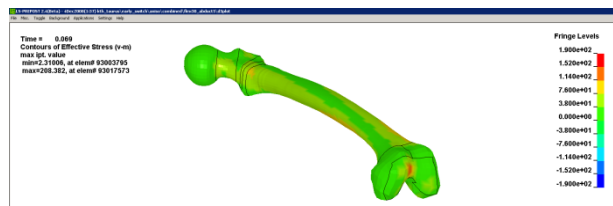
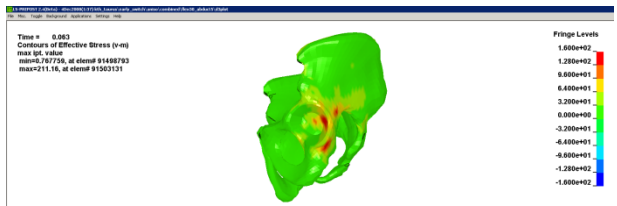
Femur Forces



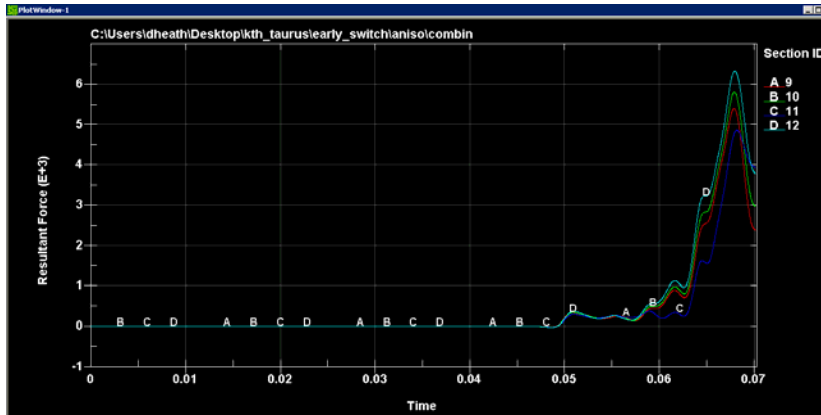
Left Leg Femur Axial Forces

Fracture Force Summary:

Parameter	Time (sec)	Force (kN)	Notes
Peak Force	0.068	8.01	
Acetabulum	0.061	3.88	
Femoral Head			
Femoral Neck			
Trochanter			
Proximal Femur			
Femoral Shaft			
Femoral Condyle	0.069	6.79	Medial Condyle; after peak



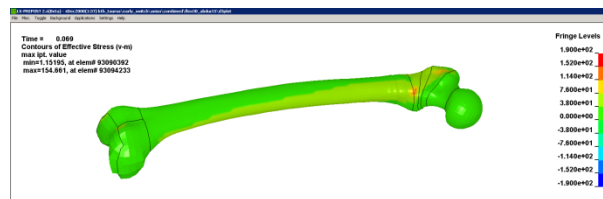
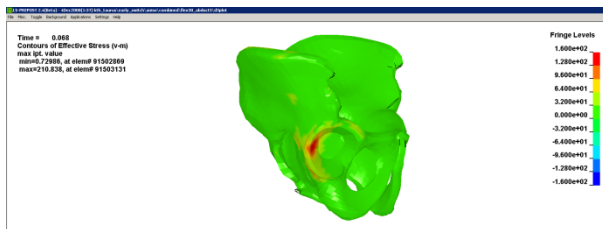
Left Leg Stresses at time of Max. Stress (t=0.069 for both)



Right Leg Femur Axial Forces

Fracture Force Summary: Right

Parameter	Time (sec)	Force (kN)	Notes
Peak Force	0.068	6.32	
Acetabulum	0.067	5.18	
Femoral Head			
Femoral Neck			
Trochanter			
Proximal Femur			
Femoral Shaft			
Femoral Condyle			



Right Leg Stresses at time of Max. Stress

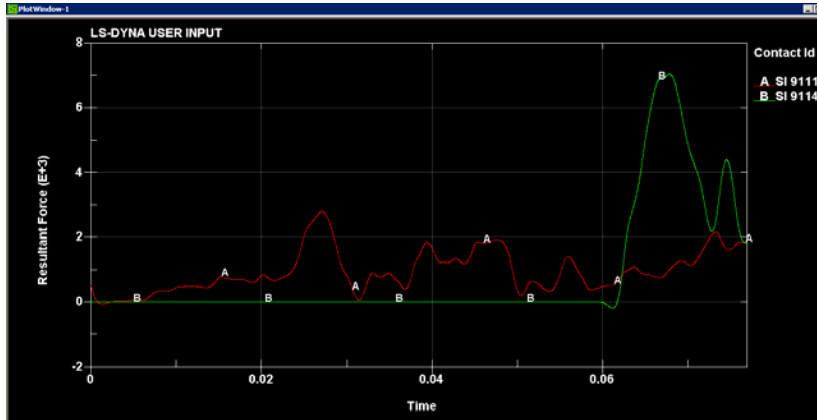
Combined Flex30° Adduct5° Results Summary

Summary: Patella fracture occurred shortly after contact with knee bolster. Little sign of correlation between maximum femur forces and foot contact forces. The left leg experienced higher force and more serious injury. Upon contact with the knee bolster, the right leg moved downward along it, causing downwards rotation of the hip. The left leg had a more direct impact, pushing the knee bolster upward and causing upward rotation at the hip. The impact appears to have been taken almost exclusively by the left leg.

Contact Forces

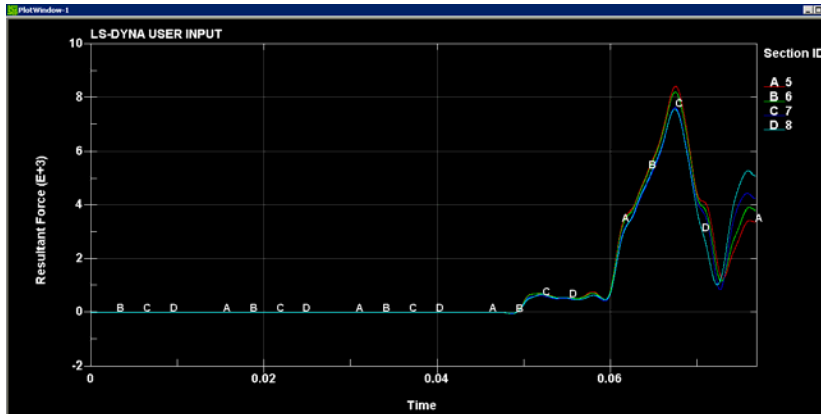


Knee Bolster Contact Forces



Foot Contact Forces

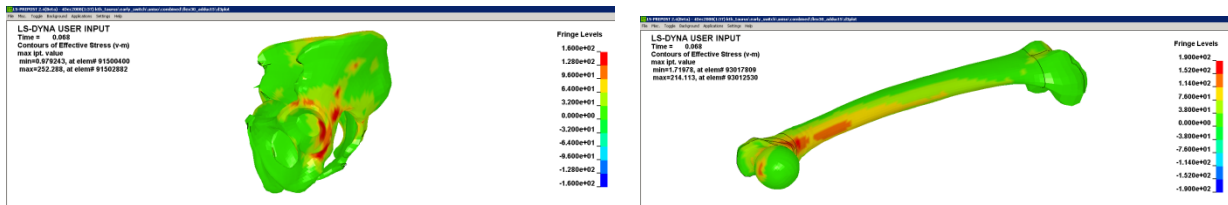
Femur Forces



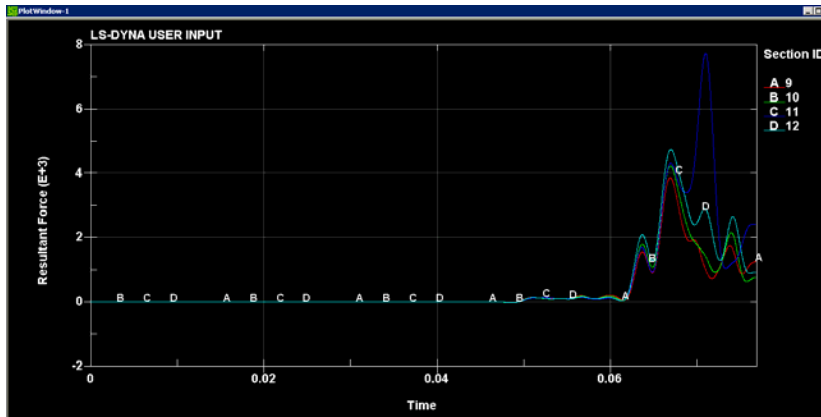
Left Leg Femur Axial Forces

Fracture Force Summary:

Parameter	Time (sec)	Force (kN)	Notes
Peak Force	0.068	8.43	
Acetabulum	0.063	4.24	
Femoral Head			
Femoral Neck			
Trochanter			
Proximal Femur	0.066	7.42	
Femoral Shaft			
Femoral Condyle			



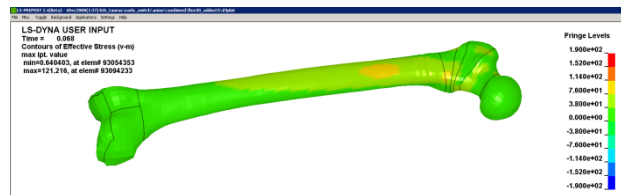
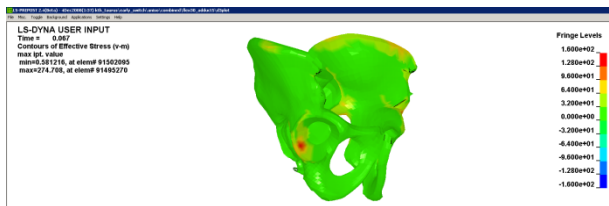
Left Leg Stresses at time of Max. Stress (t=0.069 for both)



Right Leg Femur Axial Forces

Fracture Force Summary: Right

Parameter	Time (sec)	Force (kN)	Notes
Peak Force	0.067	4.76	
Acetabulum	0.067	4.76	Peak force
Femoral Head			
Femoral Neck			
Trochanter			
Proximal Femur			
Femoral Shaft			
Femoral Condyle			



Right Leg Stresses at time of Max. Stress

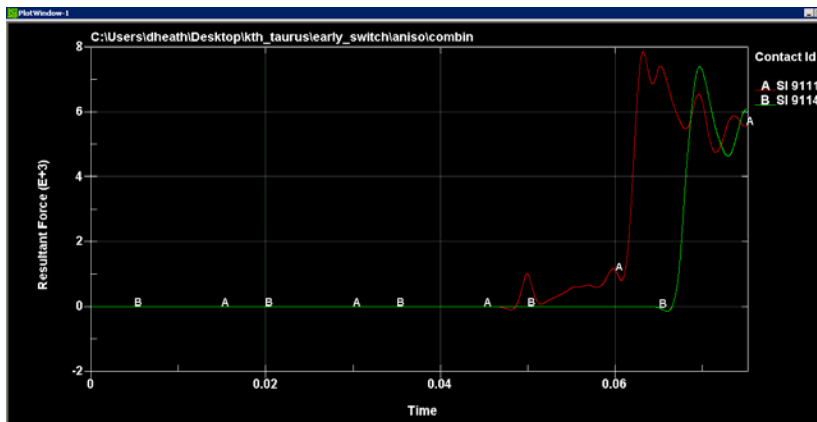
Combined Flex15° Abduct10° Results Summary

Summary: Patella fracture occurred shortly after contact with knee bolster. Signs of correlation between maximum femur forces and foot contact forces (~0.07 seconds). The left leg experienced higher force and more serious injury. Upon contact with the knee bolster, the right leg moved downward along it, causing downwards rotation of the hip. The left leg had a more direct impact, pushing the knee bolster upward and causing upward rotation at the hip.

Contact Forces

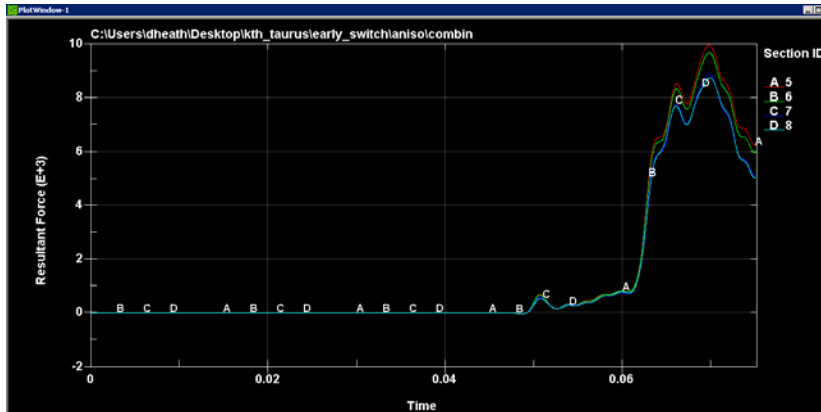


Knee Bolster Contact Forces



Foot Contact Forces

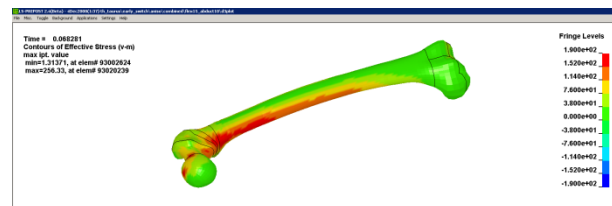
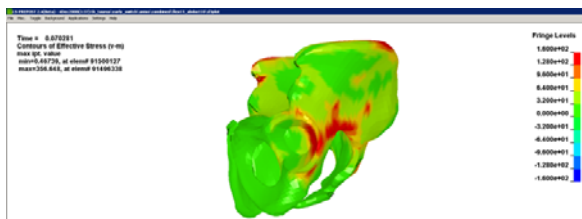
Femur Forces



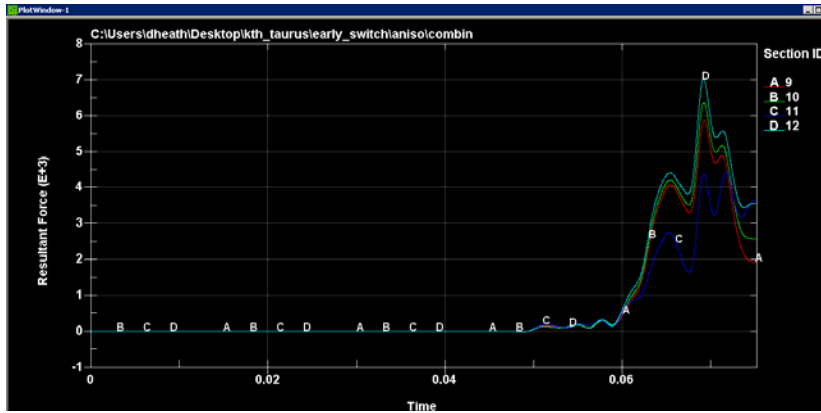
Left Leg Femur Axial Forces

Fracture Force Summary:

Parameter	Time (sec)	Force (kN)	Notes
Peak Force	0.070	9.98	
Acetabulum	0.063	4.80	
Femoral Head	0.065	6.86	
Femoral Neck	0.066	8.50	
Trochanter			
Proximal Femur	0.065	6.86	
Femoral Shaft	0.067	8.04	
Femoral Condyle			



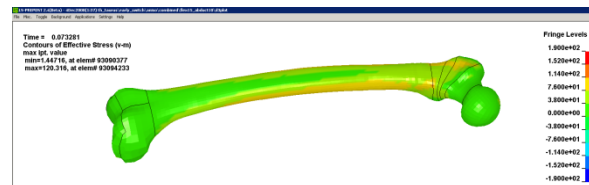
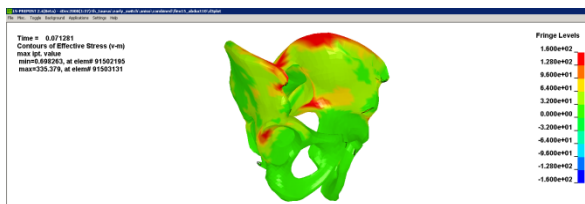
Left Leg Stresses at time of Max. Stress (t=0.069 for both)



Right Leg Femur Axial Forces

Fracture Force Summary: Right

Parameter	Time (sec)	Force (kN)	Notes
Peak Force	0.069	7.00	
Acetabulum	0.070	5.94	Spread to rim
Femoral Head			
Femoral Neck			
Trochanter			
Proximal Femur			
Femoral Shaft			
Femoral Condyle			



Right Leg Stresses at time of Max. Stress

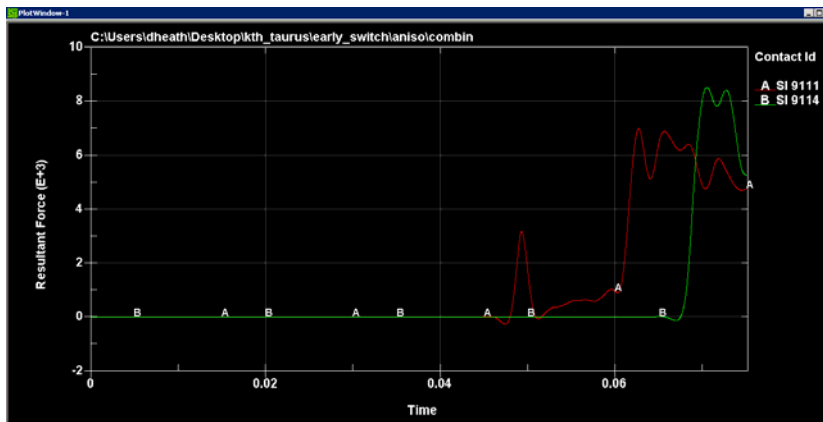
Combined Flex15° Adduct10° Results Summary

Summary: Patella fracture occurred shortly after contact with knee bolster. Signs of correlation between maximum femur forces and foot contact forces (~0.07 seconds). The left leg experienced higher force and more serious injury. Upon contact with the knee bolster, the right leg moved downward along it, causing downwards rotation of the hip. The left leg had a more direct impact, pushing the knee bolster upward and causing upward rotation at the hip.

Contact Forces

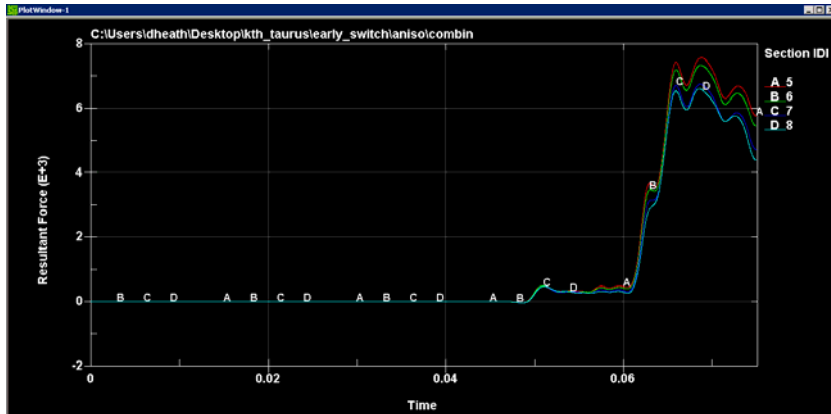


Knee Bolster Contact Forces



Foot Contact Forces

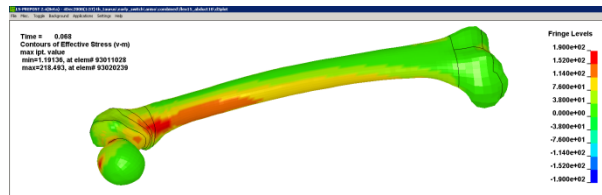
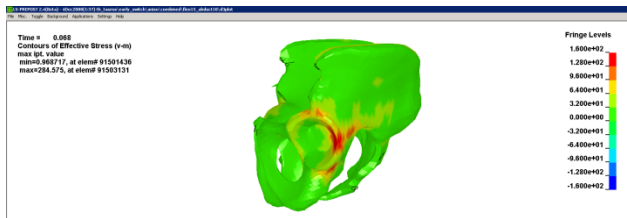
Femur Forces



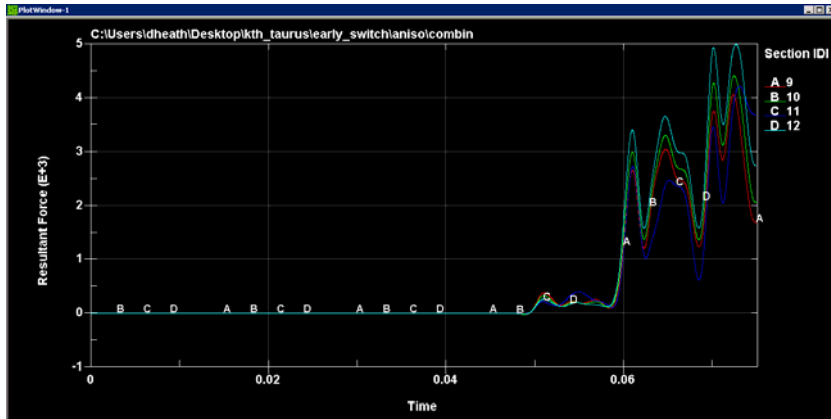
Left Leg Femur Axial Forces

Fracture Force Summary:

Parameter	Time (sec)	Force (kN)	Notes
Peak Force	0.069	7.58	
Acetabulum	0.064	3.76	
Femoral Head	0.068	7.22	
Femoral Neck			
Trochanter			
Proximal Femur	0.068	7.22	
Femoral Shaft			
Femoral Condyle			



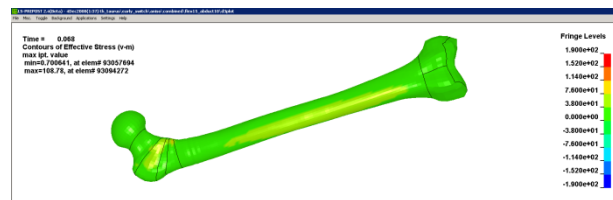
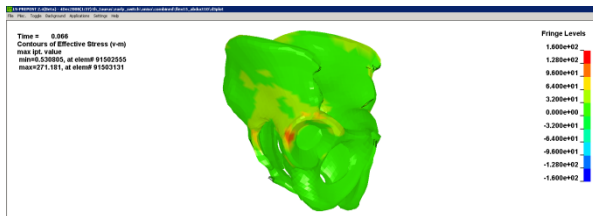
Left Leg Stresses at time of Max. Stress (t=0.069 for both)



Right Leg Femur Axial Forces

Fracture Force Summary: Right

Parameter	Time (sec)	Force (kN)	Notes
Peak Force	0.07	4.94	
Acetabulum			
Femoral Head			
Femoral Neck			
Trochanter			
Proximal Femur			
Femoral Shaft			
Femoral Condyle			

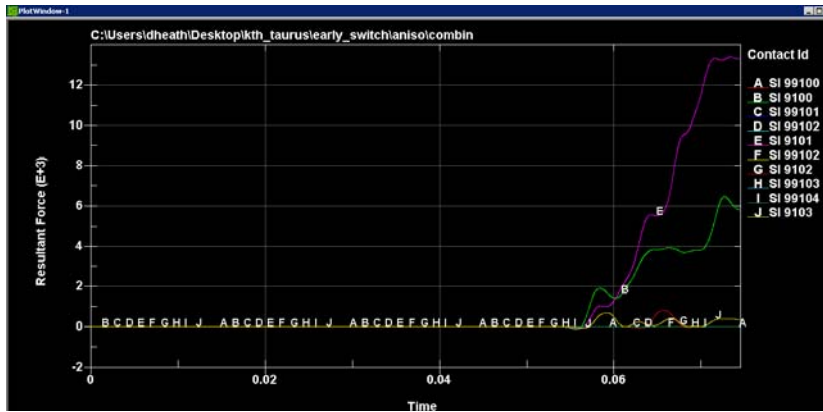


Right Leg Stresses at time of Max. Stress

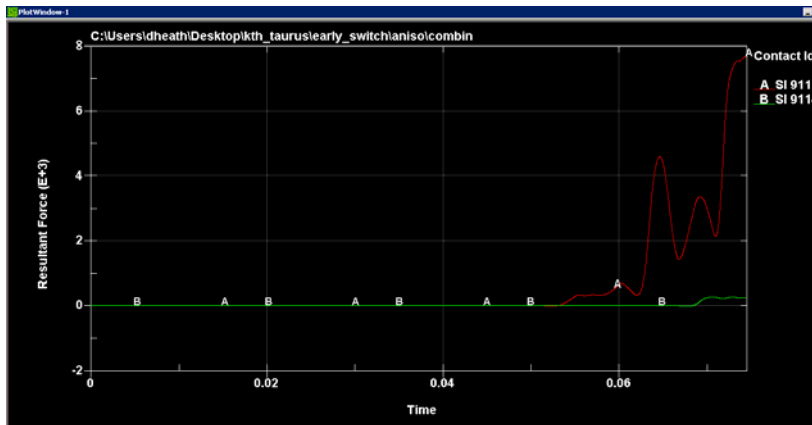
Combined Flex15° Abduct5° Results Summary

Summary: Patella fracture occurred shortly after contact with knee bolster. No signs of correlation between maximum femur forces and foot contact forces. The right leg experienced higher force and more serious injury. Upon contact with the knee bolster both legs had a direct impact, pushing the knee bolster upward and causing upward rotation at the hip.

Contact Forces

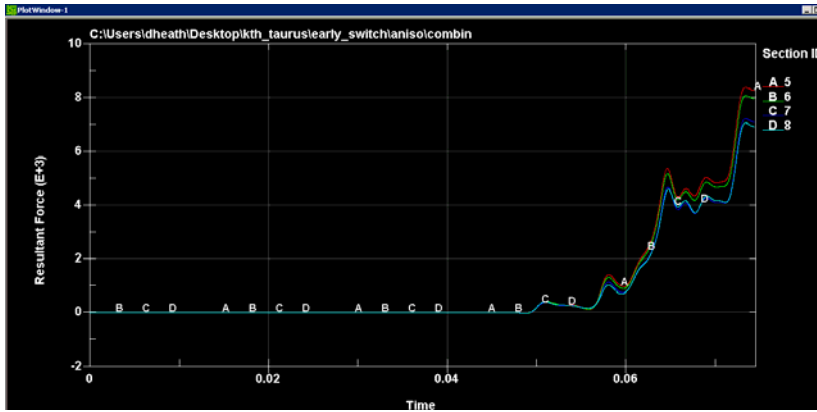


Knee Bolster Contact Forces



Foot Contact Forces

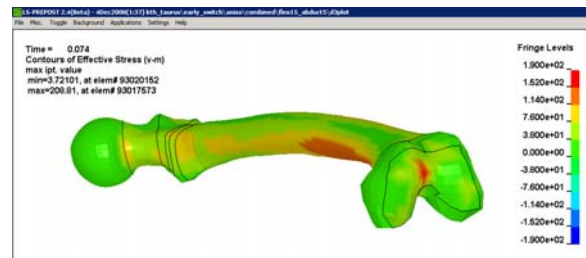
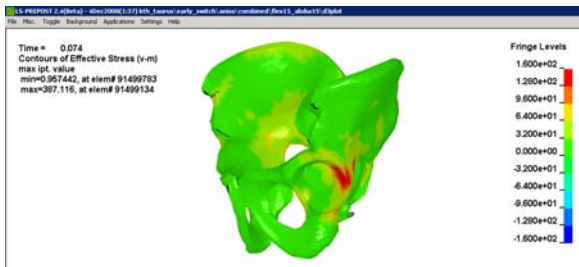
Femur Forces



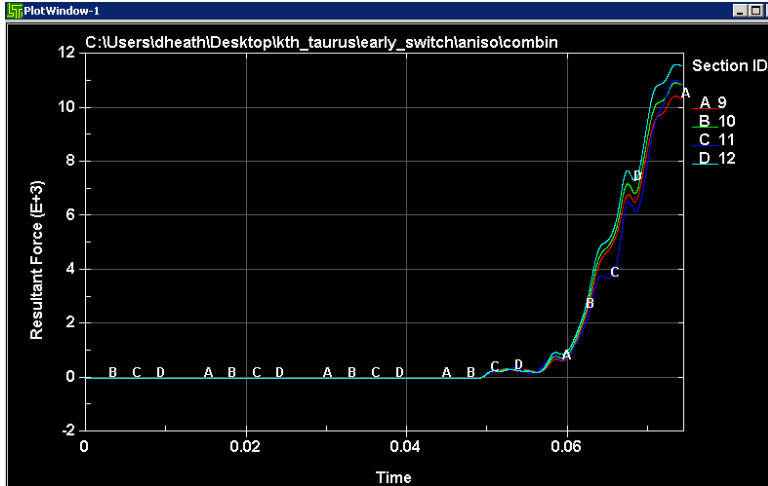
Left Leg Femur Axial Forces

Fracture Force Summary:

Parameter	Time (sec)	Force (kN)	Notes
Peak Force	0.074	8.37	
Acetabulum	0.065	5.18	
Femoral Head			
Femoral Neck			
Trochanter			
Proximal Femur			
Femoral Shaft			
Femoral Condyle	0.074	8.37	Medial condyle; peak



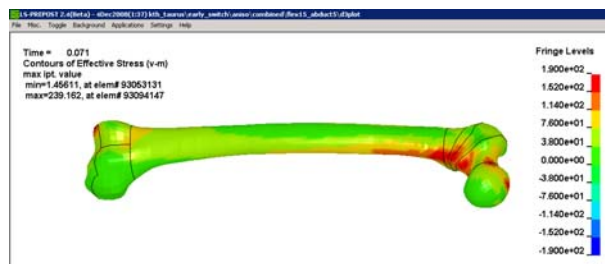
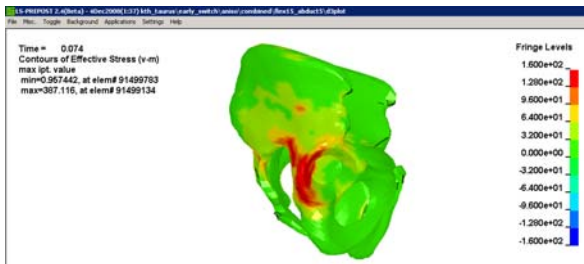
Left Leg Stresses at time of Max. Stress (t=0.069 for both)



Right Leg Femur Axial Forces

Fracture Force Summary: Right

Parameter	Time (sec)	Force (kN)	Notes
Peak Force	0.073	11.6	
Acetabulum	0.065	5.09	
Femoral Head	0.070	9.24	
Femoral Neck	0.069	7.60	
Trochanter			
Proximal Femur	0.069	7.60	
Femoral Shaft	0.072	10.9	
Femoral Condyle	0.071	10.7	Lateral condyle

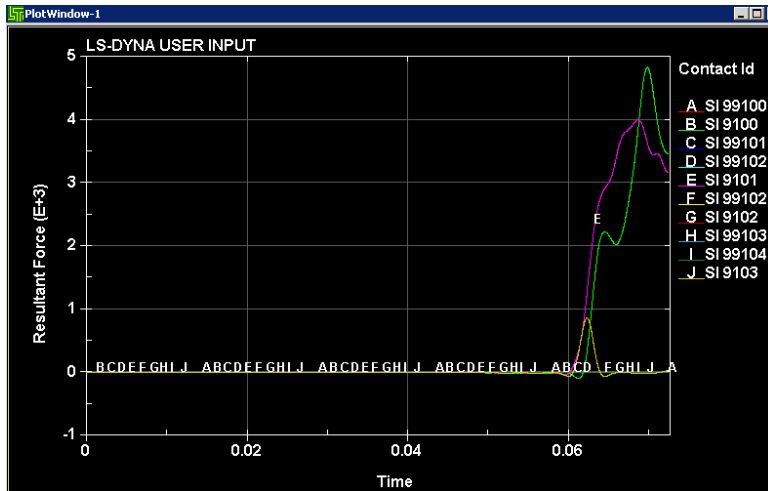


Right Leg Stresses at time of Max. Stress

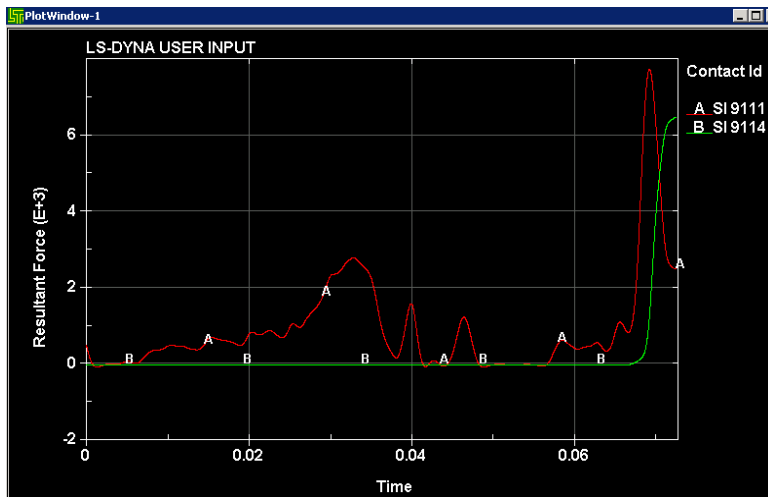
Combined Flex15° Adduct5° Results Summary

Summary: Patella fracture occurred shortly after contact with knee bolster. Signs of correlation between maximum femur forces and foot contact forces (~0.070 seconds). The right leg experienced higher force (barely), and both legs had comparable injury severity. Upon contact with the knee bolster both legs had a direct impact, pushing the knee bolster upward and causing upward rotation at the hip however, the right leg rotated medially to some degree.

Contact Forces

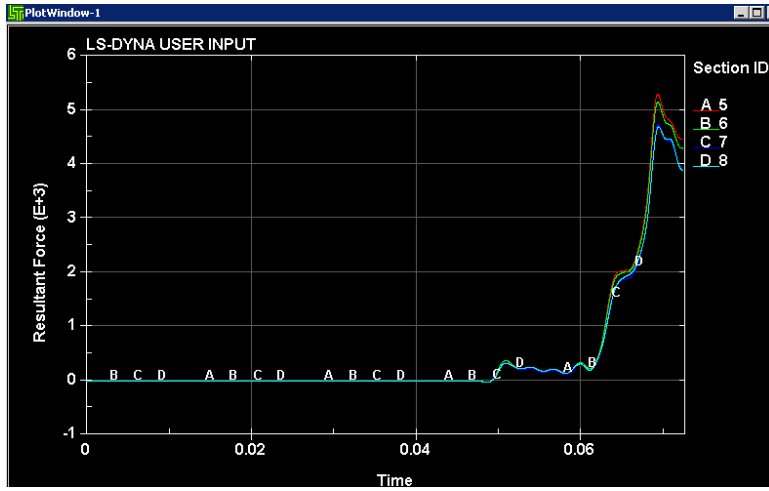


Knee Bolster Contact Forces



Foot Contact Forces

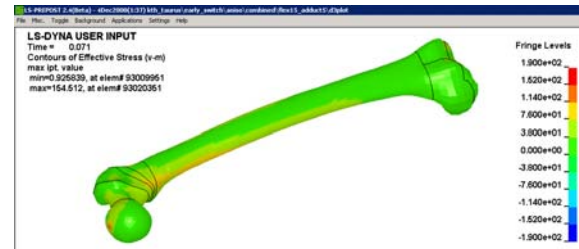
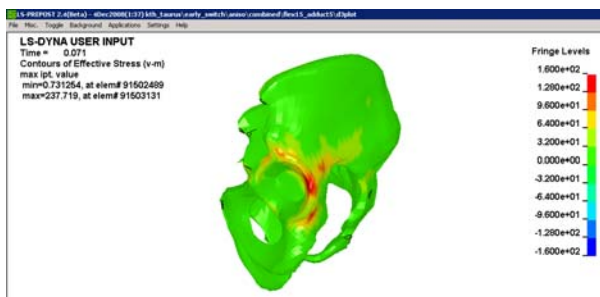
Femur Forces



Left Leg Femur Axial Forces

Fracture Force Summary:

Parameter	Time (sec)	Force (kN)	Notes
Peak Force	0.069	5.27	
Acetabulum	0.069	5.27	Peak
Femoral Head			
Femoral Neck			
Trochanter			
Proximal Femur			
Femoral Shaft			
Femoral Condyle			



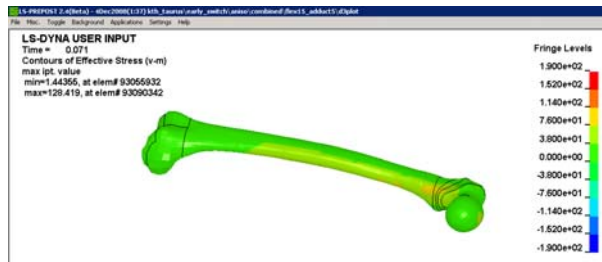
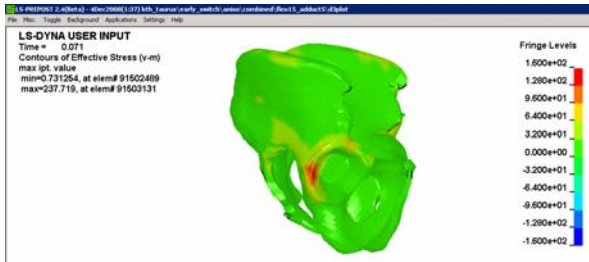
Left Leg Stresses at time of Max. Stress (t=0.069 for both)



Right Leg Femur Axial Forces

Fracture Force Summary: Right

Parameter	Time (sec)	Force (kN)	Notes
Peak Force	0.071	5.17	
Acetabulum	0.070	4.46	
Femoral Head			
Femoral Neck			
Trochanter			
Proximal Femur			
Femoral Shaft			
Femoral Condyle			

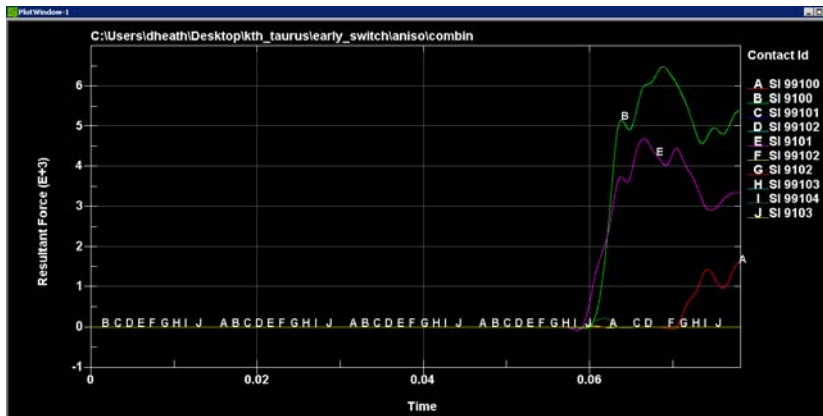


Right Leg Stresses at time of Max. Stress

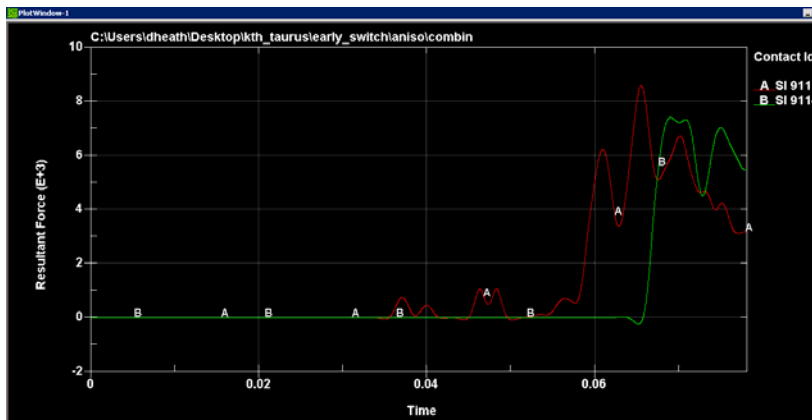
Combined Flex7.5° Abduct10° Results Summary

Summary: Patella fracture occurred shortly after contact with knee bolster. Signs of correlation between maximum femur forces and foot contact forces (~0.07 seconds). The left leg experienced higher force and more serious injury. Upon contact with the knee bolster, the right leg moved downward along it, causing downwards rotation of the hip. The left leg had a more direct impact, pushing the knee bolster upward and causing upward rotation at the hip.

Contact Forces

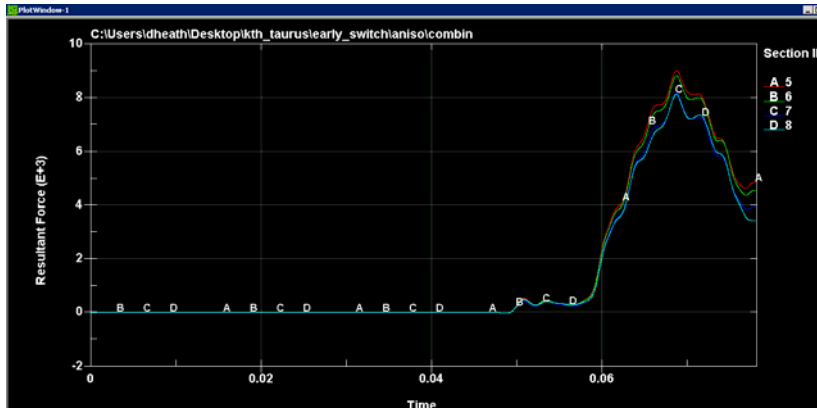


Knee Bolster Contact Forces



Foot Contact Forces

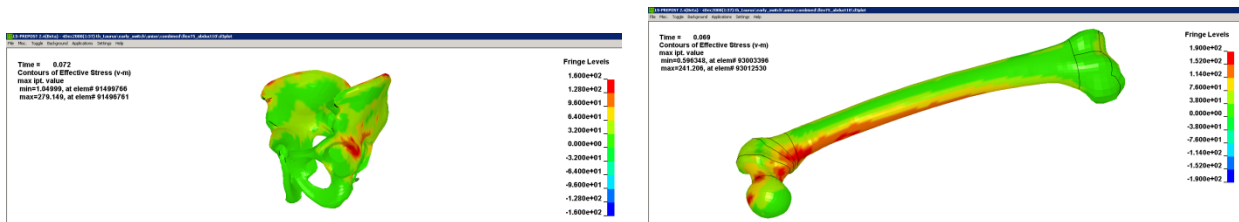
Femur Forces



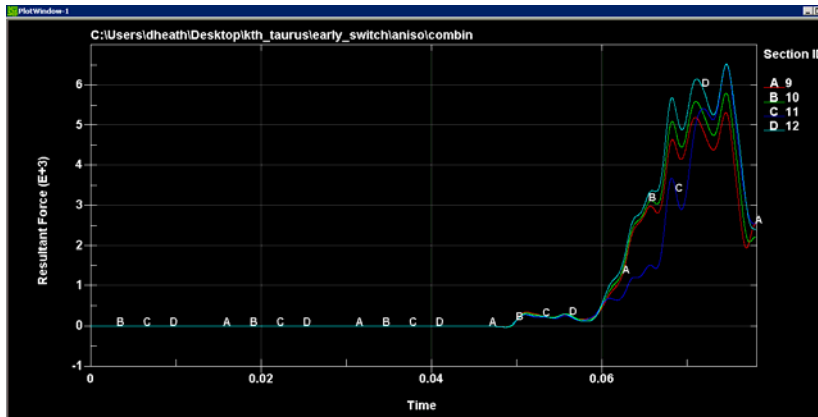
Left Leg Femur Axial Forces

Fracture Force Summary:

Parameter	Time (sec)	Force (kN)	Notes
Peak Force	0.069	9.01	
Acetabulum	0.063	4.81	
Femoral Head	0.068	8.28	
Femoral Neck	0.068	8.28	
Trochanter			
Proximal Femur	0.067	7.76	
Femoral Shaft	0.070	8.27	After peak
Femoral Condyle			



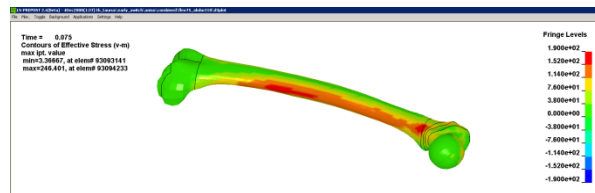
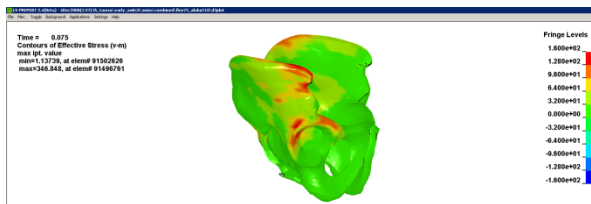
Left Leg Stresses at time of Max. Stress (t=0.069 for both)



Right Leg Femur Axial Forces

Fracture Force Summary: Right

Parameter	Time (sec)	Force (kN)	Notes
Peak Force	0.075	6.54	
Acetabulum	0.072	5.90	
Femoral Head			
Femoral Neck			
Trochanter			
Proximal Femur	0.073	5.29	
Femoral Shaft	0.075	6.54	Peak
Femoral Condyle			

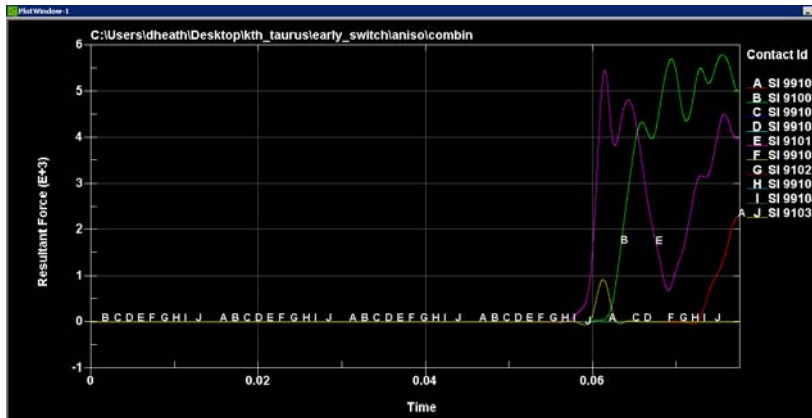


Right Leg Stresses at time of Max. Stress

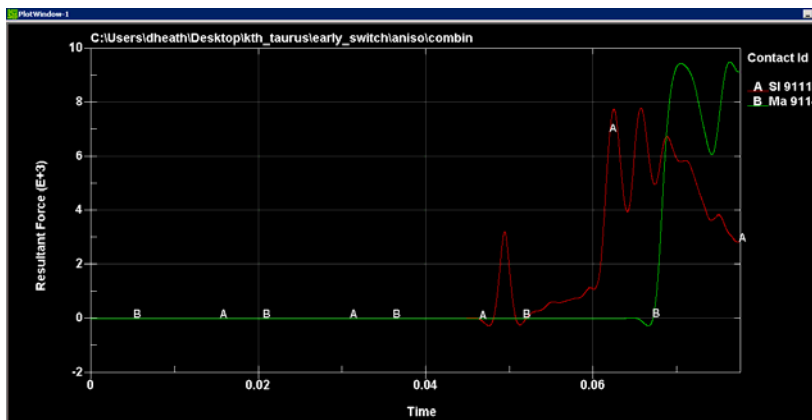
Combined Flex7.5° Adduct10° Results Summary

Summary: Patella fracture occurred shortly after contact with knee bolster. Signs of correlation between maximum femur forces and foot contact forces (~0.07 seconds). The left leg experienced higher force and more serious injury. Upon contact with the knee bolster, the right leg moved downward along it, causing downwards rotation of the hip. The left leg had a more direct impact, pushing the knee bolster upward and causing upward rotation at the hip.

Contact Forces

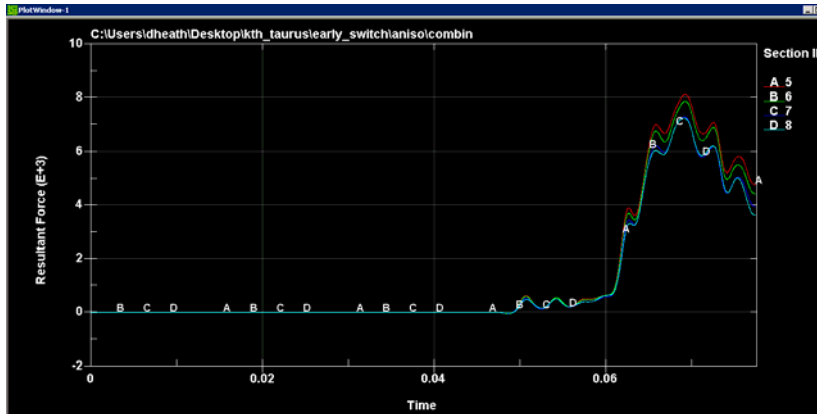


Knee Bolster Contact Forces



Foot Contact Forces

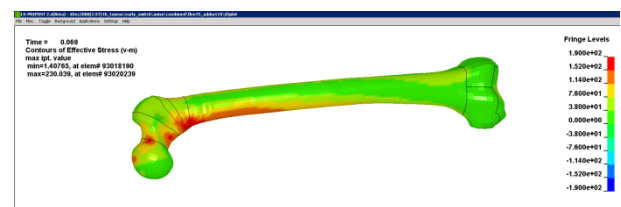
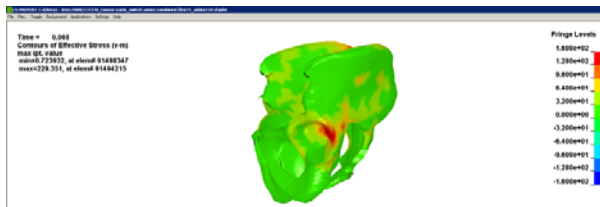
Femur Forces



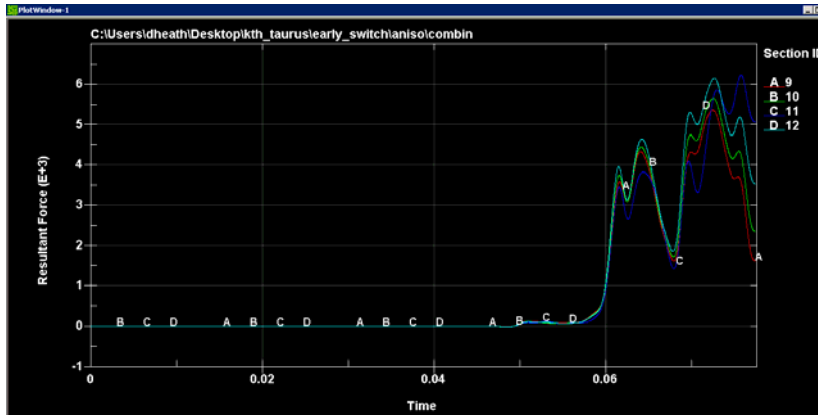
Left Leg Femur Axial Forces

Fracture Force Summary:

Parameter	Time (sec)	Force (kN)	Notes
Peak Force	0.069	8.11	
Acetabulum	0.064	3.99	
Femoral Head			
Femoral Neck	0.069	8.11	Peak
Trochanter			
Proximal Femur	0.068	7.46	
Femoral Shaft			
Femoral Condyle	0.077	4.86	Medial condyle; after peak



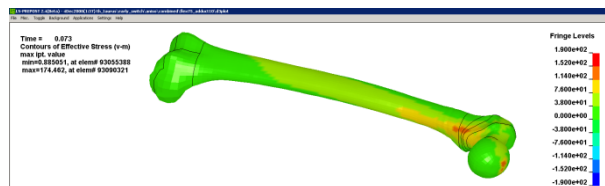
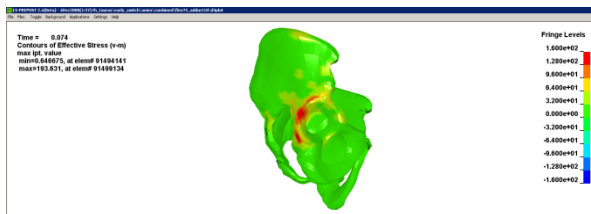
Left Leg Stresses at time of Max. Stress (t=0.069 for both)



Right Leg Femur Axial Forces

Fracture Force Summary: Right

Parameter	Time (sec)	Force (kN)	Notes
Peak Force	0.073	6.11	
Acetabulum	0.062	3.67	
Femoral Head			
Femoral Neck			
Trochanter			
Proximal Femur			
Femoral Shaft			
Femoral Condyle			

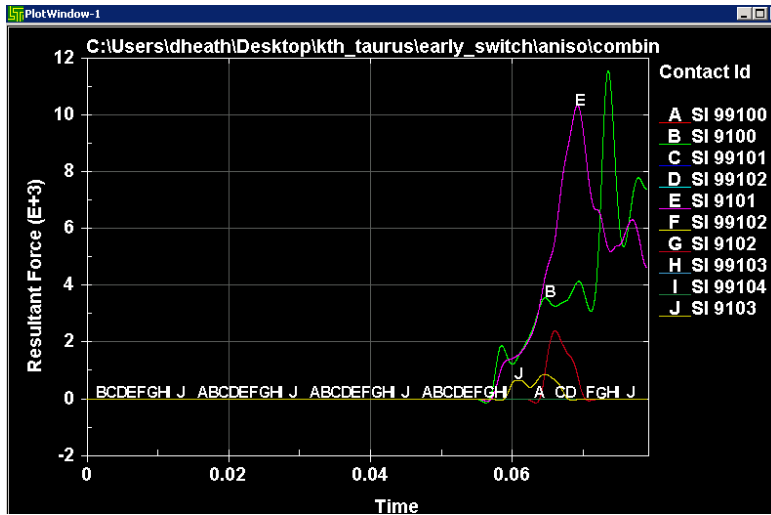


Right Leg Stresses at time of Max. Stress

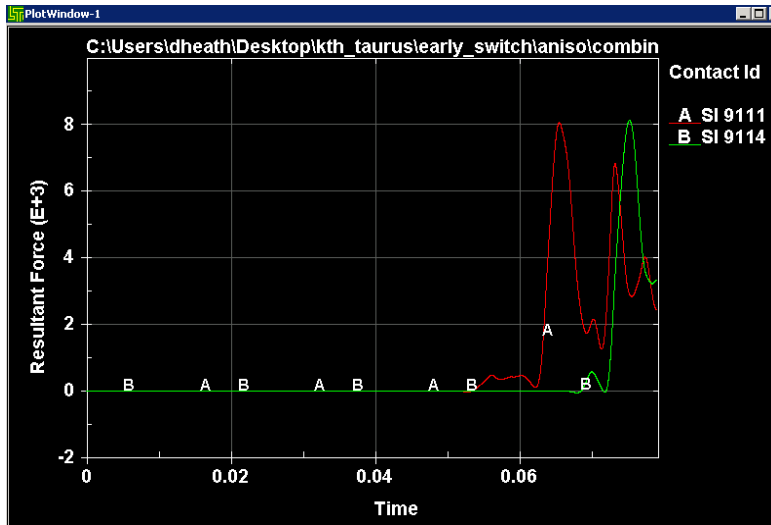
Combined Flex7.5° Abduct5° Results Summary

Summary: Patella fracture occurred shortly after contact with knee bolster. Signs of correlation between maximum femur forces and foot contact forces (~0.07 seconds). The left leg experienced higher force but both legs experienced similar injury. Both legs had a fairly direct impact with the knee bolster, pushing the knee bolster upward and causing upward rotation at the hip.

Contact Forces



Knee Bolster Contact Forces



Foot Contact Forces

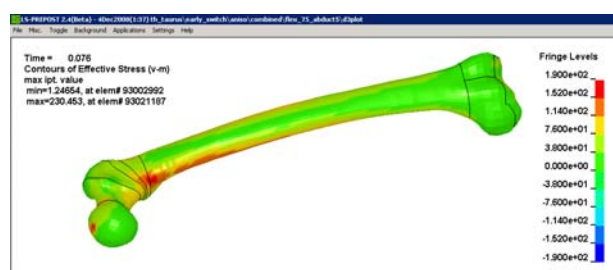
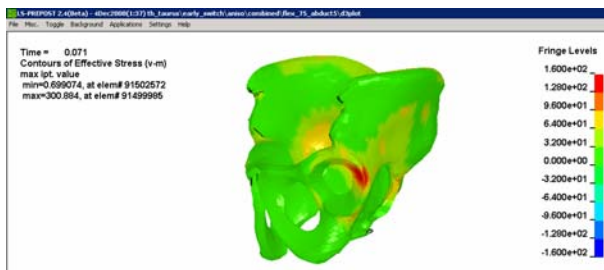
Femur Forces



Left Leg Femur Axial Forces

Fracture Force Summary:

Parameter	Time (sec)	Force (kN)	Notes
Peak Force	0.074	9.27	
Acetabulum	0.065	5.85	
Femoral Head	0.068	6.40	
Femoral Neck			
Trochanter			
Proximal Femur	0.070	6.57	
Femoral Shaft	0.078	6.83	After peak
Femoral Condyle			



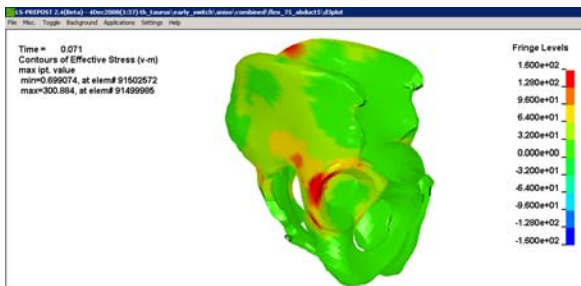
Left Leg Stresses at time of Max. Stress (t=0.069 for both)



Right Leg Femur Axial Forces

Fracture Force Summary: Right

Parameter	Time (sec)	Force (kN)	Notes
Peak Force	0.070	8.67	
Acetabulum	0.065	4.38	
Femoral Head	0.070	8.67	Peak
Femoral Neck	0.071	7.25	After Peak
Trochanter			
Proximal Femur	0.070	8.67	Peak
Femoral Shaft			
Femoral Condyle			



Right Leg Stresses at time of Max. Stress

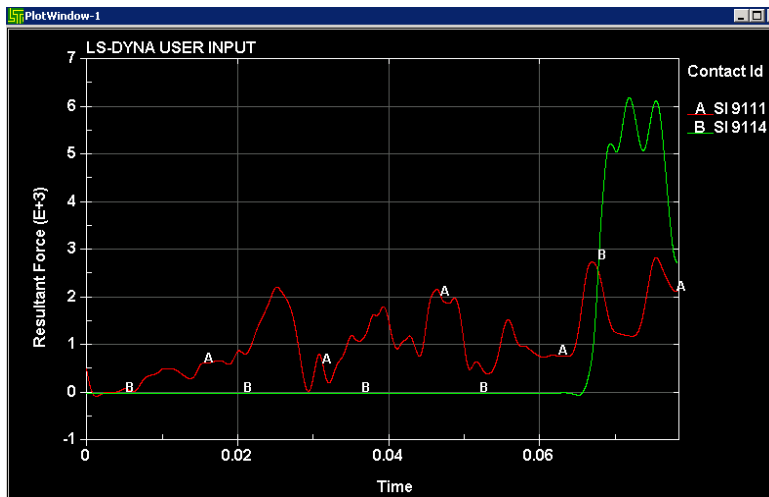
Combined Flex7.5° Adduct5° Results Summary

Summary: Patella fracture occurred shortly after contact with knee bolster. No signs of correlation between maximum femur forces and foot contact forces. The left leg experienced higher force and more serious injury. Upon contact with the knee bolster, the right leg moved downward along it, causing downwards rotation of the hip. The left leg had a more direct impact, pushing the knee bolster upward and causing upward rotation at the hip.

Contact Forces

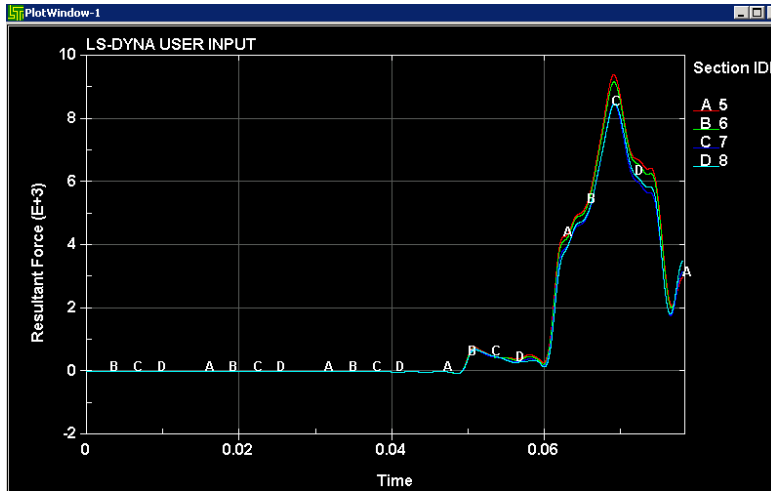


Knee Bolster Contact Forces



Foot Contact Forces

Femur Forces

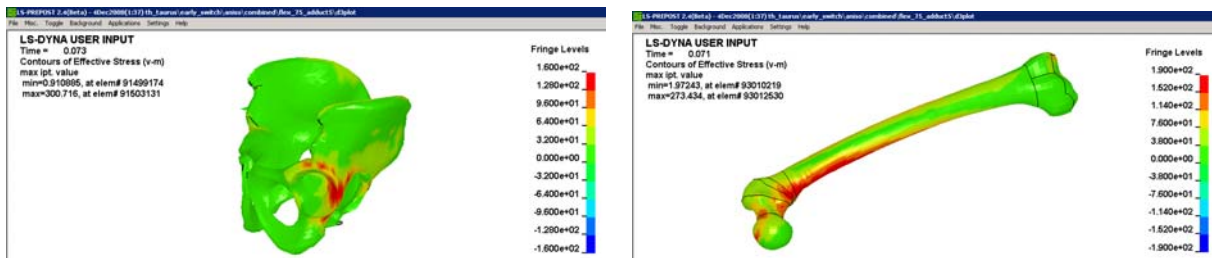


Left Leg Femur Axial Forces

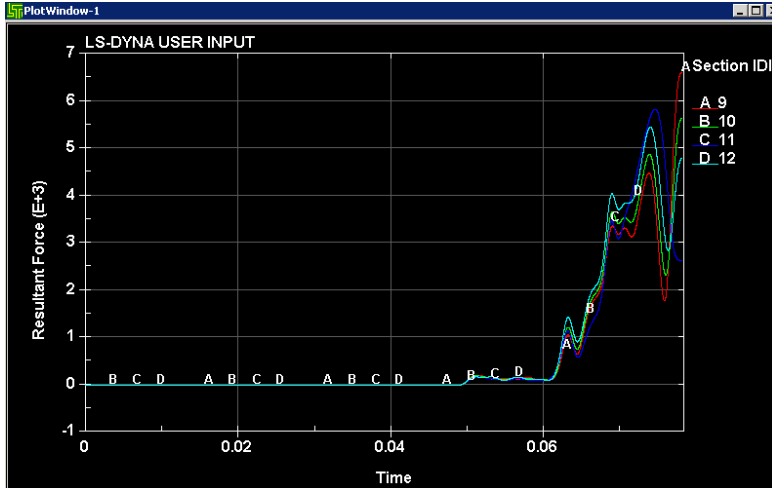
Fracture Force Summary:

Parameter	Time (sec)	Force (kN)	Notes
Peak Force	0.069	9.44	
Acetabulum	0.063	4.36	
Femoral Head	0.068	8.10	
Femoral Neck	0.070	8.96	After peak
Trochanter			
Proximal Femur	0.068	8.10	
Femoral Shaft	0.070	8.96	After peak

Femoral Condyle



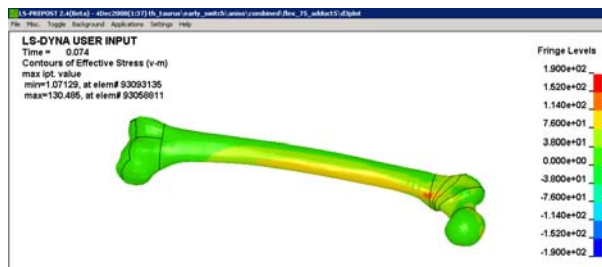
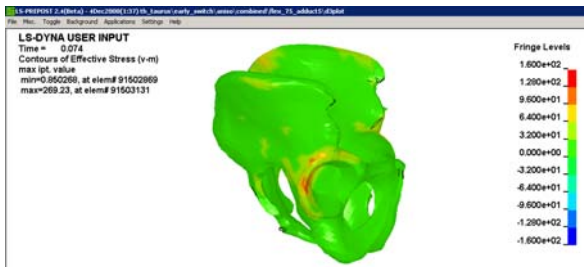
Left Leg Stresses at time of Max. Stress (t=0.069 for both)



Right Leg Femur Axial Forces

Fracture Force Summary: Right

Parameter	Time (sec)	Force (kN)	Notes
Peak Force	0.074	5.47	
Acetabulum			
Femoral Head			
Femoral Neck			
Trochanter			
Proximal Femur			
Femoral Shaft			
Femoral Condyle			

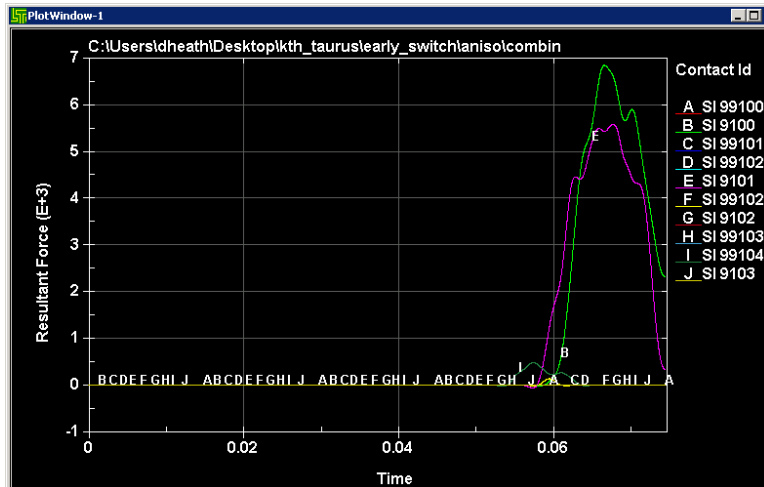


Right Leg Stresses at time of Max. Stress

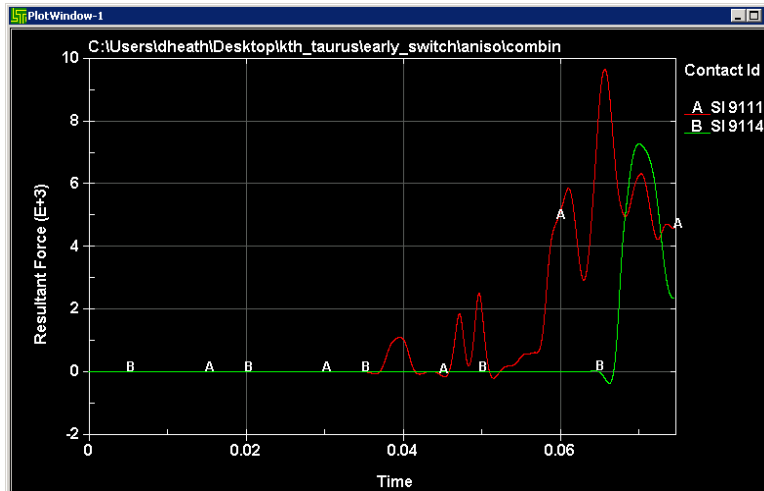
Combined Flex22.5° Abduct10° Results Summary

Summary: Patella fracture occurred shortly after contact with knee bolster. Signs of correlation between maximum femur forces and foot contact forces. The left leg experienced higher force and more serious injury. Upon contact with the knee bolster, the right leg moved downward along it, causing downwards rotation of the hip. The left leg had a more direct impact, pushing the knee bolster upward and causing upward rotation at the hip.

Contact Forces

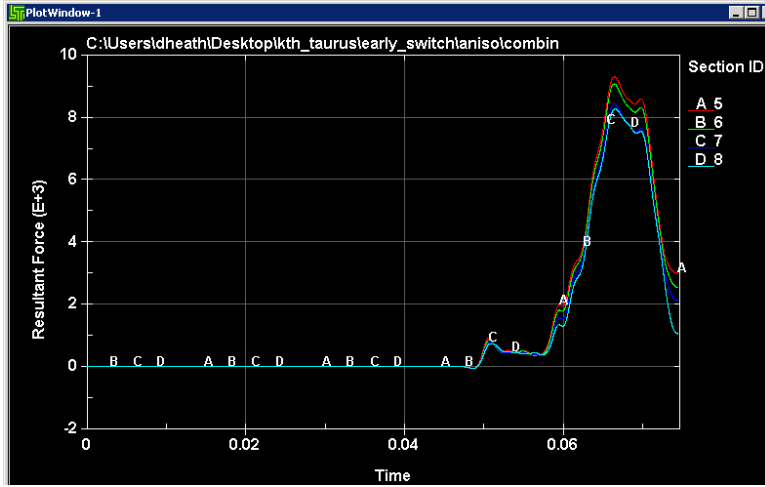


Knee Bolster Contact Forces



Foot Contact Forces

Femur Forces

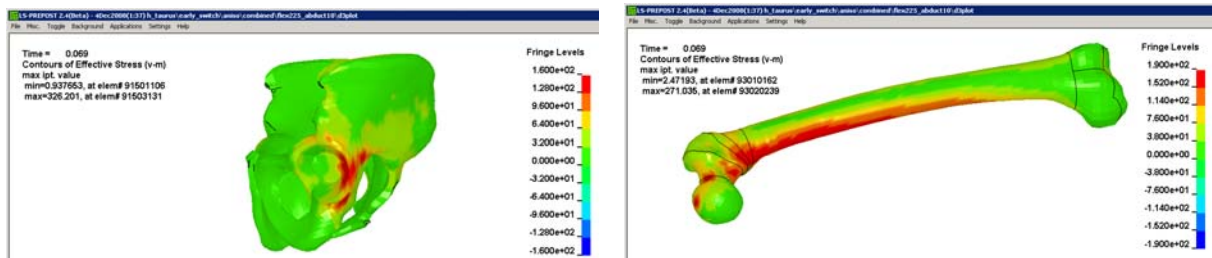


Left Leg Femur Axial Forces

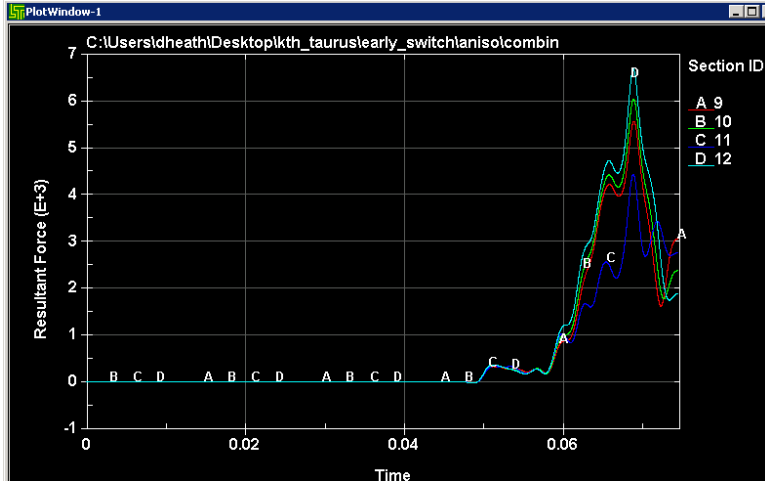
Fracture Force Summary:

Parameter	Time (sec)	Force (kN)	Notes
Peak Force	0.067	9.30	
Acetabulum	0.063	4.54	
Femoral Head	0.067	9.30	Peak
Femoral Neck	0.067	9.30	Peak
Trochanter	0.073	3.44	After peak
Proximal Femur	0.066	9.02	
Femoral Shaft	0.067	9.30	Peak

Femoral Condyle



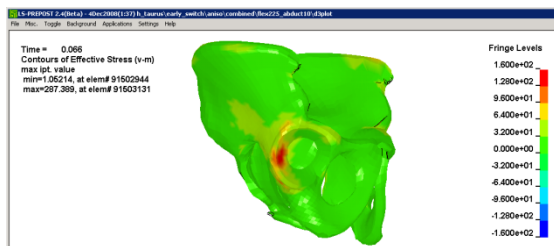
Left Leg Stresses at time of Max. Stress (t=0.069 for both)



Right Leg Femur Axial Forces

Fracture Force Summary: Right

Parameter	Time (sec)	Force (kN)	Notes
Peak Force	0.069	6.68	
Acetabulum	0.064	3.23	
Femoral Head			
Femoral Neck			
Trochanter			
Proximal Femur			
Femoral Shaft			
Femoral Condyle			



Right Leg Stresses at time of Max. Stress

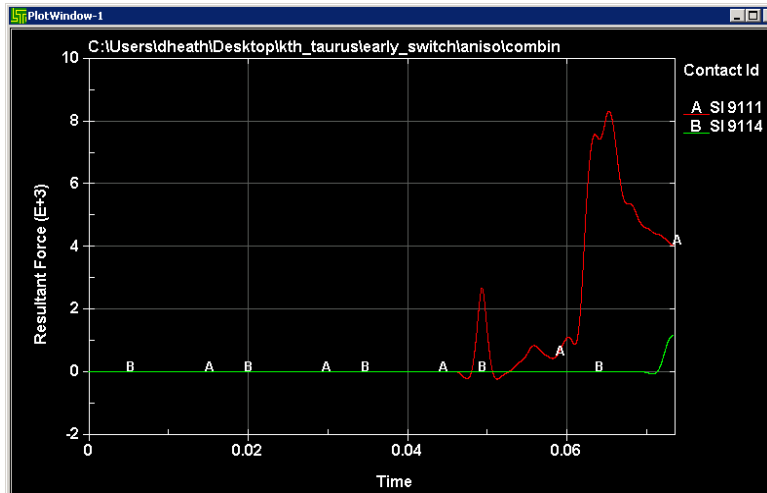
Combined Flex22.5° Adduct10° Results Summary

Summary: Patella fracture occurred shortly after contact with knee bolster. Signs of correlation between maximum femur forces and foot contact forces. The right leg experienced higher force and slightly more serious injury. Upon contact with the knee bolster, both legs had a direct impact, pushing the knee bolster upward and causing upward rotation at the hip. Because the right leg did not impact the floor very hard, the phenomena described by Meyer was observed.

Contact Forces

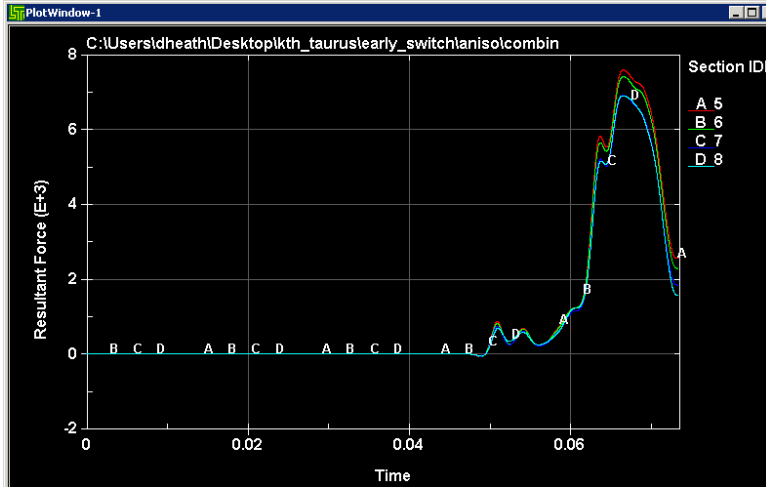


Knee Bolster Contact Forces



Foot Contact Forces

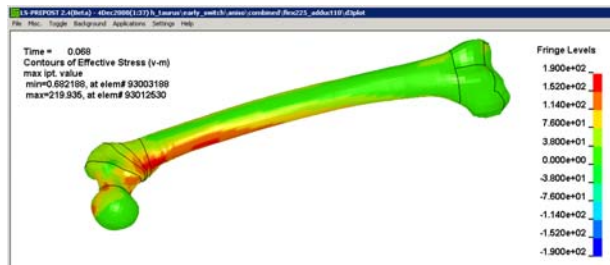
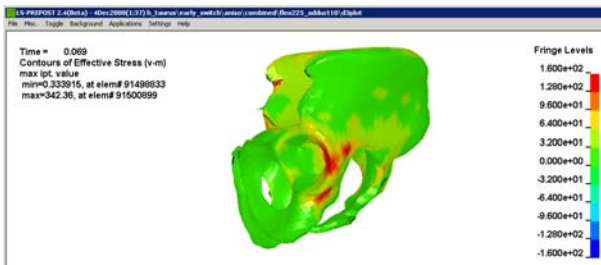
Femur Forces



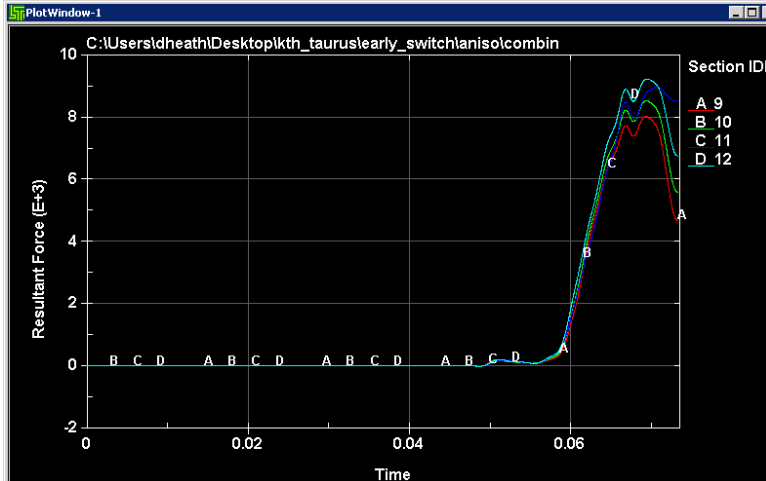
Left Leg Femur Axial Forces

Fracture Force Summary:

Parameter	Time (sec)	Force (kN)	Notes
Peak Force	0.067	7.59	
Acetabulum	0.064	5.75	
Femoral Head	0.067	7.59	Peak
Femoral Neck			
Trochanter			
Proximal Femur	0.066	7.23	
Femoral Shaft	0.068	7.32	After peak
Femoral Condyle			



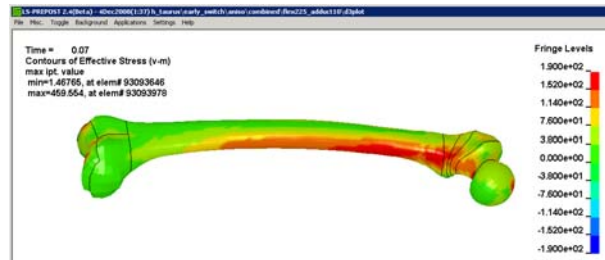
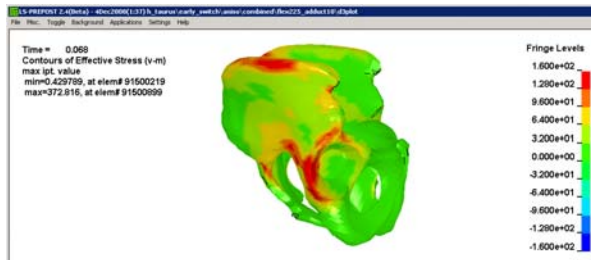
Left Leg Stresses at time of Max. Stress (t=0.069 for both)



Right Leg Femur Axial Forces

Fracture Force Summary: Right

Parameter	Time (sec)	Force (kN)	Notes
Peak Force	0.070	9.19	
Acetabulum	0.062	4.16	
Femoral Head	0.064	6.39	
Femoral Neck	0.065	7.35	
Trochanter			
Proximal Femur	0.065	7.35	
Femoral Shaft	0.069	9.03	
Femoral Condyle	0.065	7.35	

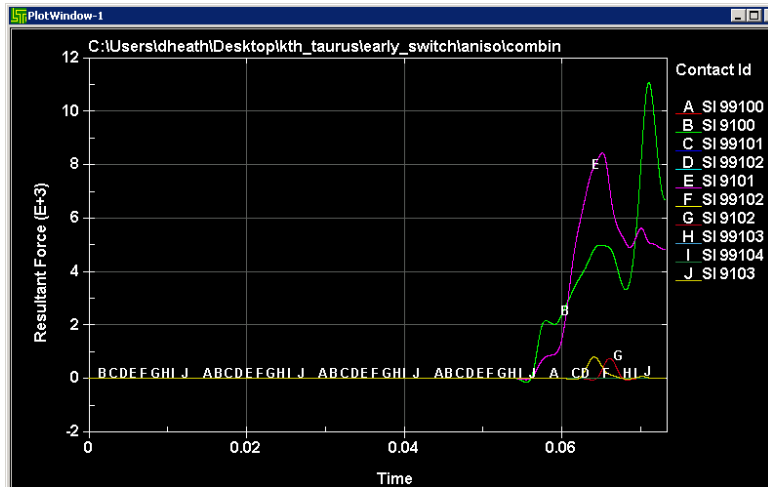


Right Leg Stresses at time of Max. Stress

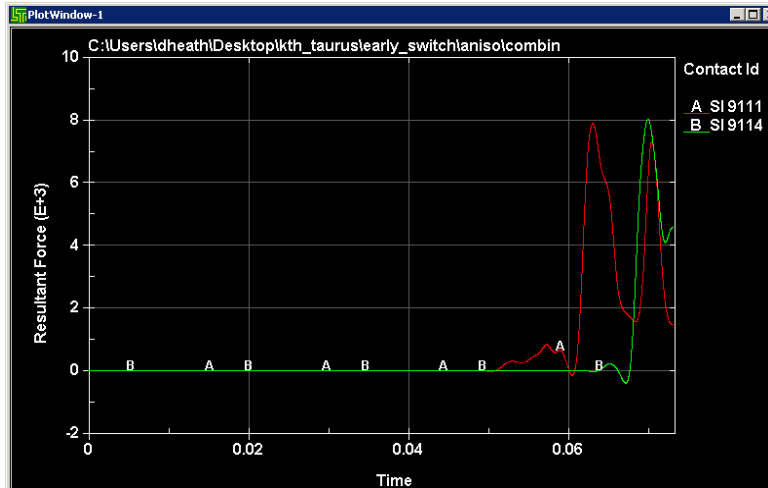
Combined Flex22.5° Abduct5° Results Summary

Summary: Patella fracture occurred shortly after contact with knee bolster. Signs of correlation between maximum femur forces and foot contact forces. The left leg experienced higher force however, the right leg experienced more serious injury. Upon contact with the knee bolster, both legs had a direct impact, pushing the knee bolster upward and causing upward rotation at the hip.

Contact Forces

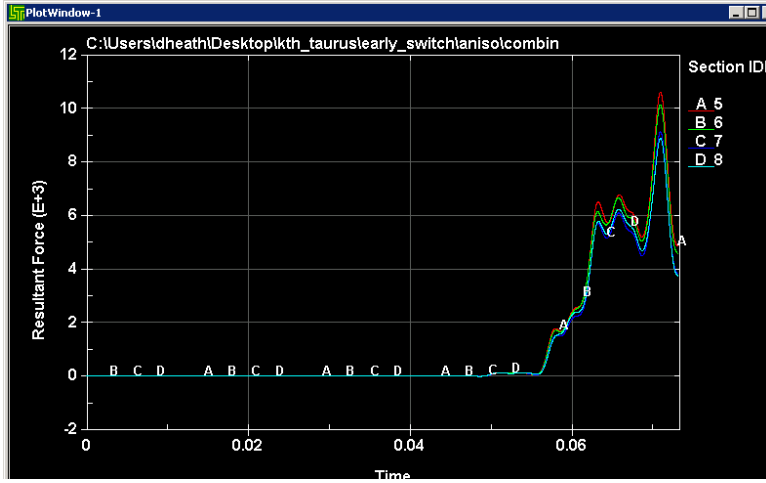


Knee Bolster Contact Forces



Foot Contact Forces

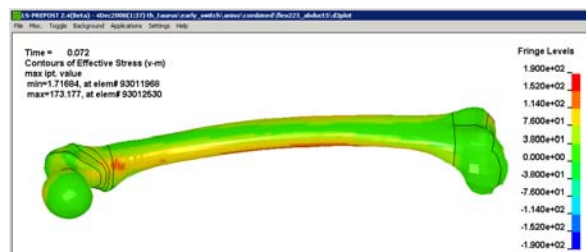
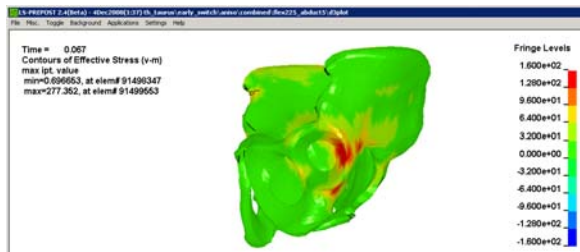
Femur Forces



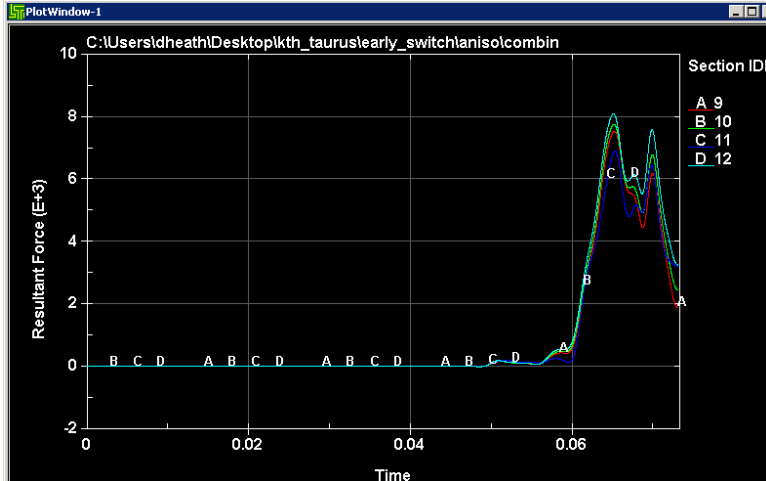
Left Leg Femur Axial Forces

Fracture Force Summary:

Parameter	Time (sec)	Force (kN)	Notes
Peak Force	0.071	10.1	
Acetabulum	0.061	2.61	
Femoral Head			
Femoral Neck			
Trochanter			
Proximal Femur			
Femoral Shaft			
Femoral Condyle			



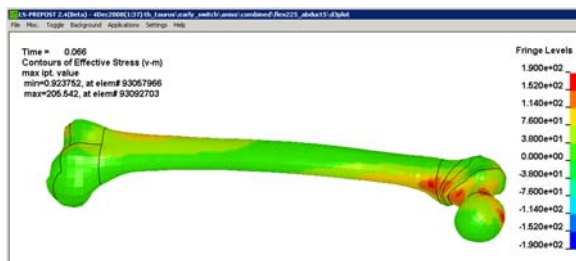
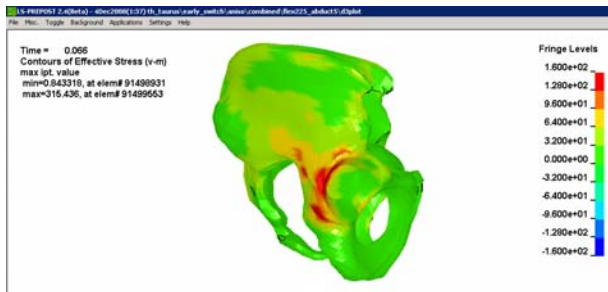
Left Leg Stresses at time of Max. Stress (t=0.069 for both)



Right Leg Femur Axial Forces

Fracture Force Summary: Right

Parameter	Time (sec)	Force (kN)	Notes
Peak Force	0.065	8.06	
Acetabulum	0.063	4.79	
Femoral Head	0.066	7.33	After peak
Femoral Neck	0.066	7.33	After peak
Trochanter			
Proximal Femur	0.066	7.33	After peak
Femoral Shaft			
Femoral Condyle			

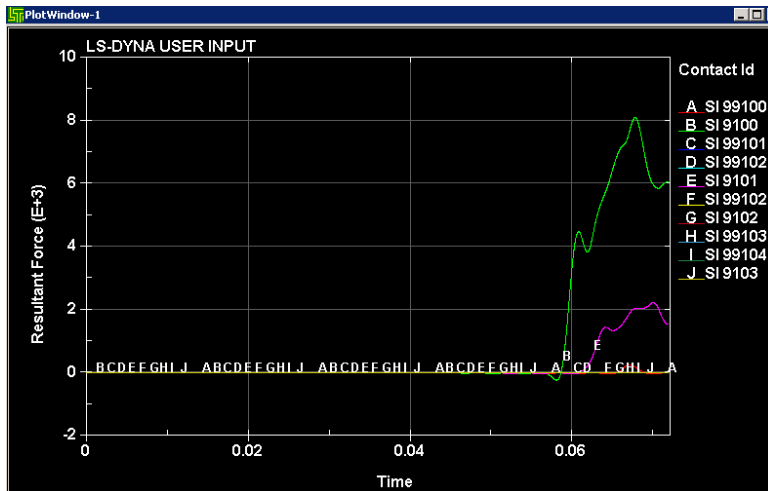


Right Leg Stresses at time of Max. Stress

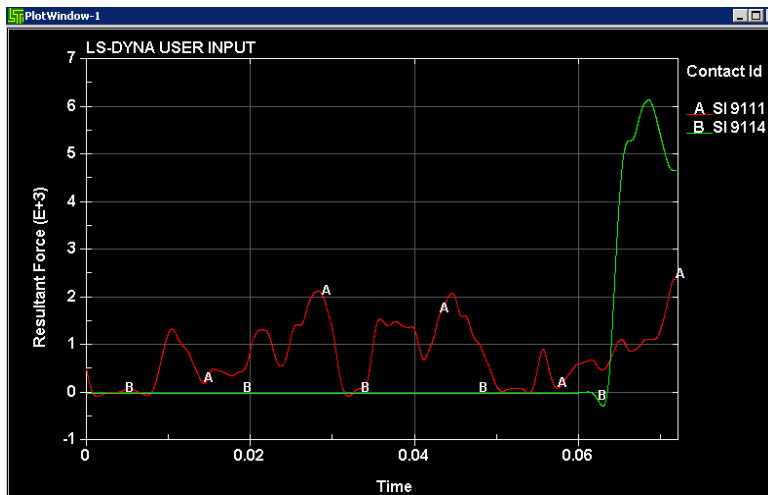
Combined Flex22.5° Adduct5° Results Summary

Summary: Patella fracture occurred shortly after contact with knee bolster. Signs of correlation between maximum femur forces and foot contact forces. The left leg experienced higher force and more serious injury. Upon contact with the knee bolster, the left leg had a direct impact, pushing the knee bolster upward and causing upward rotation at the hip. The right leg slid along the knee bolster, causing downward rotation of the hip.

Contact Forces

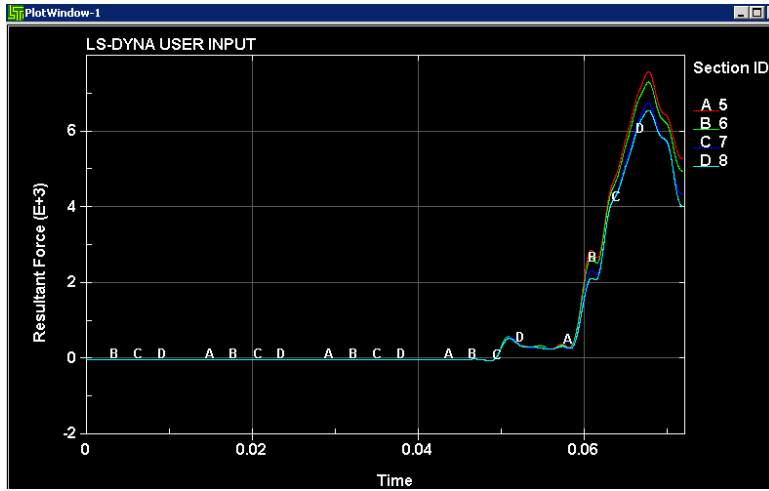


Knee Bolster Contact Forces



Foot Contact Forces

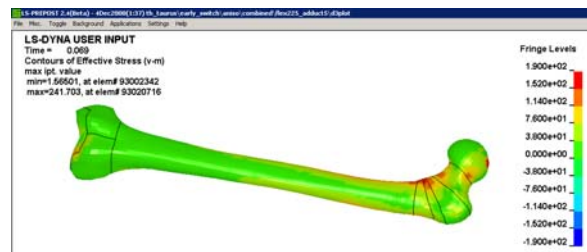
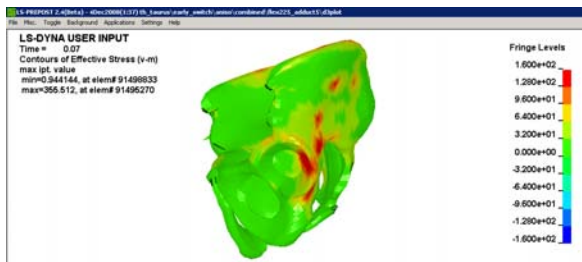
Femur Forces



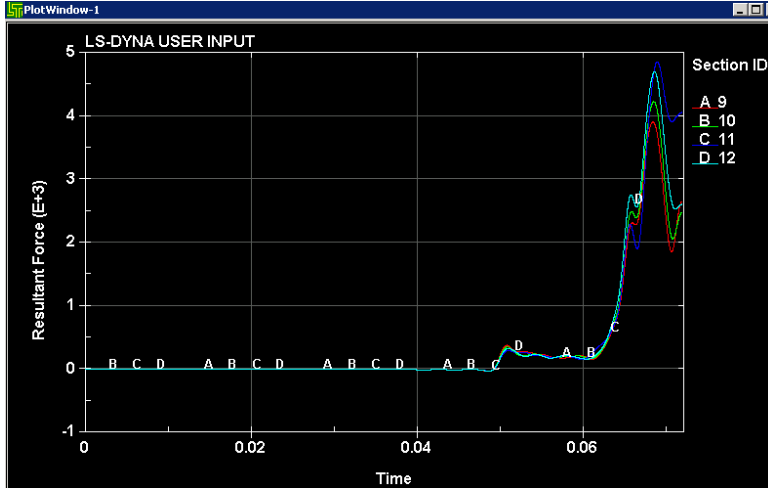
Left Leg Femur Axial Forces

Fracture Force Summary:

Parameter	Time (sec)	Force (kN)	Notes
Peak Force	0.068	7.56	
Acetabulum	0.063	4.33	
Femoral Head	0.065	5.69	
Femoral Neck			
Trochanter			
Proximal Femur	0.070	6.45	After peak
Femoral Shaft			
Femoral Condyle	0.068	7.49	Lateral condyle, after peak



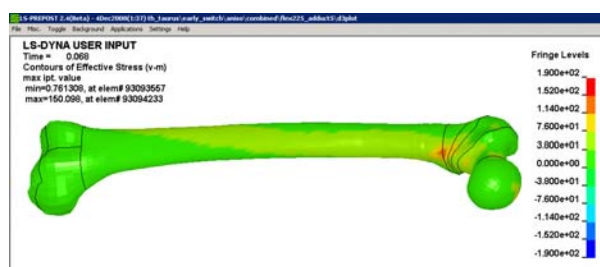
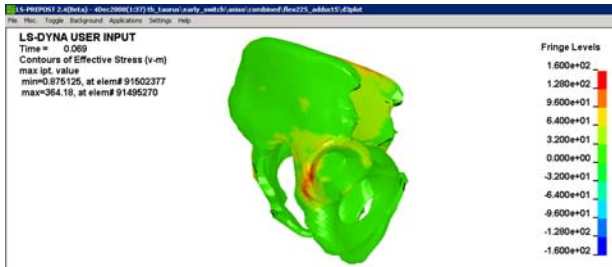
Left Leg Stresses at time of Max. Stress (t=0.069 for both)



Right Leg Femur Axial Forces

Fracture Force Summary: Right

Parameter	Time (sec)	Force (kN)	Notes
Peak Force	0.069	4.71	
Acetabulum	0.069	4.71	Peak
Femoral Head			
Femoral Neck			
Trochanter			
Proximal Femur			
Femoral Shaft			
Femoral Condyle			



Right Leg Stresses at time of Max. Stress